UNIVERSITY OF CALIFORNIA

Los Angeles

# Design and Characterization of Gene Activated Porous Hyaluronic Acid Hydrogels for Cutaneous Wound Healing

A dissertation submitted in partial satisfaction

of requirements for the degree Doctor of Philosophy

in Bioengineering

by

Cynthia Cam

2015

ABSTRACT OF THE DISSERTATION

Design and Characterization of Gene Activated Porous Hyaluronic Acid Hydrogels for Cutaneous Wound Healing

by

Cynthia Cam

Doctor of Philosophy in Bioengineering

University of California, Los Angeles, 2015

Professor Tatiana Segura, Chair

The vital wound healing process is critically dependent on sequential and overlapping stages that can be hindered by factors including diseases/conditions, systemic variables, or aging. Thus, there exists a need to aid the body when it is unable to repair tissue on its own. Currently, there is limited success in bioengineered matrices for tissue repair. Vascularization of the scaffold remains the primary cause of construct and host-integration failure. Vascularization ensures a route for nutrient, oxygen, and waste transport to facilitate cell survival deep within the construct for new tissue formation. Thus, we proposed to develop a porous hyaluronic acid (HA) hydrogel system to deliver non-viral genes to promote angiogenesis for improved wound healing.

Our lab had previously shown that porous HA hydrogels facilitated more cellular infiltration *in vivo* in murine subcutaneous implant and wound healing models when compared to non-porous gels of the same composition. With newfound validation that porous hydrogel

architecture was necessary, new techniques were developed and reduced the microsphere template processing time from 17-22 h to 1-2 h with introduction of liquid handling to minimize human error and inconsistencies with comparable results. The investigation of natural scaffolds in cutaneous wound healing further demonstrated that porous hydrogel architecture results in more rapid wound closure with more stable, mural-covered blood vessels, even when compared to fibrin—a scaffold commonly chosen due to its inherent role in natural wound healing. Incorporation of non-viral DNA aimed to enhance the therapeutic capacity of the scaffolds and was tested by loading DNA via caged nanoparticle encapsulation (CnE) and comparing it to methods utilized in literature. DNA loading was paired with hyaluronidase (HAase) treatment of the gel to loosen the polymer network for cell-mediated degradation and resultant transfection. *In vitro* and *in vivo* transfection was significantly improved with CnE loaded gels and transgene expression was a function of HAase concentration. HAase treatment was then applied to efforts in developing a sequential gene delivery system. Two hydrogel systems (surface coated and two phase) were tested *in vitro* that led to an *in vivo* application of a hybrid system. Bioluminescence imaging showed that *in vivo* transgene expression profiles suggested dual gene delivery rather than sequential. Investigation of the effect of spatio-temporal presentation of pro-angiogenic plasmids showed that a homogenous presentation of pVEGF and pPDGF polyplexes resulted in more rapid wound closure and mural-covered blood vessels than hydrogels with spatially separated polyplexes by day 7.

With further optimization and modification, we believe the proposed hydrogel system(s) are capable of controlled delivery of non-viral genes for cutaneous tissue repair. Although the focus of this dissertation was focused on repairing skin wounds, a well developed hydrogel system can deliver any type or combination of genes to yield numerous therapeutic effects.

The dissertation of Cynthia Cam is approved.

Daniel Kamei

William Lowry

Harold Monbouquette

Tatiana Segura, Committee Chair

University of California, Los Angeles

2015

*Dedication*

I dedicate this dissertation to my family.

Mom and Dad

Anthony

Charlie and Anh

Lucas

Without all your love and support, this dissertation would not have been possible.

# TABLE OF CONTENTS

CHAPTER 1: OVERVIEW OF DISSERTATION AND SPECIFIC AIMS ..... 1
1.1 Motivation and Objectives ..... 1
1.2 Specific Aims ..... 4
1.2.1 Specific Aim 1 (Chapter 4) ..... 4
1.2.2 Specific Aim 2 (Chapter 5) ..... 5
1.2.3 Specific Aim 3 (Chapter 6) ..... 5
1.2.4 Specific Aim 4 (Chapter 7) ..... 6
1.3 Dissertation Outline ..... 7
CHAPTER 2: SCAFFOLDS FOR IMPROVED TISSUE REPAIR ..... 10
2.1 Vascularization: critical role in wound healing ..... 10
2.2 Scaffold architecture: porosity and angiogenesis ..... 12
2.3 Scaffolds: type and material choice ..... 13
2.3.1 Hydrogels ..... 13
2.3.2 Hyaluronic acid (HA) ..... 14
CHAPTER 3: SCAFFOLD-MEDIATED NON-VIRAL GENE DELIVERY ..... 16
3.1 Introduction ..... 16
3.2 Vector Design ..... 18
3.3 Delivery of the Vector ..... 22
3.4 Design of the Matrix ..... 24
3.4.1 Controlled Release ..... 26
3.4.2 Controlling Cellular Infiltration ..... 27
3.4.3 Surface Associated ..... 28
3.4.4 Biochemical Cues ..... 29
3.5 Summary ..... 30
CHAPTER 4: OPTIMIZING POROUS HYALURONIC ACID HYDROGELS GENERATION FOR CELLULAR INVASION AND VASCULARIZATION ..... 31
4.1 Introduction ..... 31
4.2 Materials and methods ..... 33
4.2.1 Materials ..... 33
4.2.2 Hyaluronic acid-acrylate modification ..... 33

4.2.3 Design template using PMMA microspheres ..... 34
4.2.4 Hydrogel formation ..... 35
4.2.6 Characterization of hydrogel structural and mechanical properties ..... 36
4.2.7 Cell culture ..... 37
4.2.8 Cell seeding onto porous hydrogels ..... 37
4.2.9 Cell viability and spreading ..... 37
4.2.10 Cell proliferation ..... 38
4.2.11 Subcutaneous implant model ..... 39
4.2.12 Immunohistochemistry and immunofluorescence ..... 40
4.2.13 Quantification and characterization of cellular infiltration and blood vessels *in vivo* ..... 40
4.2.14 Statistical analysis ..... 41
4.3 Results ..... 42
4.3.1 Effect of PMMA sintering technique on hydrogel formation ..... 42
4.3.2 Effect of PMMA sintering technique on structural and mechanical properties ..... 43
4.3.3 Effect of PMMA sintering technique on cell behavior *in vitro* ..... 44
4.3.4 Effect of PMMA sintering technique *in vivo* ..... 45
4.4 Discussion ..... 47
4.5 Conclusions ..... 51
CHAPTER 5: SYSTEMATIC EVALUATION OF NATURAL SCAFFOLDS IN CUTANEOUS WOUND HEALING ..... 52
5.1 Introduction ..... 52
5.2 Materials and methods ..... 53
5.2.1 Materials ..... 53
5.2.2 Hyaluronic acid-acrylate modification ..... 54
5.2.3 Design template using PMMA microspheres ..... 54
5.2.4 Hydrogel formation ..... 55
5.2.4.1 Porous hyaluronic acid hydrogel (μ) ..... 55
5.2.4.2 Fibrin gel formation (F) ..... 55
5.2.4.3 Composite hydrogel formation ..... 56
5.2.5 VEGF nanocapsule synthesis ..... 56
5.2.6 Splinted wound healing model ..... 56
5.2.7 *In vivo* quantification and analysis ..... 58
5.2.7.1 Wound closure ..... 58

5.2.7.2 Immunohistochemistry and immunofluorescence analysis ....58
5.2.7.3 Histology evaluation ....58
5.2.8 Statistical analysis ....60
5.3. Results and Discussion ....60
5.3.1 Effect of conductive scaffolds on wound closure ....60
5.3.2 Pathological findings of conductive scaffolds ....61
5.3.3 Blood vessel characterization of conductive scaffolds ....63
5.3.4 Effect of composite gel on wound closure ....63
5.3.6 Blood vessel characterization of composite gels ....66
5.3.7 Effect of inductive composite scaffold on wound closure ....66
5.3.8 Pathological findings of inductive composite scaffolds ....68
5.3.9 Blood vessel characterization of inductive composite scaffolds ....68
5.4. Conclusions ....70
CHAPTER 6: ENHANCED TRANSFECTION FROM DNA-LOADED POROUS HYALURONIC ACID HYDROGELS ....71
6.1 Introduction ....71
6.2 Materials and methods ....73
6.2.1 Materials ....73
6.2.2 Hyaluronic acid-acrylate modification ....73
6.2.3 DNA/PEI polyplex formation ....74
6.2.4 CnE, polyplex lyophilization ....74
6.2.5 PMMA microsphere template for porous hydrogel formation ....75
6.2.6 Porous hydrogel formation ....75
6.2.7 Polyplex visualization ....76
6.2.8 Radiolabeled DNA ....76
6.2.8.1 Radiolabeling and purification ....76
6.2.8.2 DNA loading and release ....76
6.2.9 *In vitro* transfection ....77
6.2.10 Gaussia luciferase assay ....78
6.2.11 Mechanical Characterization ....78
6.2.12 Engineering pEF1α-eGFP-2A-VEGF, biscistronic vector ....79
6.2.13 Splinted wound healing model ....79
6.2.14 Wound closure ....81

6.2.15 Immunofluorescence and Immunohistochemistry ..... 81
6.2.16 Quantification and characterization of transfection and immune response in vivo ..... 81
6.2.17 Quantification and characterization of cellular infiltration and blood vessels in vivo ..... 82
6.3 Results and Discussion ..... 83
6.3.1 Effect of HAase on DNA loading and release ..... 83
6.3.2 HAase pre-treatment enhances *in vitro* transfection ..... 84
6.3.3 HAase pre-treatment enhances transfection *in vivo* ..... 88
6.3.4 *In vivo* transfection with a therapeutic plasmid encoding for VEGF ..... 90
6.4 Conclusions ..... 93
CHAPTER 7: DUAL GENE DELIVERY FROM TWO HYDROGEL SYSTEMS: SURFACE COATED VS. TWO PHASE HYDROGELS ..... 94
7.1 Introduction ..... 94
7.2 Materials and methods ..... 96
7.2.1 Materials ..... 96
7.2.2 Hyaluronic acid-acrylate modification ..... 96
7.2.3 DNA/PEI polyplex formation and surface coating ..... 97
7.2.4 CnE, polyplex lyophilization ..... 97
7.2.5 PMMA microsphere template for surface-coated and two phase hydrogel formation ..... 97
7.2.6 Hydrogel formation ..... 98
7.2.7 Hydrogel composition and mechanical characterization ..... 99
7.2.7.1 Visual characterization via confocal microscopy and SEM ..... 99
7.2.7.2 Mechanical characterization ..... 99
7.2.8 Radiolabeled DNA ..... 100
7.2.8.1 Radiolabeling and purification ..... 100
7.2.8.2 DNA release ..... 100
7.2.9 *In vitro* transfection ..... 101
7.2.10 Gaussia luciferase assay ..... 102
7.2.11 SEAP assay ..... 102
7.2.12 Cell proliferation ..... 103
7.2.13 Splinted wound healing model ..... 103
7.2.14 Bioluminescence Imaging ..... 104
7.2.15 Engineering biscistronic vectors ..... 105
7.2.16 Wound closure ..... 106

7.2.17 Immunofluorescence and Immunohistochemistry ..... 107
7.2.18 Quantification and characterization of cellular infiltration and blood vessels *in vivo* ..... 107
7.3 Results and discussion ..... 108
7.3.1 Characterization of surface coated vs. two phase gene delivery systems ..... 108
7.3.2 *In vitro* evaluation of surface coated vs. two phase gene delivery systems ..... 111
7.3.3 *In vivo* transfection ..... 113
7.4 Conclusions ..... 117
CHAPTER 8: CONCLUSIONS AND FUTURE DIRECTIONS ..... 119
8.1 Introduction ..... 119
8.2 Specific Aim 1 (Chapter 4) ..... 119
8.3 Specific Aim 2 (Chapter 5) ..... 120
8.4 Specific Aim 3 (Chapter 6) ..... 121
8.5 Specific Aim 4 (Chapter 7) ..... 123
CHAPTER 9: REFERENCES ..... 126

LIST OF FIGURES AND TABLES

**Figure 1.1 General dissertation overview**..... 9

**Figure 3.1 Schematic overview of protein expression.** For gene delivery, nDNA (**1**) is released from the scaffold through either hydrolysis or cellular migration (**2**) and internalized into the endosome (**3**). The endosome matures changing its oxidative and acidity resulting in endosomal escape of nDNA polyplexes (**4-5**). nDNA polyplexes can enter the nucleus (**7**) to be unpacked (**8**) or be de-coupled in the cytosol (**6**) for nuclear entry (**7**), where transcription and translation occurs (**9**) for protein expression. Growth factors or other bioactive signals can be used to induce intracellular signaling pathways that prime cells for transfection (**10**). .....17

**Figure 3.2** The design of scaffolds for tissue repair that use genes as a bioactive signal goes beyond incorporating the nDNA polyplexes into the scaffold. .....18

**Figure 3.3** Novel approaches to investigate the effect of design parameters on transgene expression. Different plasmid promoters (UbC vs. CMV) showed to have an effect on in vivo transgene expression (**A**), while stiffness had an inverse correlation with in vitro transgene expression in hyaluronic acid hydrogels (**B**). To decrease nDNA aggregation at higher nDNA concentrations, a caged nanoparticle encapsulation (CnE) technique was developed and applied to porous hydrogels for in vivo transfection (arrows show transfected cells, **C**).....21

**Table 3.1** Vector and carrier design characteristics .....25

**Figure 4.1 Schematic representation of steps taken to generate porous hyaluronic acid hydrogels via chemical and non-sintering of PMMA microspheres.** The appropriate sintering suspension solution is described in 2.3. The resultant porous hydrogel is achieved after step 6, following PMMA dissolution via acetone and serial hydration. .....35

**Figure 4.2** (**A**) PMMA microspheres packed with each respective sintering technique imaged via SEM demonstrated comparable microsphere structure and organization prior to hydrogel formation. (**B**) Quantification of PMMA microsphere diameter following packing showed no marked difference in microsphere size immediately following the various sintering methods. ...41

**Figure 4.3** Porous hydrogels with 60 μm pores generated from HS, NS, and CS have apparent open pore and interconnected pore structure in SEM, phase, and fluorescent orthogonal projections and 3D renderings. .....42

**Figure 4.4** (**A**) Quantification of interconnected pore diameters indicates similar interconnectivity between hydrogels generated with HS, NS, and CS. (**B**) Water content was similar for hydrogels generated with the various techniques. (**C**, **D**) Conversely, PMMA microsphere packing technique affects gel stiffness, where gels generated via HS were comparable to CS but stiffer than NS-generated gels. (***) $p < 0.001$. Values represent the mean and standard deviation. ..43

**Figure 4.5 In vitro characterization and quantification of mMSCs seeded onto hyaluronic acid hydrogels following 7 days.** (**A**) mMSC viability (green = live and red = dead cells) and (**B**) spreading (red = f-actin and blue = nuclei) was assessed at day 2 and 7 by fluorescent microscopy. (**C**) Quantification of day 2 viability and (**D**) cell growth at days 1, 4, and 7 showed no significant differences among groups. (**E**) Quantification of cell spreading by measuring end-

to-end cell length (**F**) at days 2 and 7 showed no difference among the groups at each time point. (*) $p < 0.05$. Values represent the mean±SD. .....44

**Figure 4.6 *In vivo* characterization and quantification of aceullar hyaluronic acid hydrogels (60 μm pores) implanted subcutaneously in balb/c mice for 14 days.** (**A**) H&E stained sections of porous hydrogels generated from the different techniques showed similar levels of cellular infiltration. (**B**) Staining for an endothelial cell marker showed PECAM positive cells within the hydrogels generated by all three sintering techniques. (**C**) Quantification of cellular infiltration showed comparable invasion within gels generated from all three techniques. (**D**) Vessels in 30 images over 3 sections separated by 100-150 μm were quantified and normalized to the total image area. The bar graph represents the average of 4 separate samples. (**E**) For those samples that contained vessels, vessel diameters were measured. Approximately half of the vessels in all samples were less than 6 μm in diameter. Red = PECAM positive staining (endothelial cells), yellow = erythrocytes, and blue = nuclei. Values represent the mean and standard error of the mean. .....46

**Figure 4.7** (**A**) Scanning electron micrographs of non-porous (n-pore) 3.5 w/v% hyaluronic acid hydrogels confirm that no pores are present. (**B**) H&E staining of samples of n-pore hydrogels implanted subcutaneously in balb/c mice demonstrate that host cells are only penetrate the hydrogel periphery at 14 days. The asterisk denotes the remaining n-pore hydrogel and (M) denotes muscle.....47

**Table 5.1** Scoring of epidermis/re-epithelialization.....59

**Table 5.2** Scoring of granulation tissue/vascularization.....59

**Table 5.3** Scoring of collagen deposition/fibroplasia .....59

**Table 5.4** Scoring of inflammation.....59

**Figure 5.1 Evaluation of solely conductive natural scaffolds in vivo.** (**A**) Schematic representation of untreated (U), fibrin (F), and microporous HA (μ) filled wounds following initial wound creation. Digital images of wounds were taken at regular time intervals for wound closure analysis (**B**, **C**). .....60

**Figure 5.2 Evaluation of solely conductive natural scaffolds in vivo.** H&E stained wounds depict granulation tissue formation and were scored by a pathologist for re-epithelialization, granulation tissue/vessel formation, fibroplasias, and inflammation (**A**). OCT embedded sections were stained for vascular cell populations (**B**), where CD31+, NG2+, and nuclei imaged in red, green, and blue, respectively, and quantified via imageJ (**C**).....62

**Figure 5.3 Evaluation of composite natural scaffolds *in vivo***. (**A**) Schematic representation of wound treated with fibrin (F), microporous HA (μ), or composite (μ/F) hydrogels. Digital images of wounds were taken at regular time intervals for wound closure analysis (**B**, **C**). .....64

**Figure 5.4 Evaluation of composite natural scaffolds *in vivo*.** H&E stained wounds depict granulation tissue formation and were scored by a pathologist for re-epithelialization, granulation tissue/vessel formation, fibroplasias, and inflammation (**A**). OCT embedded sections were stained for vascular cell populations (**B**), where CD31+, NG2+, and nuclei imaged in red, green, and blue, respectively, and quantified via imageJ (**C**).....65

**Figure 5.5 Evaluation of inductive scaffolds *in vivo*.** (**A**) Schematic representation of $_{n}$V synthesis. (**B**) Schematic representation of wounds with various treatments. Digital images of wounds were taken at regular time intervals for wound closure analysis (**C**, **D**).....67

**Figure 5.6 Evaluation of inductive scaffolds *in vivo*.** H&E stained wounds depict granulation tissue formation and were scored by a pathologist for re-epithelialization, granulation tissue/vessel formation, fibroplasias, and inflammation (**A**). OCT embedded sections were stained for vascular cell populations (**B**), where CD31+, NG2+, and nuclei imaged in red, green, and blue, respectively, and quantified via imageJ (**C**).....69

**Figure 6.1. Approach for releasing DNA/PEI polyplexes for enhanced transfection.** (**A**) Schematic of DNA loading, porous hyaluronic acid (HA) gel formation, and the effect of hyaluronidase (HAase) (**B**).....82

**Figure 6.2 DNA/PEI polyplexes release as a function of HAase concentration.** DNA loaded porous HA gels via direct encapsulation (-A/S) were imaged via fluorescent microscopy to evaluate stained DNA intensity before and after 5 kU/ml HAase treatment (**A**), and DNA retention (*p<0.05, t-test; **B**) and release due to enzymatic degradation (**C**, **D**) was quantified with radiolabeled DNA as a result of various HAase treatments. Similarly, DNA loaded porous HA gels via caged nanoparticle encapsulation (+A/S) were (**E**) imaged via fluorescent microscopy to evaluate stained DNA intensity before and after 5 kU/ml HAase treatment, and DNA retention (*p<0.05, t-test; **F**) and release due to enzymatic degradation (**G**, **H**) was quantified with radiolabeled DNA. Data represent the mean±SD. Scale bars, 50 μm.....83

**Figure 6.3 HAase improves *in vitro* transfection with gels containing high DNA payload**. (**A**) Schematic of gaussia luciferase assay conducted to test in vitro transfection with fluorescent image of mMSCs migrating within the porous hyaluronic acid hydrogel. Gel, green; phalloidin, red; nuclei, blue. DNA loaded porous HA gels via direct encapsulation (-A/S) were assayed for gaussia luciferase and transfection was represented in kinetic relative light units (RLU) (**B**), and cumulative RLU (**C**) DNA loaded porous HA gels via caged nanoparticle encapsulation (+A/S) were evaluated for changes in mechanical properties due to HAase treatment (****p<0.0001, t-test; **p<0.01, t-test; **D**) and similarly assayed for gaussia luciferase, where transfection was represented in kinetic RLU (*p<0.05, t-test; †p<0.01, t-test; **E**) and cumulative RLU (*p<0.05, t-test; †p<0.01, t-test; **F**). To decouple the effect of stiffness from HAase treatment, softer gels were generated and confirmed with rheology, where the asterisk by 441Pa denotes the gel with HAase treatment (****p<0.0001, t-test; *p<0.05, t-test; **G**) and employed to test transfection of plasmid encoding for gaussia luciferase (*p<0.05, t-test; **H**, *p<0.05, t-test; **p<0.01, t-test; **I**). Data represent the mean±SD. Scale bar, 50 μm.....86

**Figure 6.4 HAase pre-treatment enhances transfection *in vivo* in murine wound healing model.** (**A**) Representative staining of tissue cross sections for GFP (green), Ly6G (red), and nuclei (blue) of wounds 5 and 10 days post-implantation with DNA loaded porous HA gels following various HAase treatment. Quantification of GFP+ and Ly6G+ area was evaluated at day 5 (***p<0.001, t-test; **B**, **C**) and day 10 (*p<0.05, t-test; **p<0.01, t-test; **D**, **E**) by measuring area from 5 random regions per tissue section across three different sections at least 150 μm apart (n=4-6). GFP transfection increased over time (***p<0.001, t-test; ****p<0.0001, t-test; **F**)

while the immune response became quiescent (**p<0.01, t-test; **G**). Data represent the mean±SEM. Scale bars, 50 μm.....88

**Figure 6.5 HAase pre-treatment of porous HA gels loaded with therapeutic proangiogenic plasmid leads to more rapid wound closure in a murine wound healing model.** (**A**) Schematic of initial wound, implantation with DNA loaded porous HA gel, and newly formed tissue over time. (**B**) Wound closure was visually observed via digital photography over time and wound area was quantified to assess the effect of HAase-mediated transfection with a therapeutic plasmid (n=10-11) (**p<0.01, t-test; ***p<0.001, t-test; **C**). (**D**) Representative H&E stained wound cross sections show the degree of cellular infiltration from the edge to the center at day 5 and 10 as a result of various HAase pre-treatments. Scale bars, 125 μm (**D**).....90

**Figure 6.6 HAase pre-treatment of porous HA gels loaded with therapeutic proangiogenic plasmid leads to more enhanced vascularization in a murine wound healing model.** (**A**) Representative images of granulation tissue stained for CD31 (red), NG2 (green), and nuclei (blue) show more vascularization as a result of HAase pre-treatments. Quantification of CD31+, NG2+, and DAPI+ area was evaluated at day 5 (***p<0.001, t-test; **B**, **p<0.01, t-test; **C**, *p<0.05, t-test; **p<0.01, t-test; ****p<0.0001, t-test; **D**) and day 10 (*p<0.05, t-test; **E**, **F**, *p<0.05, t-test; **G**) by measuring area from 3 random regions per tissue section across three different sections at least 150 μm apart (Figure 6.5A) (n=4-6). HAase pre-treated gels loaded with plasmid encoding for VEGF achieved sustained vascularization and larger cell populations in the newly formed granulation tissue, in general (**H**, **I**, **p<0.01, t-test; **J**). Data represent the mean±SEM. Scale bars, 100 μm (**A**).....92

**Figure 7.1 Surface coated gene delivery system** (A) Schematic representation of the surface coated gene delivery system where condensed polyplexes are encapsulated and coated on the surface of the pores. Porous hydrogels before (B) and after (C) surface coating with DNA polyplexes; HA gel = blue, DNA = green. (D) Minimal DNA release was observed from surface coated or encapsulated polyplexes in this delivery system.....108

**Figure 7.2 Two phase gene delivery hydrogel system.** (**A**) Schematic representation of the proposed two phase hydrogel system for sequential gene delivery. (**B**) SEM and (**C**) fluorescent images demonstrate a mated interface between gel phases following separate polymerization. (**D**) Mechanical characterization shows that the two phase (TP) gel has a bulk modulus similar to porous HA gels. (**E**) DNA polyplex release from each respective phase is minimal.....109

**Figure 7.2 *in vitro* evaluation of surface coated hydrogels as a gene delivery system.** (**A**) mMSCs exhibited spreading throughout the porous HA gels at day 5 and 14 of culture; HA gel = green, F-actin = red, nuclei = blue. (**B**) Cell health monitored by an alamarBlue® assay demonstrated that the DNA loaded gels were not cytotoxic. (**C**) Transfection from two secreted plasmids incorporated within each region (encapsulated vs. surface coated) was monitored for 40 days and showed similar transgene expression profiles.....110

**Figure 7.4 *in vitro* evaluation of two phase hydrogels as a gene delivery system.** (**A**) mMSCs exhibited spreading throughout the porous HA gels at day 5 and 14 of culture; HA gel = green, F-actin = red, nuclei = blue. (**B**) Cell health monitored by an alamarBlue® assay demonstrated that the DNA loaded gels were not cytotoxic. (**C**) Transfection from two secreted

plasmids incorporated within each region (μ-pore vs. n-pore) was monitored for 40 days and showed distinct transgene expression profiles. .....112

**Figure 7.5 Bioluminescence imaging of balb/c mice wounds implanted with two phase gels.** (**A**) Bioluminescence imaging was conducted regularly for 21 days to monitor transfection due to each region (μ-pore vs. n-pore) or in combination. (**B**, **C**) Quantification of total flux over time suggests that transgene expression profiles are similar and the signal is not additive. The μ-pore + n-pore condition was only imaged until day 17; the animals had removed their wound dressings thereafter. .....113

**Figure 7.6 Wound closure.** (**A**) Digital images of wounds taken at regular time intervals. (**B**) Quantification of wound area demonstrated that wounds treated with V/P and V→P gels closed more rapidly than untreated wounds (U). .....114

**Figure 7.7 Delivery of pro-angiogenic plasmids from two phase gels.** (**A**) H&E stained wound cross sections demonstrate untreated wounds with very little dermal volume by day 7. (**B**) Staining for endothelial and mural cell markers indicated significantly more positive staining in two phase gels when compared to untreated wounds; CD31= red, NG2=green, nuclei = blue. Quantification of CD31+, NG2+, and DAPI+ area (**C**, **D**, **E**) demonstrate that the two phase gels containing the pro-angiogenic plasmids significantly increase vascular cell populations within the newly formed tissue. .....115

ACKNOWLEDGEMENTS

This dissertation would not have been possible without the help, guidance, and support of so many individuals. First, I would like to thank my family. Mom and Dad, you are the most caring, loving, and selfless people in the world. You have made so many sacrifices to ensure that our body, mind, and heart are well cared for without compromise or regard for anything but the best for us. Even though you could not help me with my research, you did everything else anyone could imagine and for that, I thank you so much! Mom and Dad, you are the best parents anyone could ask for. I know I do not say it enough, but I love you both very much and I hope that I have made and continue to make you proud. Charlie and Anh, you guys are the best. You have been with me every step of the way, whether it was to just lend an ear or to provide help in any way possible. Your love and partnership in everything is something I look up to; I love you guys. I would also like to thank you guys for having my little man, Lucas! Lucas, you are not old enough to read yet, but I wanted to thank you for being such a cute adventurer! Your mom and dad have helped brighten my days with pictures of you exploring and of course, eating extreme amounts of food. Anthony, I can say that most people do not have a sibling in graduate school at the same time! I am so glad we can swap stories and share this unique experience together. Even though you make it a mission to terrorize me, I know it is only fueld by sibling adoration; I love you bro!

I would also like to thank Tatiana. Tatiana, you have been a great mentor to me for the past five years. You have provided so much guidance and support with an open mind to new ideas that has helped me and the lab grow as successful researchers. I admire your ability to maintain a balanced style despite being a profressor, principal investigator, and mother; it is really inspiring.

I also cannot forget about all of the friends and colleagues that have made these past five years so memorable. Garrett, you are one of my best friends. It has been very special

sharing this graduate school experience with you. I am glad to have someone understand my humor, and me, as well as you do. Thank you for always being there for me. I cannot really express how appreciative I am. Talar, I wanted to thank you for being a great mentor. We worked closely in the last year that you were in the lab, and you taught me so much! I learned a lot of techniques from you, but I also learned and admired how patient, respectful, and willing to help you were. It definitely influenced how I approached lab. Thank you to Jon and Shiva. All I can say is that you two made the lab dynamic very entertaining and it definitely made my experience memorable. Allyson, Don, and Lina, thanks for being great postdocs. You all are so knowledgeable in your respective discipline, and it has enriched the lab; thank you for answering all the questions I had along the way. Suwei! Thank you Suwei for being so sweet and great; I am so glad you were there every step along the way of this five-year journey! Giovanny, thanks for serenading us with your sweet songs in the tissue culture room; it always made me smile. Thank you to Sandy, Norman, Nikki, and Victor. You guys have been great labmates and taught me to be a better mentor. Elias, I am so glad you joined the lab and that I was able to work closely with you for the last few months. Thank you for all your help; you learn fast and undoubtedly will be a great researcher. Sasha Cai, you barely just started, but I welcome you to the lab and have no doubt that you will contribute valuable technologies to the lab. Thank you to Phil Scumpia for kindly providing your expertise in pathology to help evaluate my experimental tissue samples. I also cannot forget all the undergrads and high school students I mentored throughout the years. HoMing, Chris, Issac, Zach, and Andrea, thank you so much for helping make my graduate student experience memorable. You learned as I learned and it was really great having different perspectives spanning different years of scientific experience. Mentoring you helped me improve time management and encouraged me to find different ways to explain ideas. I hope that your experience with me was as positive as it was for me with all of you. You are all bright, creative minds; I wish you the best in all your endeavors. I

would also like to acknowledge the funding sources that made the research in this dissertation possible: NIH (R01HL110592).

# VITA

**EDUCATION:** **Bioengineering, B.S.** at University of California, San Diego (2010)

**EXPERIENCE:**

**Graduate Student Researcher**, Principal Investigator: Tatiana Segura
Cell-Instructive Materials Laboratory at University of California, Los Angeles Sept. 2010 – Present

- Engineering and implementing scaffolds for gene and growth factor delivery to promote angiogenesis for improved wound healing
  - Investigating optimal design parameters for *in vitro* and *in vivo* transfection
  - Investigating scaffold design for sequential delivery of bioactive signals (growth factors, DNA)
  - Optimized and executed murine models (subcutaneous and wound healing model)
- Characterizing release kinetics and structural/mechanical properties of engineered scaffolds with fluorescent microscopy (inverted and confocal), scanning electron microscopy (SEM), rheology, and radioactivity
- Analyzing *in vivo* studies via bioluminescence imaging, immunofluorescence and histological staining to assess cellular infiltration, immune response, angiogenesis, wound healing and closure, and transfection efficiency

*Collaborations*
Di Wu, UCLA Chemical and Biomolecular Engineering Department, Principal Investigator: Yunfeng Lu

- Implementation of tumor-targeting nanoparticles in a murine breast cancer model for cancer diagnostic

Natalie Boehnke, UCLA Chemistry Department, Principal Investigator: Heather Maynard

- Characterization of *in vitro* cell response to novel "self-healing" hydrogels

**R&D Engineer**, Neurospectrum LLC Dec. 2013 – Sept. 2014

- Actively involved in Class I orthopedic device product development activities from concept to clinical trial
- Engaged in design control activities:
  - Project strategy, plan, feasibility, development
  - Built preliminary constructs for in-house testing
  - Market and product specifications
  - Developed risk analysis file
  - Conducted pre-clinical research
  - 510(k) submission
- Clinical trial:
  - Designed data entry forms for clinical trial administrators
  - In charge of preliminary statistical analysis
  - Determined minimal clinically important difference (MCID) and relevant significant values

**Research Assistant**, UCSD Biomaterials & Regenerative Medicine Lab Sept.2008 – Aug. 2010

- Investigated the effect of naturally derived extracellular matrix based (decellularized tissue) scaffolds on *in vitro* adhesion, migration, and spreading.

**Intern/Laboratory Assistant**, FFA Sciences Jul. 2007 – Sept. 2008

**PUBLICATIONS:**

Tokatlian, T., **Cam, C.**, and Segura T. "Porous Hyaluronic Acid Hydrogels for Localized Nonviral DNA Delivery in a Diabetic Wound Healing Model." Advanced Healthcare Materials, Feb. 2015.

Tokatlian, T., **Cam, C.**, and Segura T. "Non-viral DNA delivery from porous hyaluronic acid hydrogels in mice." Biomaterials, Oct. 2013.

**Cam, C.**, and Segura T. "Chemical Sintering Generates Uniform Porous Hyaluronic Acid Hydrogels." Acta Biomaterialia, Oct. 2013.

**Cam, C.**, and Segura T. "Matrix-based gene delivery for tissue repair." Current Opinion in Biotechnology, May 2013.

Tokatlian, T., **Cam, C.**, Siegman, S., Lei, Y., and Segura, T. "Design and Characterization of Microporous

Hyaluronic Acid Hydrogels for in vitro Gene Transfer to mMSCs." Acta Biomaterialia, November 2012.

DeQuach, J. A., Lin J., **Cam, C.**, Hu, D., Salvatore, M. A., Sheikh, F., and Christman, K. L. "Injectable skeletal muscle matrix hydrogel promotes neovascularization and muscle cell infiltration in a hindlimb ischemia model." European Cells and Materials, June 2012.

**HONORS & AWARDS:**

April 2013: Materials Research Society (MRS) Conference Travel Award
April 2011: National Science Foundation Graduate Research Fellowship Program (NSF GRFP) Honorable Mention
June 2009 – Aug 2009: National Science Foundation Research Experience for Undergraduates (NSF-REU) in Regenerative Medicine, Multi-Scale Bioengineering, and Systems Biology program participant, UCSD, La Jolla, CA

**POSTERS & PRESENTATIONS:**

April 2013: Materials Research Society (MRS) Spring Meeting Oral Presentation, San Francisco, CA
Title: "Design of DNA-Loaded Macroporous Hydrogels to Promote Vascularization"
Authors: Cynthia Cam and Dr. Tatiana Segura

Oct 2012: Society for Biomaterials (SFB) Symposium Oral Presentation, New Orleans, LA
Title: "Design of DNA Loaded Macroporous HA Hydrogels to Promote Vascularization"
Authors: Cynthia Cam, Talar Tokatlian, and Dr. Tatiana Segura

March 2012: UCLA Tech Forum Poster Presentation, Los Angeles, CA
Title: "Application of Macroporous Hydrogels in vitro and in vivo for Tissue Engineering and Enhanced Angiogenesis"
Authors: Cynthia Cam, Talar Tokatlian, and Dr. Tatiana Segura

June 2010: UC Systemwide Bioengineering Symposium, Davis, CA
Title: "An Injectable Decellularized Muscle Matrix for Skeletal Muscle Tissue Engineering"
Authors: Jessica A. DeQuach, Cynthia Cam, Michael A. Salvatore, Diane Hu, and Dr. Karen L. Christman

May 2010: UCSD Bioengineering Day Poster Presentation, La Jolla, CA
Title: "A Catheter Design for Intestinal Lavage: Externally-Driven Shearing Mechanism and Fluid Jet System"
Authors: Cynthia Cam, Derrick Li, Anna Luan, and Dr. Geert Schmid-Schonbein

Oct 2009: Biomedical Engineering Society (BMES) National Conference Poster, Pittsburgh, PA
Title: "Tissue Specific Migration of Rat Aortic Smooth Muscle Cells"
Authors: Cynthia Cam, Jessica A. DeQuach, Dr. Karen L. Christman

Aug 2009: UCSD Summer Research Conference Oral Presentation, La Jolla, CA
Title: "Quantifying the Haptotaxis of Vascular Cells on Tissue Specific Naturally Derived Matrices"
Authors: Cynthia Cam, Jessica A. DeQuach, Dr. Karen L. Christman

**TEACHING & MENTORING EXPERIENCE:**

Sept 2013 – Nov 2014: Graduate Student Mentor, Segura Laborartory, UCLA
June 2011 – June 2013: Graduate Student Mentor, Segura Laborartory, UCLA
June 2013 – Aug 2013: Graduate Student Mentor, HSSEAS summer program, UCLA
Sept 2011 – Aug 2012: Graduate Student Mentor, HSSEAS program/Segura lab, UCLA
June 2011 – Aug 2011: Graduate Student Mentor, HSSEAS summer program, UCLA
Fall 2011: CBE 104DL "Molecular Biotechnology Lab"
Spring 2011: CBE 104DL "Molecular Biotechnology Lab"
Fall 2012: CBE 104DL "Molecular Biotechnology Lab"
Winter 2013: CBE 104DL "Molecular Biotechnology Lab"

# CHAPTER 1

# OVERVIEW OF DISSERTATION AND SPECIFIC AIMS

## 1.1 Motivation and Objectives

Skin is the body's largest organ, where the average adult human's skin has a surface area of approximately 20 square feet [1]. It protects our internal organs from microbes and extreme elements, and functions to regulate body temperature in addition to facilitating sensations such as heat/cold, pain, and touch. Thus, although the skin is a versatile organ, its external nature makes it susceptible to numerous injuries over a lifetime. The repair process is a well orchestrated process that is critically dependent on many factors that allows it to complete the four sequential, overlapping stages of wound healing: hemostasis, inflammation, proliferation, and remodeling [2]. However, this crucial tissue repair process can be affected by many systemic variables (e.g. nutrition, age, sex, psychological stress, immobility, etc.), diseases/conditions (e.g. diabetes, autoimmune diseases, predisposition to various scar types, genetic skin diseases, obesity, etc.), and other factors such as wound-specific issues or medication that can hinder healing at any one stage [3]. Furthermore, whether or not we possess an underlying heath condition that hampers our ability to heal normally, delayed wound healing occurs naturally as we age, where changes are seen in every healing phase (e.g. increased platelet aggregation and secretion of inflammatory mediators, delayed or impaired macrophage function, delayed angiogenesis, etc.) [4, 5]. Thus, it is paramount that wound

healing strategies are available to assist the body in cutaneous tissue repair to salvage or recover the important functions of our largest organ.

Currently, there exists a large variety of treatments to assist the cutaneous wound healing process when the body cannot naturally repair its tissue. Treatments include simply maintaining a clean moist wound environment with occlusive dressings, mechanical support, or electrical stimulation [6-8]. Skin grafts have also been used; its origins date back to 800 BC and their success depends heavily on its tissue source, where autografts (recipient and donor are the same) are surgically invasive but result in better tissue integration compared to allografts (donor is different but same species as recipient) or xenografts (donor is different species from recipient), where immunologic rejection is a major concern [3]. However, in this dissertation, we will focus our attention on localized therapies that contain matrices and/or bioactive signals to promote tissue repair. Composite bioengineered skin substitutes (Apligraf®, Orcel®) have been developed for full thickness wounds that contain bilayer matrices composed of allogeneic skin cells (epidermal keratinocytes and dermal fibroblasts) cultured on a type I bovine collagen sponge [9]. Although these skin substitutes have improved treatment for chronic wounds, disadvantages include high cost, short shelf life (5 days for Apligraf®, 9 months for Orcel®), concern of patient allergy to animal products, and minimal vascularization [3, 10]. Growth factors also have the potential to heal repaired tissue by guiding the repair through bioactive cues however, to date, Regranex® (becaplermin) is the only FDA approved topical gel containing recombinant platelet-derived growth factor BB (PDGF-BB) to heal diabetic foot ulcers. Despite this, Regranex use has been limited since it has been reported to achieve healing rates closer to controls (33% vs. 26%) in clinical practice and in 2008, the FDA placed a cancer warning on becaplermin for increased cancer risk and cancer-related death for patients who have used three or more tubes [3, 11].

Taken together, there still exists a need to improve current technologies to aid in tissue repair. Classic tissue engineering approaches include some of the strategies described above where any combination of the following factors is utilized to repair or restore tissue function: (i) a scaffold, (ii) bioactive signals (e.g. proteins, drugs, DNA, etc.), and (iii) stem cells. As seen in the composite skin substitutes, a scaffold is used in an attempt to recapitulate the layered structure of skin and deliver extracellular matrix components. However, the incorporation of allogeneic cells renders composite skin substitutes more of a temporary bioactive dressing since the allogeneic fibroblasts and keratinocytes are rejected by the host and do not survive past a few weeks post-treatment [12]. Moreover, use of stem cells in the clinical practice has been limited due to concerns of immunogenicity, viable cell source, and ethical matters. Therefore, we believe an alternative approach to aid in cutaneous wound healing is to develop a well designed acellular scaffold loaded with bioactive cues to encourage endogenous healing activities within the target site. However, the overarching challenge of scaffold implantation is achieving vascularization of the construct, limiting the size and therapeutic benefit of the scaffold [13]. Most tissues, with the exception of cartilage, are highly vascularized, thus implantation of a scaffold for tissue repair requires blood vessel ingrowth to supply newly formed tissue and cells with routes for oxygen and nutrient transport for tissue survival. Moreover, formation of functional vasculature requires the vessels to become mature and stable, otherwise vessels regress if they are unable to become perfused [14], motivating the use of bioactive signals to encourage this process (e.g. growth factors, DNA, etc.)

Thus, the overall focus of my research has been to develop bioactive scaffolds to promote angiogenesis, cell infiltration, and rapid vascular ingrowth into the implanted scaffold for cutaneous tissue repair.

## 1.2 Specific Aims

The objective of this research was to develop a porous hyaluronic acid hydrogel for localized, controlled delivery of non-viral genes to promote angiogenesis in the skin. Hydrogels are a specific type of scaffold that are generated by covalent or physical crosslinks between polymers and highly absorbent (composed of > 90% water). Their tunable mechanical properties can be modified to resemble soft tissue, and their high permeability allows for the diffusion of molecules. Although several approaches have been reported (discussed in Chapters 2 – 3) to promote angiogenesis within implanted scaffolds, there are limited reports on the strategic design of hydrogels, in particular, with or without the aid of bioactive signals to promote angiogenesis in a clinically relevant timeframe or with practical considerations (in terms of cost, resources, etc.). The research conducted and described in this dissertation attempts to engineer a hydrogel to meet these criteria and gain knowledge to advance the field of regenerative medicine for tissue repair. The following section describes the proposed specific aims, which guided the experimental research described in Chapters 4 – 7. Following each aim, the specific hypothesis will be stated.

### 1.2.1 Specific Aim 1 (Chapter 4)

This aim developed an improved technique with significantly reduced processing time to generate porous HA hydrogels for enhanced cellular infiltration *in vitro* and *in vivo*. Following rigorous *in vitro* characterization, a murine subcutaneous implant model was utilized to assess its performance *in vivo*.

*Hypothesis 1*: Resuspension of porogens in volatile solution will allow for easier liquid handling and reproducible sphere-templating to generate microporous HA hydrogels with greatly reduced manufacturing time.

### 1.2.2 Specific Aim 2 (Chapter 5)

This aim investigated the implantation of various conductive and inductive scaffolds to determine the effect of scaffold type on tissue repair in a murine splinted wound healing model over 7 days. The scaffold types used in this study was: fibrin, porous HA hydrogel, a composite of fibrin and porous HA, and an inductive composite gel with plasmin-degradable vascular endothelial growth factor (VEGF) nanocapsules embedded within the composite gel.

*Hypothesis 2*: The porous architecture of the HA hydrogel will better preserve the structure of skin for cellular infiltration when compared to fibrin.

*Hypothesis 3*: Incorporation of an inductive factor, plasmin-degradable nanocapsules delivering VEGF will enhance vascularization of the newly formed tissue.

### 1.2.3 Specific Aim 3 (Chapter 6)

This aim tested an approach to treat DNA-loaded porous HA hydrogels with hyaluronidase to enhance DNA release for improved transfection. Two different techniques (traditional vs. previously described technique by our lab [CnE]) to load DNA/poly(ethylene imine) polyplexes into the porous HA gels were discussed in this aim. Gene transfer and angiogenesis was evaluated *in vitro* and *in vivo* in a splinted murine wound healing model at days 5 and 10.

*Hypothesis 4*: Porous HA hydrogel mechanics and DNA release will be a function of hyaluronidase concentration.

*Hypothesis 5*: The large concentration of DNA loaded via caged nanoparticle encapsulation (CnE) will result in higher transgene expression as the polyplexes are released from the hydrogel.

*Hypothesis 6*: The incorporation of plasmids encoding for VEGF, a proangiogenic factor, into porous HA gels treated with hyaluronidase will enhance wound closure, angiogenesis, and cellular infiltration when compared to untreated porous HA gels.

### 1.2.4 Specific Aim 4 (Chapter 7)

This aim utilized the hyaluronidase pre-treatment of DNA-loaded porous hydrogels described in Aim 3 (Chapter 6) towards a strategy for sequential gene delivery. Two different hydrogel designs were investigated *in vitro* before moving forward *in vivo* with one system. Full thickness dermal wounds in mice were implanted with the engineered hydrogels and transfection was monitored via optical imaging for 21 days. A splinted murine wound healing model was used to assess transfection, angiogenesis, and wound healing as a function of spatio-temporal presentations of polyplexes encoding for pro-angiogenic factors (VEGF and PDGF).

*Hypothesis 7*: Porous hydrogels with encapsulated and surface coated polyplexes (different plasmids for each presentation) will result in transfection from surface coated polyplexes first since they are more immediately available and accessible to infiltrating cells than encapsulated polyplexes.

*Hypothesis 8*: Cells will degrade non-porous gels slower thus a two phase hydrogel system containing a central non-porous post surrounded by a porous HA gel with different plasmids within each distinct phase will result in different transgene expression profiles.

*Hypothesis 9*: The spatio-temporal presentation of pro-angiogenic plasmids within the hydrogel will affect the number and type of vascular cells present within the newly formed tissue.

### 1.3 Dissertation Outline

Following this introduction, Chapters 2 – 3 will provide relevant background to the dissertation topic. In Chapter 2, the important role of vascularization will be discussed, as well as its implications in scaffold design and recent approaches to achieve construct vascularization. In addition, key scaffold design parameters will be described to explain our scaffold material and architecture choice. Next, in Chapter 3, matrix-based gene delivery will be rigorously discussed with a major focus on non-viral gene delivery. Design parameters to achieve transfection will be described and justification will be provided for the use of non-viral DNA polyplexes in comparison to use of growth factors, other transfection agents, and viral vectors. Following these introductory background chapters, the remainder of the dissertation will detail the research conducted to design a hydrogel system to promote angiogenesis and cutaneous tissue repair via rational considerations of scaffold material, structure, and controlled, localized delivery of non-viral DNA. **Figure 1.1** outlines the flow of the dissertation.

Chapter 4 will begin with an introduction to porous HA hydrogels. The technique employed at the time to generate a sphere-template for porous hydrogel formation was very time consuming and laborious. Thus, other proposed techniques to generate comparable sphere-templated molds employed liquid handling to reduce processing time and operator

error/inconsistencies. Chemical sintering was developed as a technique that reduced processing time from 17-22 h to 1-2 h and was applied to porous hydrogel formation in future studies. Chapter 5 discusses a systematic approach in determining the effect of conductive and inductive scaffolds on cutaneous wound healing. Interestingly, the presence of a porous architecture in a hyaluronic acid hydrogel had a more significant impact on wound closure and vessel maturation than fibrin, a highly regarded popular natural scaffold. With the support of porous architecture validated in Chapter 5, transfection from non-viral DNA-loaded porous HA gels were studied in Chapter 6. More specifically, two approaches in DNA loading was employed *in vitro* and the effect of hyaluronidase treatment on DNA release and transfection via each technique was studied. Chapter 6 validated a technique to load large amounts of DNA into porous HA gels previously developed by the Segura lab, and showed that hyaluronidase treatment facilitates significant transfection and vascularization *in vivo* with a murine splinted wound healing model. With knowledge gained from Chapter 6, the main goal of Chapter 7 was to develop a hydrogel system to achieve sequential non-viral gene delivery to not only promote cell infiltration and angiogenesis, but encourage the maturation of blood vessels for more functional healing in full thickness dermal wounds. Chapter 7 will describe two proposed sequential non-viral gene delivery hydrogel systems in detail and elaborate on a hybrid system that was applied *in vivo* to study transgene expression via bioluminescence. Moreover the developed gene delivery system was applied in a splinted wound healing model to study the effect of spatio-temporal presentation of plasmids encoding for two different pro-angiogenic factors. Finally, Chapter 8 will provide conclusions and possible future directions to advance this project and field of study for improved cutaneous wound healing with controlled, localized non-viral gene delivery.

## Aim 1 (Chapter 4)

Optimize hydrogel production time

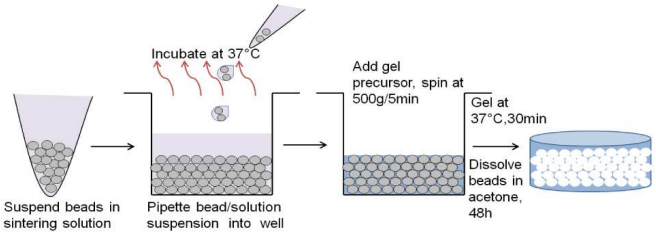


## Aim 2 (Chapter 5)

Determine the effect of conductive vs. inductive scaffolds on cutaneous wound healing

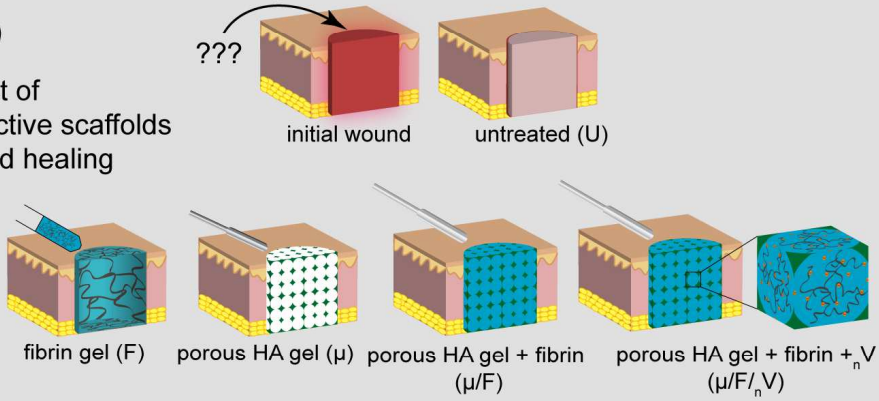


## Aim 3 (Chapter 6)

Validate high DNA loading via caged nanoparticle encapsulation (CnE)

Facilitate DNA polyplex release for enhanced transfection *in vitro* and *in vivo*

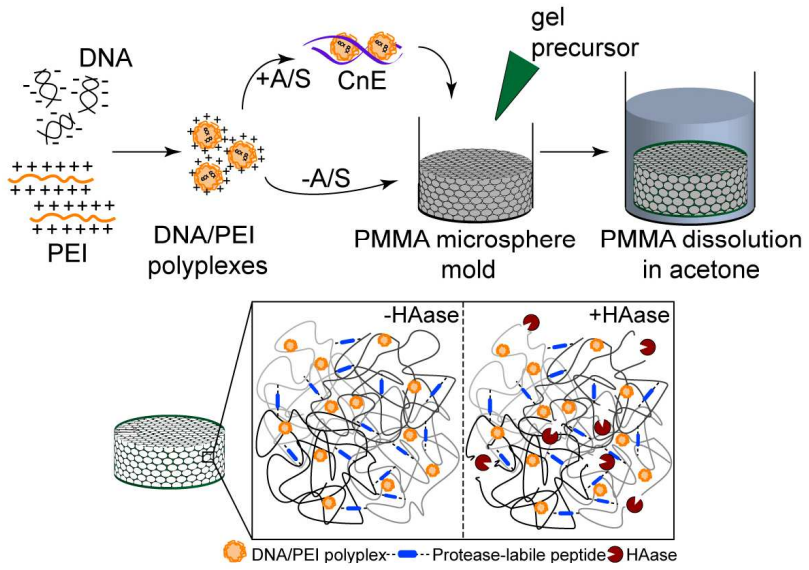


## Aim 4 (Chapter 7)

Develop hydrogel system(s) for sequential gene delivery

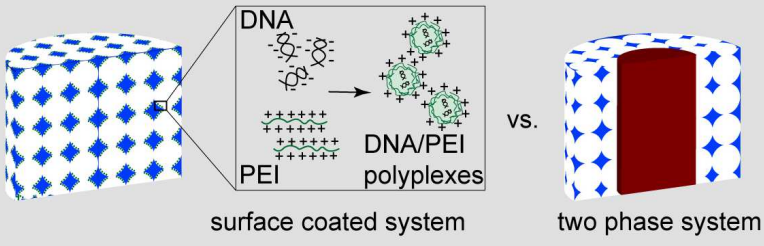


**Figure 1.1 General dissertation overview.**

# CHAPTER 2

# SCAFFOLDS FOR IMPROVED TISSUE REPAIR

## 2.1 Vascularization: critical role in wound healing

Blood vessels are an essential component in the circulatory system, supplying and transporting blood throughout the body. The human microvasculature is comprised of a hierarchy of vessel types that branch into smaller sizes, ranging from arteries (1 – 2 mm) and meta-arterioles (80 – 100 μm) to capillaries (10 – 15 μm) [15]. In adults, with the exception to skeletal muscle healing and the female menstrual cycle, microvascular remodeling occurs only due to pathological situations (e.g. inflammation, wound healing, ischemia, hypoxia, etc) since it is a mechanistic process that responds to specific environmental stimuli [15, 16]. Thus, in the common case of adult wound healing, angiogenesis (the growth of blood vessels from pre-existing vessels) is an essential stage of tissue repair in response to injury. The formation of new blood vessels is critical to sustain newly formed tissue during the wound healing cascade since vessels provide routes for oxygen and nutrient diffusion, as well as waste product removal [17, 18].

To this end, many systemic factors (e.g. diabetes mellitus, vessel disease, or genetic predisposition) alone or in combination with local factors (e.g. prolonged inflammation, presence of bacterial toxins and reactive oxygen species, or imbalance of proteases and biomolecules) may disrupt any critical stage in tissue repair leading to impaired wound healing [19, 20]. Moreover, even in the absence of an underlying disease, it has been shown that aging results in

delayed wound repair response due to alterations in the inflammatory cell content and functional response [4]. These factors may contribute to prolonged inflammation leading to inadequate vascularization and tissue formation [19]. Thus, there exists a need for an external therapy to assist the wound healing process when the body's biological healing capacity is hindered, however the primary cause of implant failure *in vivo* has been due to the lack of construct vascularization [13, 21]. Without rapid scaffold vascularization, implanted cells or endogenous cells surrounding the construct cannot infiltrate and survive deep within the scaffold for subsequent tissue formation since the oxygen diffusion limit is approximately 200 μm, a distance that correlates with maximum distance between capillaries to sustain tissues *in vivo* [21]. Consequently, the importance of promoting angiogenesis is twofold: successful implantation of a construct aiding in tissue repair requires vascularization to sustain new tissue growth and viability of the scaffold, as well as integration with the host tissue for overall remodeling.

Prevascularization of scaffolds has been one approach to promote rapid anastomosis, the connection between two vessels, with host tissue following implantation. *In vitro* prevascularization was investigated by Tremblay et al., where an endothelialized reconstructed skin was created by seeding a combination of human umbilical vein endothelial cells, fibroblasts, and keratinocytes on a collagen/glycosaminoglycan/chitosan scaffold. Capillary-like structures were spontaneously realized *in vitro* and upon implantation in nude mice, the structures contained mouse blood in less than four days, suggesting successful anastomosis [22]. Although this study demonstrated the potential of *in vitro* prevascularization of tissue constructs, drawbacks of this approach include the long *in vitro* culture time (31 days) limiting this approach to smaller implants, and the need for simultaneous extraction of keratinocytes, fibroblasts, and endothelial cells from a patient biopsy which may be considered invasive. On the other hand, *in vivo* prevascularization of constructs has also been studied as an approach

by various groups [23, 24], where the host cells create a perfusable vascular network within the initial acellular construct to be re-implanted in the ischemic wound site. Although these studies have shown to improve vascularization of scaffolds, its main drawback is the need for three invasive surgeries: namely the implantation of the acellular construct, explantation of the vascularized construct, and re-implantation into the target site. Although advances in prevascularized constructs have improved efforts to better aid in tissue repair, the clinical application remains unclear due to culture times limiting construct size and cell sources for *in vitro* prevascularization, and the invasive nature of *in vivo* prevascularized constructs. For these reasons, we have focused our efforts on promoting angiogenesis in acellular scaffolds.

The promotion of vascular ingrowth into acellular scaffolds for a variety of therapies has been investigated since the 1970s. Since then, many critical design parameters have been realized that include scaffold material, architecture, and incorporation of bioactive cues (growth factors, genes, etc). Herein, the importance and influence of scaffold material and architecture on angiogenesis will be discussed. Localized delivery of bioactive cues will be expanded on in Chapter 3.

**2.2 Scaffold architecture: porosity and angiogenesis**

Efforts to promote construct vascularization have focused on rationally designing scaffold architecture. One of the approaches utilized herein by us and other researchers is the incorporation of pores into the construct. A porous scaffold allows for better cellular infiltration, migration, and proliferation, improving mass transport of oxygen and nutrients while the scaffold provides structural integrity for tissue formation and vascular ingrowth [13]. Porous scaffolds have been formed via various techniques that include gas foaming [25], salt leaching [26], heat sintering [27], and lyophilization [28]. Even in the absence of plasmid DNA, it has been

demonstrated that hydrogels with pore sizes ranging from 30-150 μm promote angiogenesis and tissue formation *in vivo* with poly(N-isopropyl acrylamide) (poly-NIPAM) [27], poly(2-hydroxyethyl methacrylate-co-methacrylic acid) (pHEMA-co-MAA) [29], and PEG hydrogels [30]. We have previously shown that hyaluronic acid hydrogels containing ~60 or 100 μm pores allow for enhanced cellular infiltration when compared to nonporous gels of the same composition implanted subcutaneously in the backs of balb/c mice [31, 32]. By 21 days post-implantation, cells were observed to participate in bulk degradation of the nonporous gels where infiltration was limited to the periphery of the gel, therefore minimal blood vessels were observed when compared to the porous gels [31, 32]. Moreover, we showed that nonporous gels failed to degrade 14 days post-implantation and served as a mechanical barrier to wound closure when compared to porous hyaluronic acid hydrogels in a humanized diabetic wound healing model in db/db mice [33].

In all of these reports, porous architecture had significant influence on cellular migration and infiltration, and angiogenesis in regards to rate, size, and maturity of vessels. For these reasons, we have judiciously chosen to incorporate pores into our scaffolds to aid in tissue repair.

## 2.3 Scaffolds: type and material choice

### 2.3.1 Hydrogels

Although criteria for three dimensional scaffolds vary depending on application, ours include biocompatibility, degradability, porosity, and tunable mechanical properties. For these reasons, hydrogels are an attractive alternative to other scaffolds. Hydrogels are water-soluble, crosslinked polymeric networks that swell in the presence of water without dissolving [34]. Their characteristics are determined by the extent of crosslinking and molecular structure [34]. Hydrogels are ideal scaffolds for tissue engineering since their tunable mechanical properties

can closely mimic those of soft tissue, and they can be used to load and protect bioactive cues (e.g. proteins, DNA, siRNA) of varying efficiency. Naturally derived polymers such as fibrin, collagen, gelatin, alginate, and hyaluronic acid possess advantages such as biocompatibility, biodegradability, and intrinsic native cues that promote cell interactions while synthetic polymers such as poly(ethylene glycol), poly(acrylic acid), poly(vinyl alcohol), polypeptides and poly(ethylene oxide) offer a high level of reproducibility and tunability with endless variations of chemical modifications [13, 21, 35, 36]. Despite synthetic polymers' ability to be biochemically inert and ability to serve as a "blank slate," natural polymers possess natural sites for cell interaction and signaling that is sometimes difficult to recapitulate in the lab. Therefore, this dissertation will focus on the development a porous hydrogel for tissue repair based on natural polymers. For the studies described henceforth, hyaluronic acid is almost exclusively used.

### 2.3.2 Hyaluronic acid (HA)

Hyaluronic acid is an anionic, nonsulfated glycosaminoglycan and major component in the extracellular matrix (ECM), where its presence is highest in connective tissues such as the skin [37, 38]. Its high biocompatibility and low immunogenicity make it an ideal biopolymer to use *in vivo*. Moreover, HA's hygroscopic nature is believed to be important in maintaining tissue hydration, osmosis, and overall homeostasis [39, 40]. In its native state (>$10^6$ kDa), HA inhibits endothelial cell migration and proliferation, but following injury, a significant portion of HA depolymerizes to smaller fragments of HA (3 – 10 disaccharides) which bind to CD44 and RHAMM (receptor for HA-mediated motility), stimulating endothelial cell proliferation, migration, and tube formation demonstrating its importance in angiogenesis [41, 42]. The impact of HA oligosaccharides (o-HA) has also been studied *in vivo*; o-HA fragments have been shown to stimulate angiogenesis and neovascularization. Gao et al. reported that daily topical applications o-HA (2 – 10 disaccharides), as opposed to high molecular weight HA, promoted

murine dermal wound healing and neovascularization similar to VEGF-treated wounds [43]. Utilizing mild chemistries, the HA backbone can be modified to contain functional groups, such as thiols, acrylates or amines, which can be utilized as sites for crosslinking for hydrogel formation [44-48]. In addition, acrylated HA hydrogels crosslinked with matrix metalloproteinase (MMP)-sensitive peptides have been developed for culturing mouse and human mesenchymal stem cells in three dimensions [49, 50]. This design allows for cell-mediated degradation, since MMPs are upregulated in response to injury, tissue remodeling, and in diseased states [51], making it an attractive approach for controlled, localized bioactive signal delivery systems aiding in tissue repair. For the studies described henceforth, HA hydrogels with MMP sensitive crosslinkers are almost exclusively used.

# CHAPTER 3

# SCAFFOLD-MEDIATED NON-VIRAL GENE DELIVERY

## 3.1 Introduction

In the design of scaffolds for tissue repair, biochemical, biophysical, and cell-cell signals must be intricately orchestrated to guide the formation of healthy tissue at sites of injury or disease. Ideally, the manner in which these signals are incorporated allows for necessary changes during tissue growth. For example, the biochemical signals that contribute to the start of morphogenesis (tissue growth) are very often detrimental if they are present at the final stages of growth which, in many cases, cause pathological conditions. Thus, the biochemical signals (e.g. peptides, proteins, small molecules) must be introduced such that their activity can be regulated. Proteins are the most common bioactive signal introduced into scaffolds for tissue repair. Although delivery mechanisms have been designed to control release rates of one or multiple proteins, protein stability and cost are still major limitations. For example, the biological half-life of platelet-derived growth factor (PDGF), basic fibroblast growth factor (bFGF) and vascular endothelial growth factor (VEGF) are less than 2 [52], 3 [53] , and 30 minutes [54], respectively, when injected intravenously. Thus, to achieve therapeutic success, proteins often require large doses and multiple injections [55-57]. Gene delivery has been used as an alternative to protein and protein fragment delivery [58], and it holds the advantage that a universal delivery strategy can be designed for any DNA sequence. A universal delivery strategy is not possible for growth factor delivery since the tertiary and quaternary structures are

different for each protein and immobilization or other processing conditions affect each protein differently. Furthermore, the secretion of a protein by a transfected cell may be present for a longer duration. This increased residence time eliminates the need for repeated injections [59] and stimulates autocrine and paracrine signaling in tissue formation, which cannot be induced by delivery of the protein to the bulk media [60]. One major limitation of gene delivery is that the cargo is not immediately available as a bioactive signal, whereas proteins can begin their biochemical activation of targeted cells and commence tissue repair immediately after implantation. To this end, successful gene delivery and transfection depends on a series of critical steps, which take several hours to days to commence *in vivo*, with transgene expression peaking in the order of days after injection for naked plasmid, minicircles [61, 62], and polyplexes [63]. **Figure 3.1** details the steps that must occur for gene transfer to take place from the point of view of scaffolds for tissue repair. **Figure 3.2** summarizes the major design characteristics for matrix based gene delivery for tissue repair.

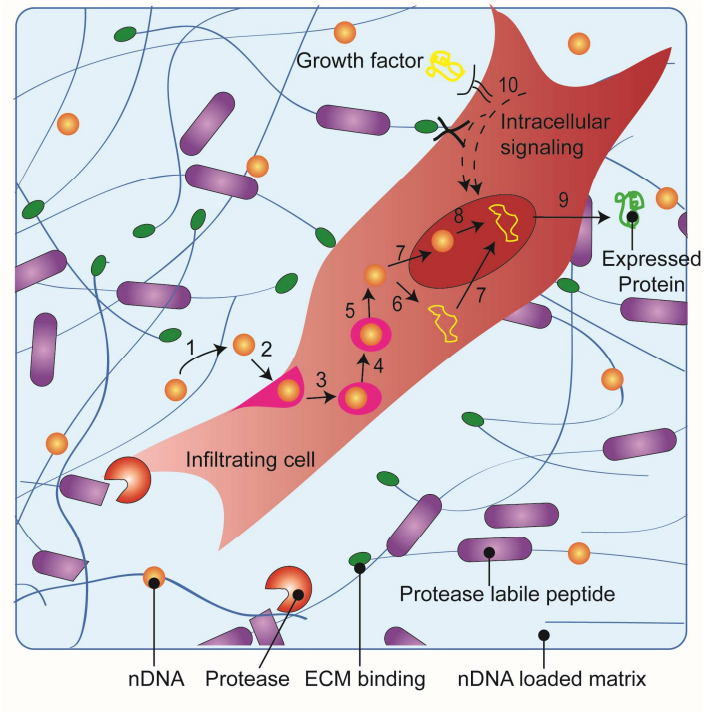


**Figure 3.1 Schematic overview of protein expression.** For gene delivery, nDNA (**1**) is released from the scaffold through either hydrolysis or cellular migration (**2**) and internalized into the endosome (**3**). The endosome matures changing its oxidative and acidity resulting in endosomal escape of nDNA (**4-5**). nDNA can enter the nucleus (**7**) to be unpacked (**8**) or be de-coupled in the cytosol (**6**) for nuclear entry (**7**), where transcription and translation occurs (**9**) for protein expression. Growth factors or other bioactive signals can be used to induce intracellular signaling pathways that prime cells for transfection (**10**).

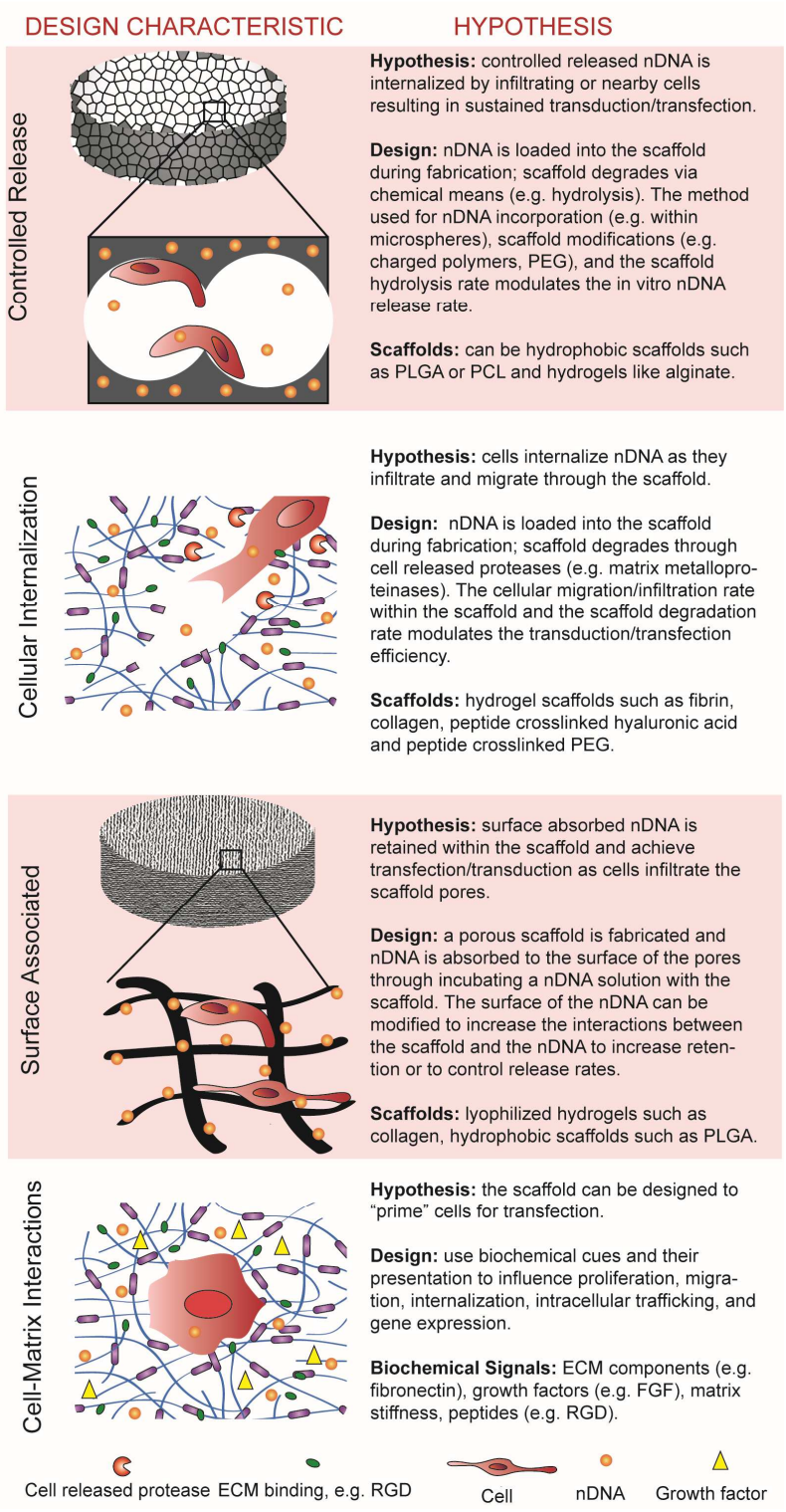


**Figure 3.2** The design of scaffolds for tissue repair that use genes as a bioactive signal goes beyond incorporating the nDNA into the scaffold.

### 3.2 Vector Design

The two main types of vectors used for gene transfer in the context of tissue repair are plasmid DNA or modified viruses. The major design characteristics for vector design are the

attenuation of the immune response, the promoters used to drive expression (**Figure 3.3A**), and the therapeutic protein expressed.

Viral vectors have been widely used for gene delivery due to its high efficiency but have been under scrutiny due to the toxicity, immunogenicity, oncogenicity by insertional mutagenesis, and uncertain long-term effects in vivo, limiting their clinical effectiveness [64-66]. Conversely, naked plasmid or non-viral vectors elicit a milder immune response while having lower *in vivo* transfection efficiency [67]. The lower transfection efficiency may be improved by complexing the nucleic acids (negatively charged) with cationic polymers or lipids to protect against degradation and condense larger amounts of DNA to promote internalization [64, 66]. Due to the potential adverse effects of viral vectors, we chose to focus our studies using nonviral plasmid DNA (pDNA).

As mentioned before, a major concern with gene delivery is immunogenicity. There are various methods to modulate the immune response by modifying the vector. The immune response to plasmids is influenced by the methylation of CpG sequences on the plasmid backbone that ultimately affects the duration of transgene expression [59, 68]. Although bacterial DNA or pDNA is often used in gene delivery vehicles, it is significantly different from mammalian DNA. The frequency of CpG dinucleotides in mammalian DNA is comparatively suppressed and most of the CpG sequences are methylated [69, 70]. The absence of CpG methylation in bacterial DNA induces immunostimulatory cytokines IL-6, IL-12, TNF-α and IFN-γ, that are both cell-mediated and humoral immune responses [71, 72]. These immune responses have been shown to be acutely toxic, thereby eliminating expressing cells and result in decreased duration of transgene expression [73]. The immune response may be decreased by either eliminating the immunostimulatory CpG sequences or inhibiting certain CpG signaling pathways [70].

An alternative method to modulate the host immune response and transgene expression is to incorporate minicircle DNA vectors. Minicircles are supercoiled DNA molecules that are smaller in size, and lack a bacterial origin of replication and an antibiotic resistance gene, ideal for nonviral gene delivery [61]. Since minicircles only carry short bacterial sequences, the decreased number of CpG sequences offer better evasion from the immune system [61, 74]. Incorporation of minicircle DNA vectors has been shown to significantly increase transgene expression *in vitro* and *in vivo* when compared to regular plasmid [61, 74, 75]. Although it is desirable to minimize the immune response to achieve better transgene expression, it is important to note that there exist other applications where an immunostimulatory effect is beneficial, as in the case of vaccinations and cancer immunotherapy.

Selective promoter incorporation into vectors has also been shown to affect transgene expression *in vitro* and *in vivo*. Viral promoters in plasmid vectors, such as the commonly used cytomegalovirus (CMV) promoter, are able to achieve high levels of gene expression but are often short-lived due to detection and silencing of viral transgene expression from eukaryotic cells, in addition to induced hepatotoxicity and immune responses [76, 77]. It has been shown that plasmids containing a mammalian ubiquitin C (UbC) promoter can achieve similar maximal gene expression as the CMV promoter *in vivo*, but its expression is sustained for 21 days while the CMV promoter results in an initial robust response followed by decrease in expression over time most likely due to silencing [78]. To improve specificity and safety, plasmid design has shifted to tissue-specific endogenous promoters. Despite its lower expression intensity, tissue-specific promoters have been able to achieve longer transgene expression and evade transcriptional silencing *in vivo* [76, 79]. In this dissertation, we moved from traditional CMV promoters to employing an EF1α promoter from human origin *in vivo* in Chapters 6 and 7. **Table 1** details these major design characteristics for vector design.

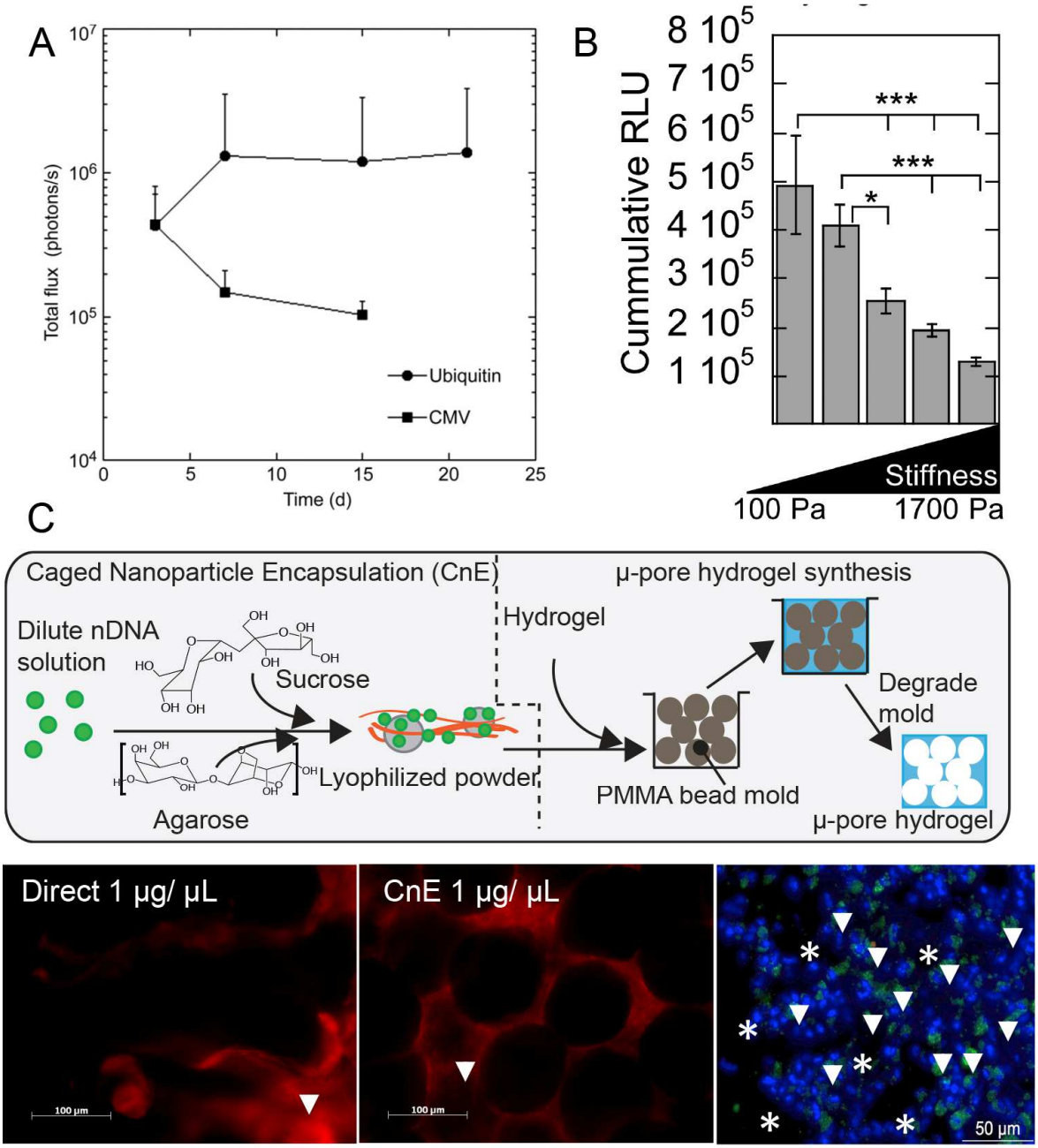


**Figure 3.3** Novel approaches to investigate the effect of design parameters on transgene expression. Different plasmid promoters (UbC vs. CMV) showed to have an effect on *in vivo* transgene expression (**A**), while stiffness had an inverse correlation with in vitro transgene expression in hyaluronic acid hydrogels (**B**). To decrease nDNA aggregation at higher nDNA concentrations, a caged nanoparticle encapsulation (CnE) technique was developed and applied to porous hydrogels for *in vivo* transfection (arrows show transfected cells, **C**).

### 3.3 Delivery of the Vector

Although naked DNA has shown success in the delivery of genes *in vivo* for tissue repair, the field has moved towards the use of packaged DNA (nDNA), either in synthetic particles or viruses. Successful gene delivery and transfection depends on a series of critical steps. Initially, the DNA must bind to the cell surface to be endocytosed and released for nuclear transport [80, 81]. Once transported to the nucleus, the vector is unpacked for translation [80, 81]. Although the direct injection of naked plasmid DNA is the simplest mode of vector delivery, it has achieved limited success [80, 82]. The large and negatively charged plasmid DNA does not allow for sufficient interaction with the negatively charged cell membrane, therefore reducing the potential for internalization and ultimately, gene transfer [67]. Complexation of the plasmid DNA with cationized materials (e.g., lipids, polymers, peptides) offers advantages such as a decrease in overall molecular size, protection of the DNA from degradation due to nucleases and serum components, and improving cellular uptake and transfection via the interaction between the positively charged complex and the cell membrane [67, 68, 81].

Lipoplexes are produced by complexing cationic lipids (e.g. DOTAP, DOTMA, DC-Chol, DOGS, DOSPA, DOPC) with plasmid DNA [81, 83]. Lipoplexes have been incorporated into three-dimensional scaffolds such as hydrogels as gene delivery vehicles. Investigation of transgene expression have been performed *in vitro* by seeding cells on top of the hydrogels (2D) or embedding cells inside the hydrogel (3D) with encapsulated lipoplexes. Stable transgene expression can be achieved for the initial days of culture in both conditions, however there are mixed accounts of superior transgene expression when 2D and 3D culture are compared [84-86]. Employment of 3D hydrogels with complexed therapeutic plasmid DNA demonstrated that lipoplexes did not have a significant effect on the amount of released protein from transfected cells, therefore successful studies of lipoplexes encapsulated in hydrogels

have been limited *in vivo* [87]. Lipoplex performance is greatly dependent on its formulation. The hydrophobic units of the lipid determine critical characteristics such as size, shape, and stability, which ultimately affect the transfection efficiency of the formed lipoplexes [80, 81]. Since these parameters are difficult to control, transfection efficiency is low and lipoplexes may become unstable over time [80, 88]. An attractive alternative to condense DNA is through the self-assembly of polyplexes; polyplexes lack interactions between polycations, allowing for more control over its properties.

Polyplexes are formed by complexing cationic polymers with plasmid DNA into nanoparticles [64]. Frequently used cationic polymers include poly(L-lysine) (PLL), chitosan, dendrimers, and poly(ethylene-imine) (PEI). PLL is a biocompatible and biodegradable linear polypeptide that has been shown to achieve low transfection efficiency when delivered alone or without any modifications when complexed with DNA [64, 89, 90]. This weak transfection efficiency may be due the lack of released PLL/DNA complexes from the endosomes necessary for gene transfer [91]. To improve transfection efficiency, PLL is commonly modified with histidine residues, oligomers and polymers such as chitosan and PEG, and lipids [81, 88]. Chitosan is a biodegradable linear polysaccharide that is highly biocompatible and commonly used to complex DNA due to its high positive charge density [88, 92]. Chitosan alone has low transfection efficiency but this may be attributed to its limited solubility and low buffering capacity at physiological pH, therefore resulting in unfavorable conditions for endosomal escape [93]. Chitosan molecular weight and chemical modifications can significantly affect complexation, stability, and intracellular release and ultimate gene transfer [83]. It has been shown that low molecular weight chitosan allows for better intracellular release and high gene transfer, while high molecular weight chitosan provides better DNA complexation with enhanced stability [94]. Dendrimers such as polyamidoamine (PAMAM) and polypropylenimine (PPI) have been used as gene delivery vehicles due to their high transfection efficiency, but possess in vivo

cytotoxicity concerns (determined by size, generation, dose, chemical structure, and surface charge) that may translate poorly to clinical applications [95]. A popular and widely studied polymer used to generate polyplexes for nucleic acid delivery is PEI. PEI has a high charge density that allows for DNA condensation and it acts as a proton sponge, which protects DNA from degradation and aids endosomal disruption for DNA to escape into the cytoplasm [64, 81]. PEI can be used in linear or branched forms for gene delivery; linear PEI is often preferred despite its lower transfection efficiency because it is less toxic than its branched counterparts (less primary amines) [93]. Transfection efficiency involves a complex interplay among various parameters that include molecular weight and the ratio of carrier protonated nitrogens to DNA phosphates (N/P). Although lower molecular weight PEI is less toxic, it also achieves less transfection [88]. While increasing the N/P ratio achieves a more condensed particle size [83] and higher gene transfer efficiency, it has cytotoxic effects which cannot be overlooked [96-98]. In this dissertation, polyplexes were exclusively employed with L-PEI as the cationic complexation agent to form stable nanoparticles with a balance between toxicity and transfection at N/P = 7.

### 3.4 Design of the Matrix

Although the primary focus to enhance transgene expression *in vivo* has been the design of the delivery vector, the matrix itself can provide alternative approaches to enhance transfection efficiency as well as promote tissue formation. Gene transfer from a matrix offers a three-dimensional distribution of complexes for more controlled, localized transfection as compared to a bolus delivery that may result in an unfavorable systemic delivery or unintended delivery to neighboring organs and tissues. In addition, delivery from a matrix can maintain the level of the vector over time, providing repeated opportunities for transfection/transduction and extending transgene expression as compared to bolus delivery. Incorporation of polyplexes into

hydrogels scaffolds have shown sustained expression compared to soluble polyplexes (35 days compared to 7 days) [63].

**Table 3.1** Vector and carrier design characteristics

| Consideration | Type | Details | References |
|---|---|---|---|
| **Immune Response** | CpG Motifs | • Mammalian DNA has less CpG motifs and most motifs are methylated whereas bacterial pDNA has more CpG motifs that are unmethylated<br>• Unmethylated CpG motifs induces pro-inflammatory cytokines (e.g. IL-6, IL-12, TNF-α, IFN-γ)<br>• Inverse correlation with number of CpG motifs and transfection | [70, 72, 79] |
| | Minicircle DNA | • Minicircles are supercoiled DNA molecules.<br>• Small in size, lack bacterial origin of replication and antibiotic resistance gene<br>• Decreased number of CpG sequences (better evasion of immune system<br>• Significantly increases transgene expression *in vitro* and *in vivo* | [61, 74, 75] |
| | Viral Capsid | • Directed evolution of adeno-associated virus (AAV) and impact on transduction | [99] |
| | | • Pro-inflammatory cytokine concentrations return to baseline by 4 weeks post-implantation of hydrogel with adenovirus | [100] |
| **Promoters** | Cytomegalovirus (CMV) | • Most widely used viral promoter.<br>• Robust expression, but short-lived due to silencing *in vivo* | [77] |
| | Ubiquitin C (UbC) | • Mammalian promoter results in sustained *in vivo* transgene expression | [78] |
| | Tissue-Specific | • Lower expression intensity, but longer transgene expression *in vivo* | [76] |
| **Bioactive Signal** | Growth Factors | • Spinal cord/nerves: BDNF, NGF, NT-3, FGF<br>• Bone: BMP-2<br>• Skin: FGF, KGF, SDF1α<br>• Cartilage: TGF-β1, TGF-β3<br>• Wound healing: PDGF, VEGF | [101] |
| | Transcription Factors | • HIF-1α lacking the oxygen-sensitive degradation domain (HIF-1αΔODD) upregulated expression of VEGF and resulted in mature vessels *in vivo* | [102] |
| | siRNA | • Induces gene silencing via mRNA degradation in cytosol<br>• Higher cargo loading required for silencing as compared to gene expression | [83] |
| **Carriers** | Polyplex | • Nucleic acids complexed with cationic polymers (e.g. linear polyethylene imine (LPEI))<br>• N/P ratio is crucial (High N/P results in higher transfection but is toxic, low N/P results in lower transfection but less toxic)<br>• Size range: 20-500nm | [83, 92, 96] |
| | Lipoplex | • Nucleic acids complexed with cationic lipids (e.g. 1,2-Dioleoyl-3-trimethylammonium-propane (DOTAP), 3β-[N-(N',N'-dimethylaminoethane)-carbamoyl]cholesterol (DC-Chol))<br>• Hydrophobic units of lipid determine: size, shape, and stability<br>• Size range:60-200nm | [81, 92] |
| | Viral | • Lentiviruses, adenoviruses, and adeno-associated viruses can infect non-dividing and dividing cells<br>• Lentiviral insert size is 7-8kb, has long duration of gene expression with risk of insertional mutagenesis<br>• Adenoviral insert size is ~30kb, has short duration of expression (does not integrate in host genome), and has risk of insertional response<br>• AAV insert size is 4.5kb, has long duration of expression with risk of insertional mutagenesis | [103, 104] |
| | Inorganic Particles | • Nano-hydroxyapatite (<200nm) particles are used to adsorb viral vectors/DNA | [105, 106] |

### 3.4.1 Controlled Release

Controlled release strategies are often described as an important design parameter for matrix mediated gene transfer, with the belief that sustained release of the transfection vector achieves prolonged transgene expression over burst-released vectors. The hypothesis is that maintaining the level of the vector in the local microenvironment constant (since vector is continuously released) provides repeated opportunities for transfection/transduction resulting in sustained transgene expression. Prolonged transgene expression of a single protein is desired in situation where the tissue takes time to mature. For example, the sustained release of VEGF is necessary to promote the formation of mature vasculature [13]. To achieve controlled release, the nucleic acid is encapsulated within the scaffold during scaffold fabrication, and the release rate is controlled through modulating the degradation rate of the scaffold. In this approach, typically the scaffold degradation rate is not dependent on cellular action but rather it is chemically mediated through processes such as hydrolysis. Additionally, the scaffolds may be highly porous to allow for cellular infiltration within the scaffold such that as the DNA is released, it can reach the infiltrating cells. Poly(lactide-co-glycolide) (PLGA) scaffolds were some of the first to be used for matrix mediated gene delivery [107] and can be designed to release plasmid DNA in hours, weeks or months *in vitro* and have resulted in sustained transgene expression for up to 105 days [25]. Although controlled release is often cited as a desired quality to ensure long lasting expression, recent data suggest that release rate *in vitro* does not lead to corresponding differences of transgene expression *in vivo*. The Shea lab designed PLGA scaffolds with vastly different DNA release rates *in vitro* and showed they all achieved the same level and duration of transgene expression *in vivo* [78]. This suggests that *in vitro* release kinetics for nDNA do not correlate well with *in vivo* release or that sustained release of DNA is not the reason sustained transgene expression is observed. Hydrogels have also been

designed to achieve controlled release. Oxidized alginate hydrogels loaded with DNA/PEI nDNA were shown to achieve sustained release *in vitro* and achieve enhanced revascularization *in vivo* [108].

### 3.4.2 Controlling Cellular Infiltration

An alternative approach to controlled release is to design scaffolds that allow cell mediated degradation and cellular infiltration within the bulk of the scaffold. These approaches involve the use of hydrogels either naturally crosslinked (e.g. collagen [106], fibrin [109, 110], gelatin [111]) or synthetically crosslinked with protease degradable peptides (e.g. PEG [112], hyaluronic acid [31, 113]). The hypothesis in this case is that cells uptake the DNA as they infiltrate the scaffold and thus the transgene expression can be sustained or increased with time. This hypothesis has been proven to be true *in vitro* with cells embedded in DNA loaded MMP-degradable PEG [85, 114] or hyaluronic acid [96] hydrogels, showing sustained transgene expression when the hydrogels were designed to enhance the cellular migration rate. The incorporation of nDNA into protease degradable scaffolds can result in aggregation either due to the interaction of nDNA with the gel precursor solutions such as in the case with fibrin or hyaluronic acid [113], or the interaction of nDNA particles with themselves as in the case for high nDNA concentrations [114]. To prevent such aggregation, a caged nanoparticle encapsulation (CnE) approach has been designed, where the nDNA are generated under dilute conditions and lyophilized in the presence of sucrose and agarose (**Figure 3.3C**). The sucrose is used as a cryo-protectant while the agarose functions as an inert polymer that prevents nDNA from interacting with the gel precursor solution and itself. This approach has been shown to result in active and non-aggregated polyplexes [113, 115], resulting in transgene expression *in vivo* in a subcutaneous model (**Figure 3.3C**). Since synthetically crosslinked hydrogels have been shown to result in poor cellular infiltration *in vivo* in areas of low protease expression [31],

micron sized pores have been introduced into PEG [116] and HA [31] hydrogels to enhance cellular infiltration and angiogenesis. Lentiviral vectors encoding for VEGF encapsulated in porous PEG hydrogels demonstrated blood vessel formation and lectin-positive cells at 2 and 4 weeks, while significant collagen deposition was observed by 4 weeks when compared to encapsulated lentivirus encoding for luciferase [116].

To achieve further control over transgene expression of encapsulated nDNA and prevent premature release of the nDNA, nDNA has been covalently immobilized to the scaffold backbone. In this case, the release rate and transfection efficiency are either related to the degradation rate of the scaffold (to allow nDNA release and internalization by infiltrating cells surrounding the implant [102]) or the degradation rate of the tether between the nDNA and the scaffold (which can control release rate or target a particular cell population) [117, 118].

### 3.4.3 Surface Associated

A complementary or stand-alone approach to control both release and cellular infiltration involves associating the DNA to the scaffold surface through nonspecific adsorption. The hypothesis in this case is that the loosely associated DNA can achieve sufficient nDNA retention to avoid premature release, allowing transgene expression to promote tissue repair soon after implantation and the embedded DNA (if present) can prolong this expression or express a different gene. Moreover, since nDNA are adsorbed following scaffold formation, it avoids the harsh processing conditions that that may occur during scaffold synthesis and can avoid polyplex aggregation [119]. *In vitro*, surface associated DNA polyplexes result in enhanced transgene expression compared to embedded polyplexes [120]. Surface associated DNA has been the most widely used approach to deliver DNA *in vivo* from scaffolds these recent years. Effective gene transfer and tissue formation was demonstrated with collagen/gelatin meshes or sponges [121-123], silk fibroin scaffolds [100], PLGA multichannel bridges [124], electrospun

fibers [125] and collagen/chitosan scaffolds [126] [127].These studies achieved regeneration of critical size defects in animal models and yielded similar results compared to the delivery of recombinant protein. Surface association/coating will be revisited in Chapter 6.

### 3.4.4 Biochemical Cues

Since gene transfer efficiency is correlated with cellular process such as proliferation rate, cellular infiltration rate into the scaffold, and actin/microtubule polymerization or de-polymerization, the scaffold itself can be engineered to enhance transgene expression. Integrin cell adhesion to the scaffold can be engineered to achieve enhanced cell migration and proliferation. Alginate hydrogels conjugated with various RGD densities for siRNA-mediated knockdown of eGFP demonstrated that increasing RGD density resulted in significantly higher knockdown of the targeted protein [128]. Moreover, RGD gradients and presentation (homogeneous vs. clustered) in different scaffolds have been used to influence transfection [96, 129]. Hydrogel stiffness can also be used to modulate migration and gene delivery rates; stiffer gels result in slower release rates of encapsulated polyplexes and decreased cell populations, spreading, and transfection [96] (**Figure 3.3B**). ECM proteins have also shown to have a significant impact on gene transfer with different ECM molecules enhancing or inhibiting gene transfer *in vitro* [130, 131]. Although the mechanism of the ECM mediated enhancement is not completely understood, RhoGTPases have been shown to play a significant role [130]. The co-delivery of proteins from the scaffold can be used to modulate the proliferative state of the infiltrating cells. Delivery of plasmid encoding for BMP-2 with along with recombinant bFGF encapsulated in PLG microspheres *in vivo* demonstrated significantly enhanced gene expression and increased blood vessel density compared to pDNA alone [132].

### 3.5 Summary

Current tissue engineering approaches to help guide wound healing and tissue repair primarily focus on developing scaffolds to deliver bioactive signals to aid these events. In this chapter, we aimed to elucidate the complexity of designing gene-loaded scaffolds for tissue engineering. Moreover, studies on gene incorporation, scaffold material, architecture, and presentation of biochemical cues highlight the importance of how cells experience the local microenvironment and their effect on gene transfer. As a result, careful consideration of these parameters must be taken to create a successful gene loaded scaffold for regenerative medicine and tissue repair. In this dissertation, nonviral gene delivery will be employed with the aid of L-PEI as the cationic condensing polymer. The importance of scaffold material and architecture on cell infiltration and vascular ingrowth will be discussed in Chapters 4 and 5. Knowledge gained from those chapters will be applied to nonviral gene delivery from porous hydrogels in Chapter 6 where *in vitro* and *in vivo* gene transfer is studied. In Chapter 7, two different gene delivery systems will study the effect of DNA presentation on gene transfer *in vitro* and *in vivo* in a wound healing model. Finally, Chapter 8 will re-visit the main conclusions of each chapter and potential interesting studies to conduct in the future.

# CHAPTER 4

# OPTIMIZING POROUS HYALURONIC ACID HYDROGELS GENERATION FOR CELLULAR INVASION AND VASCULARIZATION

## 4.1 Introduction

One of the overarching limitations of current approaches in developing scaffolds for tissue repair is the inability to achieve scaffold vascularization [13, 21]. Without blood vessels, the lack of oxygen and nutrient diffusion in and out of the scaffold does not allow for cells to infiltrate and survive deep within the scaffold for subsequent repair and new tissue formation. Therefore, much of current tissue engineering efforts have focused on developing scaffolds that promote vascular ingrowth to improve scaffold efficacy and overall success in aiding tissue repair.

Although implantation of a completely pre-vascularized tissue or scaffold may appear as an attractive option, the time course of such an approach renders it impractical. For this reason, popular strategies have been developed to more rapidly fabricate scaffolds that focus on the promotion of host vascularization and integration. One approach to improve scaffold vascularization is to rationally design the scaffold architecture to promote rapid cellular infiltration and blood vessel invasion. This can be achieved by designing a scaffold with a porous structure; pores allow for better cellular infiltration, migration, and proliferation, improving mass transport of oxygen and nutrients, as compared to non-porous scaffolds of similar composition, while the scaffold provides the necessary structural integrity for new tissue

formation and vascular ingrowth [13]. Porous scaffolds have been formed via various techniques that include gas foaming [25, 133], salt leaching [26, 30, 134, 135], heat sintering [27, 29], and lyophilization [28, 136-138]. Even in the absence of pro-angiogenic factors, porous hydrogels formed via the previously mentioned techniques with pore sizes ranging from 30-150 μm have been shown to promote angiogenesis and tissue formation *in vivo* with poly(N-isopropyl acrylamide) (poly-NIPAM) [27], poly(2-hydroxyethyl methacrylate-co-methacrylic acid) (pHEMA-co-MAA) [29], and PEG hydrogels [30]. Although gas foaming, salt leaching, and lyophilization are successful in achieving porous scaffolds, these techniques often lack uniformity in interconnected pore structure and pore size which make it difficult to accurately attribute the observed effects to these parameters. For this reason, heat sintering polymethyl methacrylate (PMMA) microspheres has been an attractive alternative, where the hydrogel is formed around a uniformly packed PMMA microsphere template.

Although heat sintering requires manual PMMA microsphere handling, the technique produces a uniform network of slightly fused PMMA microspheres following sintering at 150 °C for 17-22 h for subsequent hydrogel formation [27, 120, 139]. Due to this lengthy processing time to produce a network of PMMA microspheres for porous hydrogel formation, we proposed to develop a more efficient sintering technique. The objectives of this study were to: (i) decrease the PMMA microsphere network processing time and (ii) create a technique that minimizes manual handling and resultant error propagation. We proposed to utilize a suspension of dilute acetone in ethanol to slightly mate the microsphere interfaces to generate a highly uniform network more efficiently. We compared the proposed chemical sintering technique to the commonly used heat sintering technique and another suspension method that utilizes only ethanol by other research groups [140, 141] to determine the uniformity and efficacy in vitro and in vivo. In our studies, we used PMMA microspheres ranging from 53-63 μm in diameter to form our porous hydrogels since scaffolds with pore sizes outside 20-60 μm result in avascular,

fibrotic healing [142]. Moreover, we aimed to pair the advantages of a porous network with a hyaluronic acid (HA) scaffold since HA is a biocompatible glycosaminoglycan and key component in the extracellular matrix that has been shown to stimulate endothelial cell activity and its oligosaccharides have been shown to promote angiogenesis *in vivo* [36, 37, 43, 45]. The HA backbone was chemically modified to contain acrylates to provide sites for the inclusion of cell adhesion peptides (RGD) and matrix-metalloproteinase (MMP) - degradable peptide crosslinkers to promote cell infiltration and cell-mediated scaffold degradation, respectively. MMPs are a family of proteinases that play critical roles in many physiological processes and are upregulated during the wound healing cascade [51, 143], therefore can be utilized as an initiator for scaffold degradation and a potential delivery mechanism of pro-angiogenic bioactive signals contained within the scaffold to stimulate vascularization.

## 4.2 Materials and methods

### 4.2.1 Materials

Peptides Ac-GCRDGPQGIWGQDRCG-NH2 (HS-MMP-SH) and Ac-GCGYGRGDSPG-NH2 (RGD) were purchased from Genscript (Piscataway, NJ). Sodium hyaluronan (HA) was a gift from Genzyme Corporation (60 kDa, Cambridge, MA). All other chemicals were purchased from Fisher Scientific (Pittsburgh, PA) unless otherwise noted.

### 4.2.2 Hyaluronic acid-acrylate modification

Sodium hyaluronan was modified to contain acrylate functionalities as previously described [31]. Briefly, hyaluronic acid (2.0 g, 5.28 mmol, 60 kDa) was reacted with 18.0 g (105.5 mmol) adipic acid dihydrazide (ADH) at pH 4.75 in the presence of 4.0 g (20 mmol) 1-ethyl-3-[3-dimethylaminopropyl] carbodiimide hydrochloride (EDC) overnight and purified

through dialysis (8000 MWCO) in deionized (DI) water for 2 days. The purified intermediate (HA-ADH) was lyophilized and stored at -20 °C until used. Approximately 60% of the carboxyl groups were modified with ADH, which was determined using 1H-NMR ($D_2O$) by taking the ratio of peaks at δ = 1.6 and 2.3 corresponding to the eight hydrogens of the methylene groups on the ADH to the singlet peak of the acetyl methyl protons in HA (δ = 1.88). HA-ADH (1.9 g) was reacted with N-acryloxysuccinimide (NHS-Ac) (1.33 g, 4.4 mmol) in HEPES buffer (10 mM HEPES, 150 mM NaCl, 10 mM EDTA, pH 7.2) overnight and purified through dialysis against a 100 mM to 0 mM salt gradient for 1 day, and then against DI water for 3-4 days before lyophilization. The degree of acrylation was determined to be ~10% using 1H-NMR ($D_2O$) by taking the ratio of the multiplet peak at δ = 6.2 corresponding to the cis and trans acrylate hydrogens to the singlet peak of the acetyl methyl protons in HA (δ = 1.88).

4.2.3 Design template using PMMA microspheres

Heat sintered (HS) microsphere templates for porous hydrogels were prepared as previously described [31]. Briefly, approximately 24 mg polymethyl methacrylate (PMMA) microspheres (53–63 μm, which will be referred to as 60 μm hereafter, Cospheric, Santa Barbara, CA) were added into glass-bottom silicon wells (6 mm x 1 mm, D x H). The microspheres were then packed by slight tapping for 1–2 min and examined for homogenous packing through phase microscopy. The filled glass-bottom silicon wells were then placed into an oven and the microspheres were sintered for 17-22 h at 150 °C. Non-sintered and chemically sintered microsphere templates were prepared by suspending PMMA microspheres in a sintering solution at 0.4444 mg/μl. 55 μl of the PMMA suspension was added to flexiPERM molds (Sigma–Aldrich, St. Louis, MO) adhered to sigmacoted glass slides and placed in an incubator at 37 °C for 1-2 h to dry. The non-sintering (NS) suspension solution was optimized to

be 70 % ethanol for the 60 µm PMMA microspheres. The “chemical sintering” (CS) solutions were optimized to be 1 % acetone in 70 % ethanol for the 60 µm PMMA microspheres.

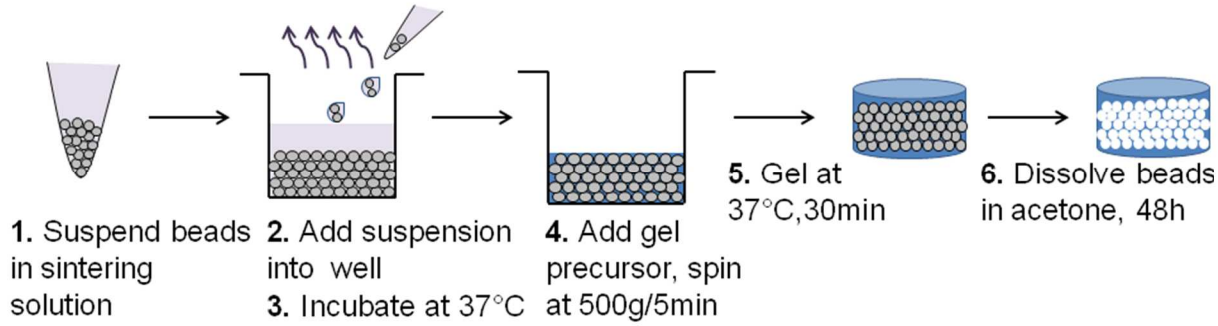


**Figure 4.1 Schematic representation of steps taken to generate porous hyaluronic acid hydrogels via chemical and non-sintering of PMMA microspheres.** The appropriate sintering suspension solution is described in 2.3. The resultant porous hydrogel is achieved after step 6, following PMMA dissolution via acetone and serial hydration.

4.2.4 Hydrogel formation

Hydrogels were formed by Michael-type addition of acrylate functionalized HA (HA-Ac) with bis-cysteine containing MMP peptide cross-linkers at pH 7.6–7.8. Prior to reaction, a hydrogel precursor solution was made by mixing HA-Ac with a lyophilized aliquot of cell adhesion peptide, RGD, for 30 min at 37 °C. After incubation, HA-RGD was mixed with the remaining HA-Ac and 0.3M triethanolamine (TEOA), pH 8.8 for a final gel concentration of 3.5 w/v% HA and 500 µM RGD. Finally, lyophilized aliquots of the cross-linker (0.9 mg HS-MMP-SH) were diluted in 18 µl of TEOA buffer pH 8.8 immediately before addition to the rest of the mixture. For porous hydrogels, 20 µl of gel solution was then added directly on top of a PMMA microsphere template and perfused into the template by centrifugation at 500 g for 5 min at 4 °C. The slide was then incubated at 37 °C for 30–45 min to induce polymerization. Once complete, the gels were removed from the silicon wells and placed directly into 100% acetone for 48 h to dissolve the PMMA microsphere template (**Figure 4.1**). The acetone solution was

replaced 2–3 times during this incubation. The gels were then serially hydrated into sterile phosphate buffered saline (PBS) and left in PBS until ready for use. For non-porous hydrogels, the gel solution was sandwiched between two sigmacoted slides using 1 mm thick plastic spacers and incubated at 37 °C for 30–45 min to induce polymerization. Once complete, the gels were placed directly into sterile PBS and left in PBS until ready for use.

### 4.2.5 Hydrogel preparation for SEM imaging

Each hydrated hydrogel was cut in half with the vertical cross section facing up and placed onto a dry carbon tape-covered holder. Samples were imaged under low vacuum at 50 Pa, 10 kV, and spot size of 3.0 using an FEI Nova Nano 230 SEM in the UCLA Molecular & Nano Archaeology (MNA) facility.

### 4.2.6 Characterization of hydrogel structural and mechanical properties

The storage and loss moduli were measured using a plate-to-plate rheometer (Physica MCR, Anton Paar, Ashland, VA) with an 8 mm (diameter) plate under a constant strain of 0.1 % and angular frequency ranging from 0.1 to 10 $s^{-1}$. Hydrogels were generated as described above and cut to 8 mm in diameter using an 8 mm biopsy punch. To prevent the hydrogel from drying, a humidity hood was utilized and the stage was set to 37 °C. Hydrogel water content was quantified by taking the ratio of equilibrated swollen hydrogel weight, subtracting the lyophilized dry hydrogel weight to the swollen gel weight. Interconnected pore diameters were manually measured using ImageJ on SEM images taken at 500X magnification (2 images per condition). NHS-Alexa488 (Invitrogen, Grand Island, NY) was used to stain the HA hydrogel by binding to the free amines (following formation). Stained hydrogels were imaged with an inverted Observer Z1 Zeiss fluorescent microscope; orthogonal projections and 3D rendering was obtained using Zen software.

4.2.7 Cell culture

Mouse bone marrow-derived mesenchymal stem cells (mMSCs) (D1, CRL12424) were purchased from ATCC (Manassas, VA) and cultured in Dulbecco's modified Eagle medium (DMEM) (Invitrogen, Grand Island, NY) supplemented with 10 % bovine growth serum (BGS, Hyclone, Logan, UT) and 1 % penicillin/streptomycin (Invitrogen, Grand Island, NY) at 37 °C and 5 % CO2. The cells were passaged using trypsin following standard cell culture protocols every 2–3 days.

4.2.8 Cell seeding onto porous hydrogels

mMSCs were seeded onto 3.5 w/v%, 500 μM RGD porous hydrogels as previously described [144]. Briefly, porous hydrogels were sterilized by 3 consecutive 10 min washes in sterile PBS. Hydrogels were then placed into dry low-binding plates and cells were seeded onto the hydrogels in two steps. First, 15,000 cells at a density of 15,000 cells/10 μl DMEM were added directly on top of each hydrogel and centrifuged down for 3 min at 700 rpm. Then, an additional 15,000 cells were seeded directly on top without further centrifugation. The hydrogels were incubated at 37 °C for 15 min and then 180 μl of fresh media was added for a final volume of 200 μl/well.

4.2.9 Cell viability and spreading

mMSC viability was studied with a LIVE/DEAD® viability/cytotoxicity kit (Molecular Probes, Eugene, OR). Briefly, 1 μl of ethidium homodimer-1 and 0.25 μl of calcein AM from the kit were diluted with 500 μl DMEM to make the staining solution. Each gel (2–3 gels per condition per time point) was stained with 150 μl of staining solution for 30 min at 37 °C in the

dark before imaging. To better analyze cell spreading, gels (2–3 gels per condition per time point) were fixed for 30 min at RT using 4 % paraformaldehyde (PFA), rinsed with PBS, treated with 0.1 % triton-X for 10 min and stained for 90 min in the dark with YOYO-1 for cell nuclei (1:250 dilution from 1 mM stock, Invitrogen, Grand Island, NY) and rhodamine-phalloidin (1:40 dilution, Invitrogen, Grand Island, NY)) in 1% bovine serum albumin solution. The samples were then washed with 0.05 % tween-20. For both cell viability and cell spreading, an inverted Observer Z1 Zeiss fluorescent microscope was used to visualize samples. To better visualize the distribution throughout the hydrogel, multiple z-stacks 1.9–2.3 μm thick were taken for each image, deconvolved to minimize background, and presented as orthogonal projections. Cell viability was assessed by quantifying the ratio of live cells to the total number of cells as manually counted from an orthogonal projection of z-stacks through 70 μm of hydrogel acquired from the LIVE/DEAD® assay. Cell spreading was quantified by manually measuring end-to-end cell length using Zen Blue 2011 (Carl Zeiss, Jena, Germany) for three images (orthogonal projections of z-stacks through 125 μm of hydrogel) per condition per time point.

#### 4.2.10 Cell proliferation

An alamarBlue® assay (AbD Serotec, Raleigh, NC) was used to quantify cell proliferation rate. 20 μl alamarBlue reagent with 200 μl DMEM was added to each well containing a hydrogel seeded with cells in a 96-well plate and incubated at 37 °C for 5 h. The solutions were transferred to a new plate and absorbance was measured at 570 nm and 600 nm using a standard plate reader. Three gels for each condition were analyzed at each time point and proliferation rate was calculated following the manufacturer's instructions.

4.2.11 Subcutaneous implant model

All in vivo studies were conducted in compliance with the NIH Guide for Care and Use of Laboratory Animals and UCLA ARC standards. 6 to 8-week old female Balb/c mice, each 20–30 g, were used to study cellular infiltration and blood vessel formation in HA hydrogels since this strain and size has been previously used for wound healing and angiogenesis assays [145, 146]. Non-porous or porous hydrogels were made exactly as described above (3.5 w/v% HA, 100 μM RGD) and cut to 6 mm in diameter using a sterile biopsy punch, for final overall dimensions of 6 mm x1 mm, D x H. All porous hydrogels were made using 60 μm beads. In fabricating the hydrogels, the starting reagents were sterilized through filtering with a 0.22 μm filter. After scaffold fabrication, the hydrogels were washed with sterile PBS and kept in PBS with 1 % P/S. Immediately prior to surgery, mice were anesthetized with 4 % isoflurane through an induction chamber. After anesthesia induction, the isoflurane concentration was lowered to 1.5–2.5% for the remainder of the surgery. The back of the mouse was subsequently shaved and washed with povidone-iodine (Betadine, Stamford, CT) and 70 % isopropyl alcohol. Two lateral incisions appropriate to the size of the implant were made in the skin (one on each side of the midline of the animal) using scissors. Two subcutaneous pockets were subsequently created by blunt dissection using rounded-end scissors. The hydrogels were inserted into each respective subcutaneous pocket and closed with a single wound clip. All animals were observed daily for signs of inflammation and pain and also administered carprofen injections for the first 48 h post-survival surgery. After 2 weeks, mice (n=4) were sacrificed with isoflurane overdose. Two 1 $cm^2$ pieces of tissue were collected from each mouse containing the implant and the surrounding tissue and skin, fixed in 2 % PFA for 16 h at 4 °C, dehydrated in 70% EtOH, and finally paraffin embedded. A total of 12 mice were used in this study, with four mice per hydrogel condition.

4.2.12 Immunohistochemistry and immunofluorescence

Paraffin embedded sections (5 μm thick) were deparaffinized by incubation in multiple xylene washes followed by serial hydration from 100 % ethanol to 100 % water. Cell membranes were permeabilized with a 15 min incubation at 37 °C in 0.1 mg/ml proteinase K solution. Sections were then washed with PBS and incubated in blocking buffer (1 % goat serum (Jackson Immuno Research Labs, West Grove, PA) + 0.05 % Tween-20 in PBS) for 1 h at RT before being incubated in primary antibody solution (1:100 dilution in blocking buffer of rat anti-mouse CD31 (BD Pharmingen, San Diego, CA)) overnight at 4 °C. Sections were again washed with PBS and incubated in blocking buffer for 10 min at RT before being incubated for 2 h at RT in secondary antibody solution (1:200 dilution in blocking buffer of goat anti-rat Alexa 568 (Invitrogen, Grand Islands, NY), which also contained α-smooth muscle actin-FITC (1:500 dilution, Sigma–Aldrich, St. Louis, MO) and DAPI nuclear stain (1:400 dilution, Invitrogen, Grand Island, NY). Sections were then washed twice in PBS, mounted and imaged using an inverted Zeiss fluorescence microscope. All hematoxylin and eosin staining of sections was conducted by the Translational Pathology Core Laboratory (TPCL) at UCLA.

4.2.13 Quantification and characterization of cellular infiltration and blood vessels *in vivo*

Hydrogels were halved and embedded in paraffin with the vertical cross sections facing up. Each paraffin embedded section contained 2 halves (vertical cross section) of the hydrogel. Three separate sections at least 100 – 150 μm apart were analyzed for each sample. 5 randomly chosen areas were imaged on each half gel, with 10 images total in per section. Cellular infiltration was quantified by using Fiji software by converting the image to an 8-bit file, applying a threshold sensitivity, and using the watershed tool to separate joined cells to analyze the cell number. Vessels were counted manually in each section, totaled from all 30 sections, and finally normalized to the total imaged area. The bar graph in **Figure 4.6D** represents the

average vessels/mm2 from 4 different animals. The diameter of each vessel was manually measured using Zen imaging and analysis software (Zeiss). Percentages were determined using the entire vessel set.

4.2.14 Statistical analysis

Statistical analyses were performed using Prism (GraphPad, San Diego, CA). Interconnected pore diameter, water content, rheology, cell viability, spreading, and proliferation data were analyzed using a one-way analysis of variance (ANOVA) followed by a Tukey post-hoc test. The results were represented as mean ± SD. The in vivo cellular invasion and blood vessel characterization data were analyzed using a Kruskal-Wallis one-way ANOVA followed by a Dunn's post-hoc test and represented as mean ± SEM. Single, double, and triple asterisks represent $p < 0.05$, $p < 0.01$, and $p < 0.001$, respectively. A p value $< 0.05$ was considered statistically significant.

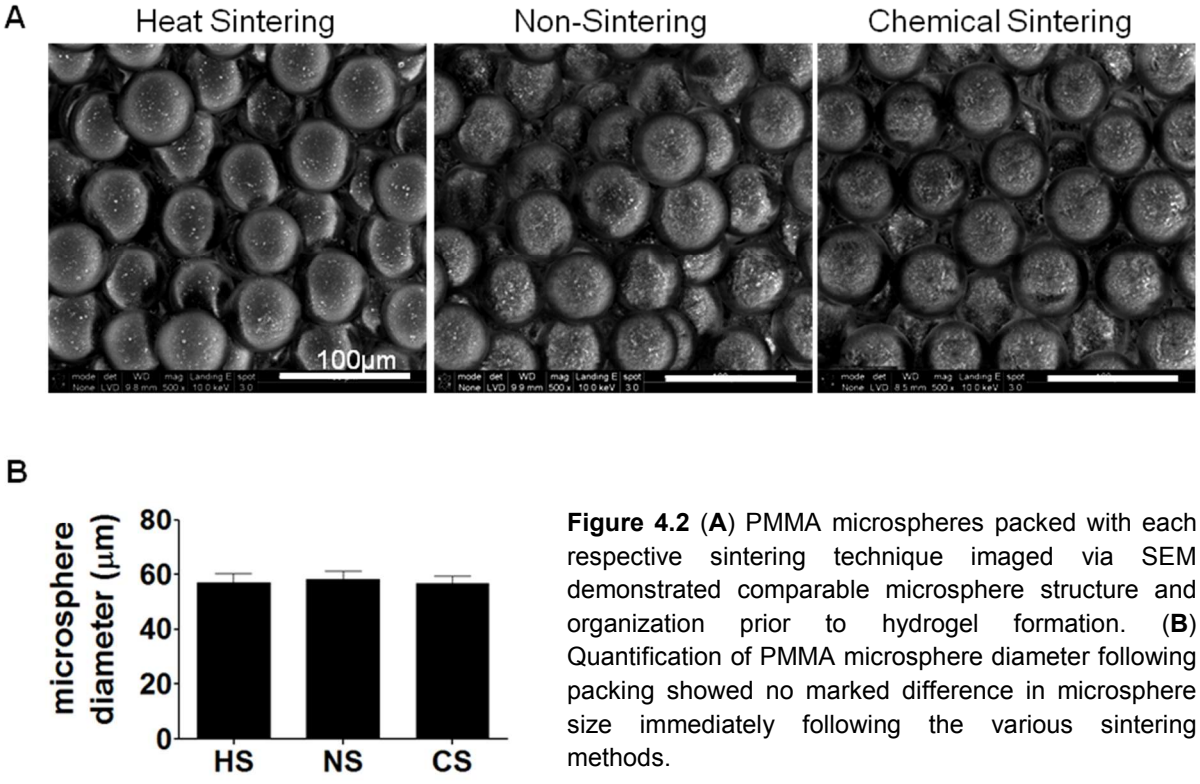


**Figure 4.2** (**A**) PMMA microspheres packed with each respective sintering technique imaged via SEM demonstrated comparable microsphere structure and organization prior to hydrogel formation. (**B**) Quantification of PMMA microsphere diameter following packing showed no marked difference in microsphere size immediately following the various sintering methods.

## 4.3 Results

### 4.3.1 Effect of PMMA sintering technique on hydrogel formation

Prior to hydrogel formation, PMMA microsphere packing was investigated as a result of each sintering technique. SEM images show similar microsphere organization (**Figure 4.2A**). 3.5 w/v% HA-MMP porous hydrogels were generated from heat sintering (HS), non-sintering (NS), and chemically sintering (CS) 60 μm PMMA microspheres to compare the differences in hydrogel structure and architecture as a function of sintering technique (**Figure 4.3**). SEM images taken at 255x, 500x, and 1000x magnification demonstrated that 60 μm pore hydrogels generated from chemical sintering had comparable uniform open pore structure and pore interconnectivity as the currently used HS and NS techniques. SEM images of non-porous gels are included as a comparison (**Figure 4.7A**). Moreover, phase and fluorescent microscopy was used to investigate the hydrogel structure in its hydrated state. Porous hydrogels were stained with NHS-Alexa488 and imaged under fluorescent microscopy. Application of orthogonal projections and 3D rendering to multiple z-stack images showed apparent pores and high interconnectivity in all hydrogels generated with each sintering technique.

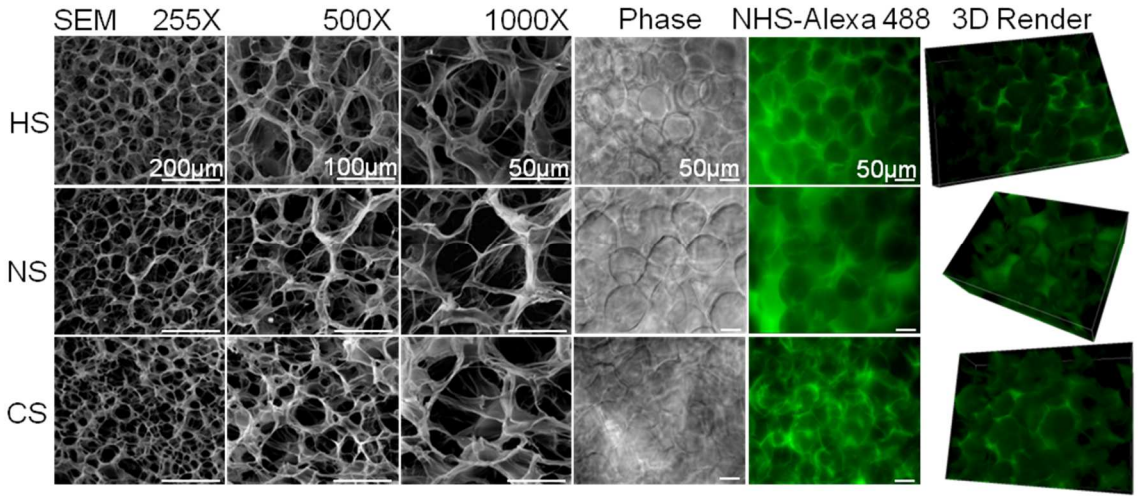


**Figure 4.3** Porous hydrogels with 60 μm pores generated from HS, NS, and CS have apparent open pore and interconnected pore structure in SEM, phase, and fluorescent orthogonal projections and 3D renderings.

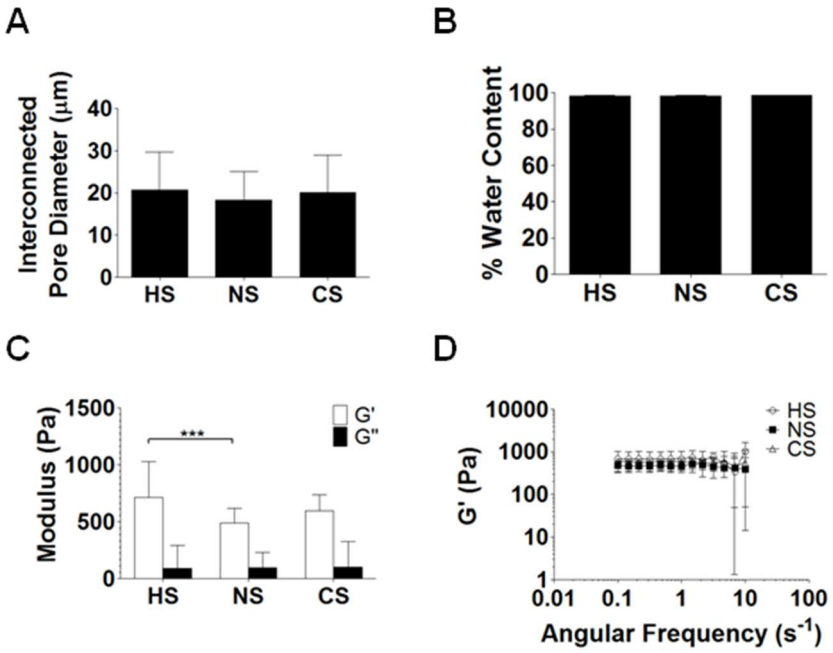


**Figure 4.4** (**A**) Quantification of interconnected pore diameters indicates similar interconnectivity between hydrogels generated with HS, NS, and CS. (**B**) Water content was similar for hydrogels generated with the various techniques. (**C**, **D**) Conversely, PMMA microsphere packing technique affects gel stiffness, where gels generated via HS were comparable to CS but stiffer than NS-generated gels. (***) $p < 0.001$. Values represent the mean and standard deviation.

### 4.3.2 Effect of PMMA sintering technique on structural and mechanical properties

Pore interconnectivity of SEM images was manually measured using ImageJ and defined as the interfacial, longitudinal distance between adjacent pores. Porous hydrogels generated via heat sintering, non-sintering, and chemical sintering had comparable interconnected pore diameters of 20.75 ± 8.93, 18.29 ± 6.81, and 20.08 ± 8.92 μm, respectively (**Figure 4.4A**). In addition, the quantification of water content of hydrogels generated from each technique revealed that the sintering technique did not significantly affect the water retention capability, where the hydrogels were 98.38 ± 0.36, 98.28 ± 0.32, and 98.49 ± 0.22 % water from with HS, NS, and CS techniques, respectively (**Figure 4.4B**). Conversely, the PMMA microsphere sintering technique appeared to significantly affect the mechanical stiffness of the resultant porous hydrogels (**Figure 4.4C, D**). Gels formed via heat sintering were comparable to

those generated with chemical sintering, but significantly stiffer than when formed with non-sintering where the storage moduli were 713 ± 317.3, 597.2 ± 140.5, and 488 ± 129.6 Pa, respectively.

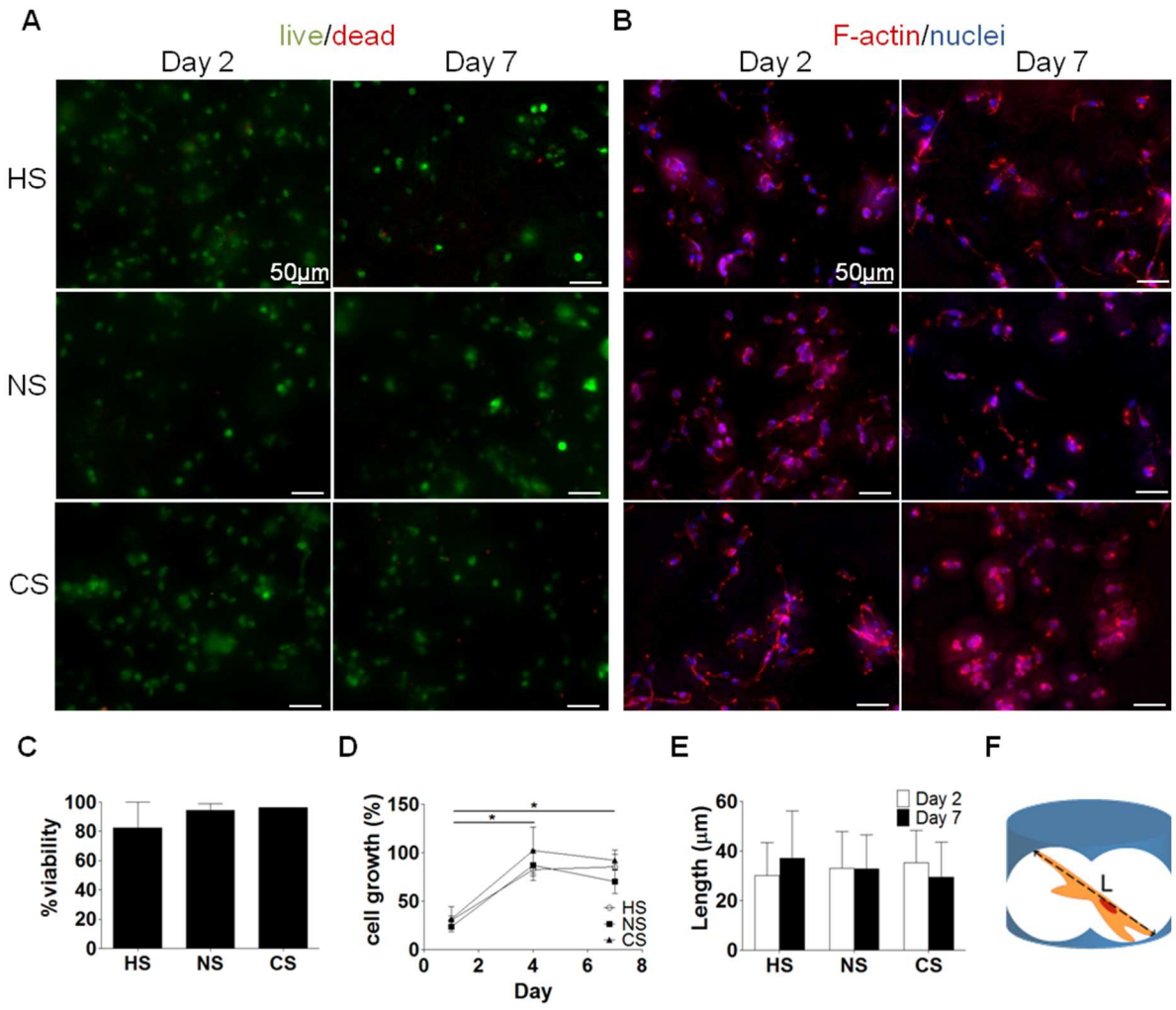


**Figure 4.5 In vitro characterization and quantification of mMSCs seeded onto hyaluronic acid hydrogels following 7 days.** (**A**) mMSC viability (green = live and red = dead cells) and (**B**) spreading (red = f-actin and blue = nuclei) was assessed at day 2 and 7 by fluorescent microscopy. (**C**) Quantification of day 2 viability and (**D**) cell growth at days 1, 4, and 7 showed no significant differences among groups. (**E**) Quantification of cell spreading by measuring end-to-end cell length (**F**) at days 2 and 7 showed no difference among the groups at each time point. (*) $p < 0.05$. Values represent the mean±SD.

### 4.3.3 Effect of PMMA sintering technique on cell behavior *in vitro*

To study the effect of sintering technique on cell morphology in vitro, mMSCs were seeded on 3.5 w/v% HA-MMP hydrogels functionalized with 500 μM RGD. Cell-seeded

hydrogels were stained at days 2 and 7 with live/dead® (**Figure 4.5A**) and rhodamine-phalloidin/dapi (**Figure 4.5B**) to study cell viability and spreading, respectively. Quantification of viability at day 2 showed no significant differences among sintering techniques with greater than 82% viability (**Figure 4.5C**). Morphological differences could not be observed in images obtained from staining the cell-seeded gels for f-actin and nuclei. This result was confirmed by quantifying cell spreading by manually measuring the end-to-end cell length (**Figure 4.5F**), where cell spreading was comparable among the hydrogels generated from the different techniques (**Figure 4.5E**). Cell proliferation was also monitored over time using an alamarBlue® assay and days 1, 4, and 7 post-seeding (**Figure4.5D**). For any time point, there was no difference among the hydrogels formed from the different sintering techniques. However, for each condition, cell growth peaked at day 4, and plateaued through day 7.

### 4.3.4 Effect of PMMA sintering technique *in vivo*

Acellular 3.5 w/v% HA-MMP hydrogels functionalized with 100 μM RGD were implanted subcutaneously in the backs of balb/c mice for 14 days to study cellular infiltration. Samples were excised at day 14 for analysis. Hematoxylin and eosin (H&E) staining of the hydrogel cross sections showed that the porous hydrogel structure was maintained through 14 days and high cellular infiltration into the hydrogels was present (**Figure 4.6A**), while host cells remained on the periphery of non-porous gels (**Figure 4.7B**). Quantification of cellular invasion was obtained by counting nuclei normalized to gel area; this data supported H&E observations where the number of cells infiltrating the hydrogels generated from chemical sintering (2424 ± 292 nuclei/mm$^2$) were comparable to hydrogels generated with heat or non-sintering (3037 ± 206 or 2672 ± 282 nuclei/mm$^2$, respectively) (**Figure 4.6C**). Immunofluorescence staining for PECAM positive endothelial cells revealed that blood vessels were present in hydrogels formed from all three different sintering techniques (**Figure 4.6B**). Quantification of the number of blood vessels

present normalized to gel area showed that the PMMA microsphere sintering and resultant porous hydrogel did not significantly affect the vessel invasion (**Figure 4.6D**). Moreover, characterization of the blood vessel diameters showed that approximately half of the vessels present were no more than 6 μm in diameter (diameter of an erythrocyte) (**Figure 4.6E**).

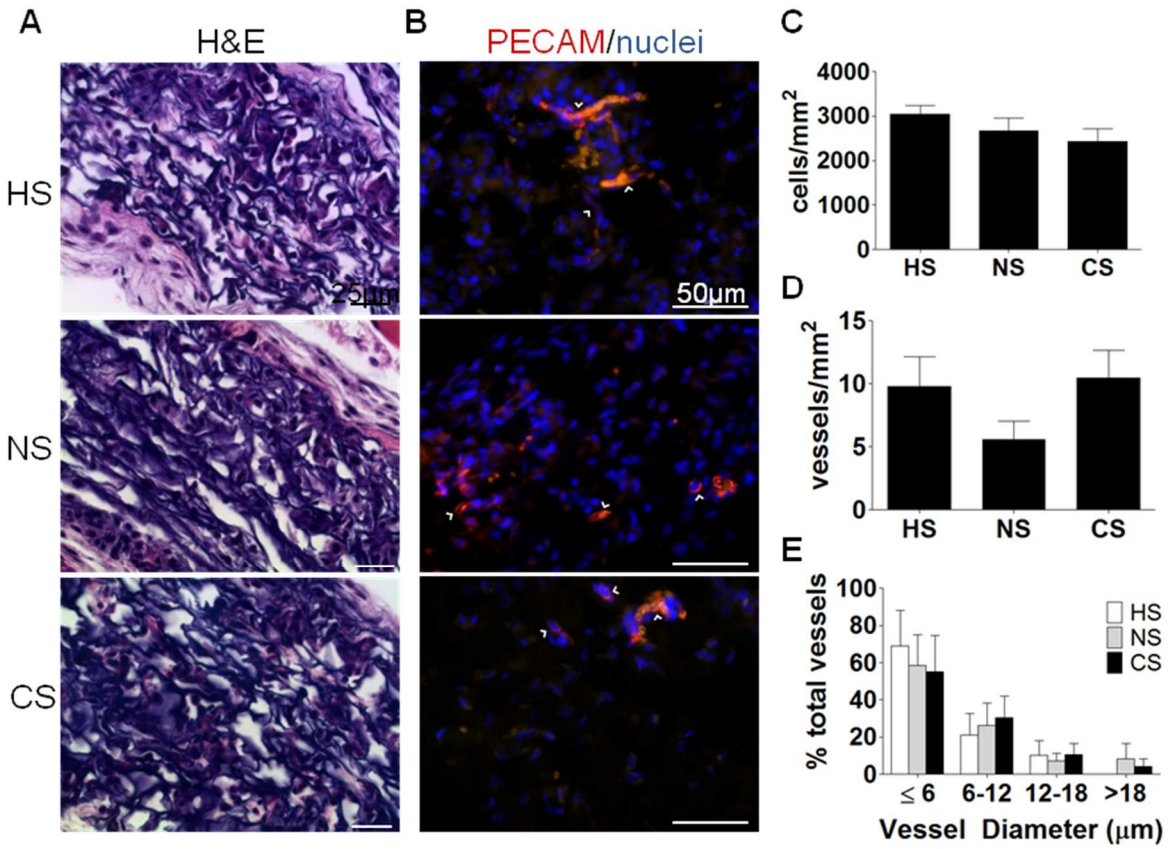


**Figure 4.6 *In vivo* characterization and quantification of aceullar hyaluronic acid hydrogels (60 μm pores) implanted subcutaneously in balb/c mice for 14 days.** (**A**) H&E stained sections of porous hydrogels generated from the different techniques showed similar levels of cellular infiltration. (**B**) Staining for an endothelial cell marker showed PECAM positive cells within the hydrogels generated by all three sintering techniques. (**C**) Quantification of cellular infiltration showed comparable invasion within gels generated from all three techniques. (**D**) Vessels in 30 images over 3 sections separated by 100-150 μm were quantified and normalized to the total image area. The bar graph represents the average of 4 separate samples. (**E**) For those samples that contained vessels, vessel diameters were measured. Approximately half of the vessels in all samples were less than 6 μm in diameter. Red = PECAM positive staining (endothelial cells), yellow = erythrocytes, and blue = nuclei. Values represent the mean and standard error of the mean.

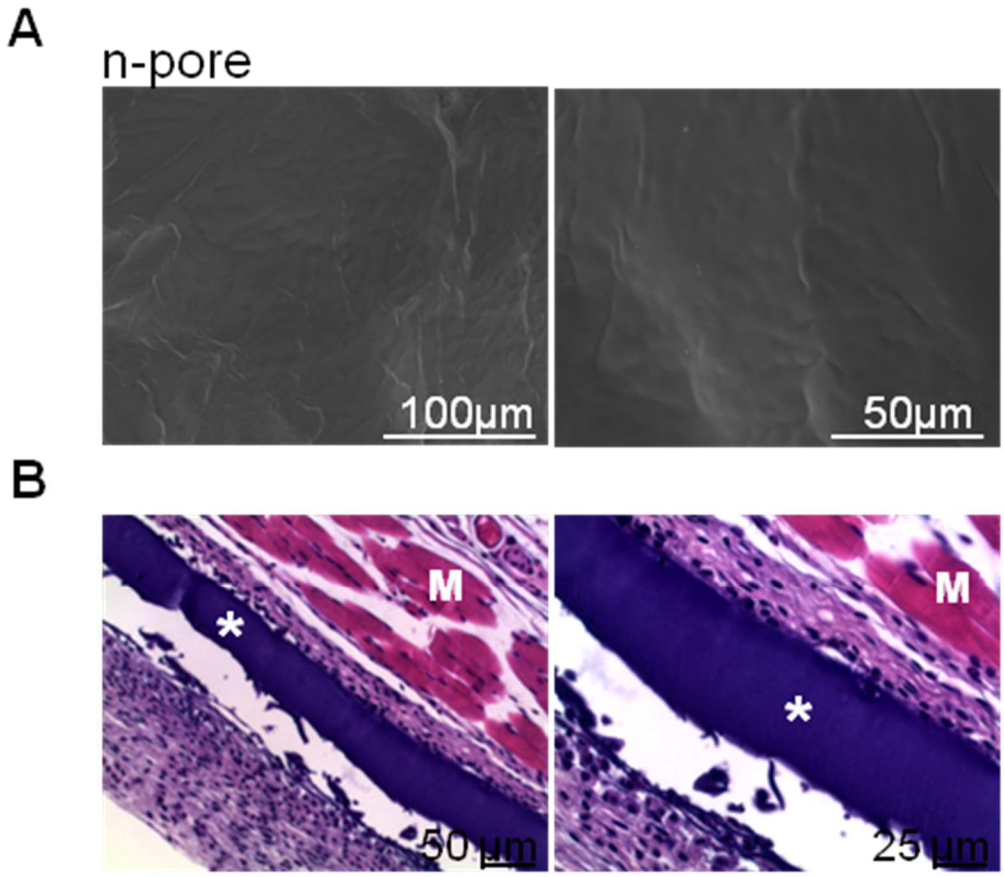


**Figure 4.7** (**A**) Scanning electron micrographs of non-porous (n-pore) 3.5 w/v% hyaluronic acid hydrogels confirm that no pores are present. (**B**) H&E staining of samples of n-pore hydrogels implanted subcutaneously in balb/c mice demonstrate that host cells are only penetrate the hydrogel periphery at 14 days. The asterisk denotes the remaining n-pore hydrogel and (M) denotes muscle.

### 4.4 Discussion

Several current approaches in generating porous hydrogels possess limited control over consistency, therefore using PMMA microspheres as a sphere template via heat sintering has offered better uniformity in pore structure and interconnectivity. However, the main limitations with heat sintering include the manual handling and long processing time (17-22 h) that carries over to delayed experimental investigation. For this reason, we proposed to chemically sinter the PMMA microspheres in a liquid suspension to (i) utilize a liquid handling technique to minimize manual handling and resultant error and (ii) slightly fuse the microspheres at its

interfacial boundary to generate a neatly packed microsphere network. Since acetone is a known solvent for PMMA, it was used in a dilute concentration with the expectation that the PMMA microspheres would slightly mate the microspheres at each adjacent interface. Moreover, the dilute acetone was suspended in ethanol to pair the volatile state of these solvents with an incubation step to expedite the drying rate of the PMMA microsphere network. In this study, we compared our proposed chemically sintered PMMA microspheres to those suspended in a 70 % ethanol solution (non-sintering) as used by Peyton et al. [140] and Stachowiak et al. [141] and to the commonly used heat sintered technique in order to investigate the resultant hydrogel pore structure and cell response in vitro and in vivo.

We report that similar uniform pore structure with the proposed chemical sintering technique was achieved when compared to hydrogels generated via heat sintering and non-sintering (**Figure 4.3**). However, the difference herein lies with the processing time, where non- and chemically sintered hydrogels only required 1-2 h for incubation while heat sintering requires more than ten times this. Unexpectedly, our studies demonstrate no quantifiable difference among the three sintering techniques with regard to pore uniformity and interconnectivity, despite the vastly dissimilar approaches (**Figure 4.3, 4.4A**). Further investigation of PMMA microsphere packing via SEM microscopy showed similar resultant microsphere networks generated with each technique (**Figure 4.2A**). This was confirmed via quantification of PMMA microsphere diameter using ImageJ following each respective sintering solution where no marked difference among the techniques was present (**Figure 4.2B**). This result indicates that the proposed chemical sintering suspension solution with dilute acetone does not significantly cause surface dissolution or fusion of the PMMA microspheres as previously hypothesized. This may be altered with slightly increasing the acetone concentration between 1-5 %; optimization studies realized that acetone concentrations exceeding 5 % acetone in ethanol resulted in complete PMMA dissolution (data not shown). Moreover, the

interconnected pore diameter achieved from heat sintering at high temperatures was comparable to chemical and non-sintering. This result is likely due to the intrinsic viscous nature of hyaluronic acid; we believe that despite centrifugation of the hydrogel into the PMMA microsphere templates, the viscous hydrogel does not penetrate the void spaces or interfacial gaps as deeply as expected, rendering the porous hydrogel interconnectivity similar among all sintering techniques.

Despite similar porous hydrogel structure and interconnectivity, the effect of sintering technique on mechanical properties was apparent (**Figure 4.4C**). Although the storage moduli of hydrogels formed via heat and non-sintering techniques were significantly different, it is important to note that hydrogels formed via chemical sintering were comparable to those generated by heat sintering. These data show that porous hydrogels can be generated via chemical sintering to achieve mechanical properties similar to the commonly used heat sintering technique with ten-fold less processing time. It was also observed that the storage moduli of the porous hydrogels varied at angular frequencies nearing 10 rad/s (**Figure 4.4D**). This result may due in part to the large pores we have introduced into the scaffold; the thin hydrogel walls between pores that may be experiencing variable deformation with increased angular frequencies.

Cell behavior in response to hydrogels generated from the three sintering techniques was evaluated via viability and proliferation assays, as well as immunofluorescent staining for cell morphology to confirm that porous hydrogels formed from the different techniques did not significantly vary in presentation to cells *in vitro*. Cell viability, spreading, and proliferation was not significantly different among the hydrogels generated from each sintering technique (**Figure 4.5A-F**), suggesting that the differences observed in mechanical properties did not largely affect cell behavior *in vitro*. This result may be attributed to the scale of interaction between the cell and scaffold, as well as the relative difference in moduli. Despite observing a statistically

significant difference in storage moduli, the difference is not extreme; the hydrogel moduli remain on the same order of magnitude. Since the cell-scaffold surface interaction more closely mimics a 2D presentation of cues, we believe that the overall cell behavior *in vitro* may not be significantly influenced by bulk mechanical stiffness with the small difference in modulus. Mechanical properties have been shown to influence mesenchymal stem cell behavior in 2D when moduli vary from 2 to 10 fold [147, 148]. The differences observed between our hydrogels are much smaller than this, where the stiffest hydrogel was 713 Pa and the softest was 488 Pa. Therefore, this small variation in moduli may not be sufficient to see differences in cellular proliferation, spreading, and viability.

To further investigate the effect of sintering *in vivo*, acellular porous hydrogels generated from heat, chemical, and non-sintering were implanted subcutaneously in the backs of balb/c mice to assess cellular infiltration and implant integration with host tissue at 14 days. H&E staining of hydrogel sections showed high cellular infiltration into the porous hydrogels generated from each technique (**Figure 4.6A**). This observation was confirmed with quantification of nuclei normalized to hydrogel area via Fiji software (**Figure 4.6C**), demonstrating that the host cells were able to invade the pores generated from each technique comparably. Moreover, staining for endothelial cells demonstrate that blood vessels were present at 14 d in porous hydrogels generated from each PMMA sintering technique (**Figure 4.6B**). Characterization of the vessels present indicated that the density of blood vessels present were comparable in hydrogels formed with each technique, and of the vessels present, most were on the dimensional order of erythrocytes suggesting capillary formation. Immunofluorescent staining confirmed this, as no PECAM+ vessels stained positive for α-SMA, a smooth muscle cell marker that exists on larger, contractile vessels. These results highlight the therapeutic potential of these porous hydrogels for tissue repair for several reasons. First, the inclusion of pores by any of the described methods allow for rapid cellular infiltration when

compared to a non-porous hydrogel of the same composition (**Figure 4.7A, B**). Secondly, even without the inclusion of pro-angiogenic factors in the porous hydrogels, we observed blood vessel invasion into the hydrogel at 14 days. Blood vessel formation and maturation could potentially be encouraged further with the incorporation of pro-angiogenic growth factors or therapeutic plasmids. More importantly, although hyaluronic acid possesses many attractive qualities that include biocompatibility and biodegradability, it was strategically chosen for our hydrogel system because its degraded fragments of HA stimulates angiogenesis in vivo [43]. Interestingly, it appears as though the degraded HA alone was not a strong enough pro-angiogenic stimulus for the non-porous hydrogels to recruit blood vessel invasion. This observation may indicate that for a HA-MMP degradable hydrogel system to promote vascular ingrowth without the presence of pro-angiogenic growth factors or therapeutic plasmids, a porous structure is necessary.

### 4.5 Conclusions

In this chapter, we report a chemical sintering method to generate porous hyaluronic acid hydrogels comparable to currently used non- and heat sintering techniques. More importantly, the proposed chemical sintering was able to achieve similar uniform pore structure and interconnectivity when compared to non- and heat sintering techniques with equal or less processing time at 1-2 h versus 1-2 h and 17-22 h, respectively. Chemical sintering was able to achieve similar *in vitro* and *in vivo* responses as ascertained by studying cell viability, spreading, proliferation, and cell and blood vessel invasion. These results indicate that porous hyaluronic acid hydrogels can be generated via chemical sintering or non-sintering comparable to the commonly used heat sintering technique with higher efficiency as these techniques minimize manual PMMA microsphere handling and significantly reduce processing time.

# CHAPTER 5

# SYSTEMATIC EVALUATION OF NATURAL SCAFFOLDS IN CUTANEOUS WOUND HEALING

## 5.1 Introduction

Tissue engineering aims to repair damaged or injured tissue by generating biological substitutes that will maintain, restore, or improve its function [149, 150]. This is generally achieved with any combination of the following three components: cells, a scaffold, and/or bioactive cues (growth factors, DNA, etc). While the ideal case would be to implant cell-laden tissue constructs, limitations include extensive cell culture time (dependent on tissue type, complexity, and size), high cost, and risk of immunological rejection if autologous cells are not used [150, 151]. An attractive alternative approach is to judiciously choose a biomaterial or scaffold to induce the host's natural processes for repair. In this chapter, we focused on systematically evaluating the role of scaffold type for cutaneous wound healing.

Hydrogels are ideal scaffolds because they are water-swollen polymer networks that can possess mechanical properties similar to soft tissue and high permeability for the diffusion of oxygen and nutrients, mimicking the native extracellular matrix (ECM). In this report, we focused on natural polymers, namely fibrin and hyaluronic acid, due to their biocompatibility, inherent biodegradability, and intrinsic biological functions in promoting angiogenesis for improved wound healing. Vascular ingrowth into the site of injury allows for the transport of nutrients, waste, and cells; it is critical for the survival of newly formed tissue.

Fibrin was chosen since it is one of the most widely used scaffolds due to its biodegradability, inherent capacity to promote cell adhesion [152], and its natural role in the wound healing cascade as a matrix for new ECM formation [153]. A porous hyaluronic acid hydrogel was utilized due to two motivations: scaffold architecture and natural material properties. Scaffold porosity has been shown to promote cellular infiltration and vascular ingrowth in a variety of materials including poly(N-isopropyl acrylamide) (poly-NIPAM) [27], poly(2-hydroxyethyl methacrylate-co-methacrylic acid) (pHEMA-co-MAA) [29], PEG [26] and hyaluronic acid (HA) hydrogels [31, 32, 154]. Moreover, along with its low immunogenicity, HA has been shown to stimulate endothelial cell activity and its degraded fragments (oligosaccharides) have demonstrated potential to promote neovascularization *in vivo* [36, 37, 43, 45, 155]. Lastly, HA scaffolds are completely resorbable into completely metabolizable degradation products.

Although hydrogel implants have been previously utilized as delivery vehicles for bioactive signals, the direct role of the scaffold and scaffold architecture in skin tissue healing and vascularization has not been previously performed in a humanized wound disease model. In this chapter, we show the tissue healing capacity for solely conductive scaffolds composed of fibrin and/or hyaluronic acid and compared them to scaffolds that deliver a pro-angiogenic protein signal.

## 5.2 Materials and methods

### 5.2.1 Materials

Peptides Ac-GCRDGPQGIWGQDRCG-NH2 (HS-MMP-SH) and Ac-GCGYGRGDSPG-NH2 (RGD) were purchased from Genscript (Piscataway, NJ). Sodium hyaluronan (HA) was a gift from Genzyme Corporation (60 kDa, Cambridge, MA). All other chemicals were purchased from Fisher Scientific (Pittsburgh, PA) unless otherwise noted.

### 5.2.2 Hyaluronic acid-acrylate modification

Sodium hyaluronan was modified to contain acrylate functionalities as previously described [31]. Briefly, hyaluronic acid (2.0 g, 5.28 mmol, 60 kDa) was reacted with 18.0 g (105.5 mmol) adipic acid dihydrazide (ADH) at pH 4.75 in the presence of 4.0 g (20 mmol) 1-ethyl-3-[3-dimethylaminopropyl] carbodiimide hydrochloride (EDC) overnight and purified through dialysis (8000 MWCO) in deionized (DI) water for two days. The purified intermediate (HA-ADH) was lyophilized and stored at -20 °C until used. Approximately 60 % of the carboxyl groups were modified with ADH, which was determined using 1H-NMR ($D_2O$) by taking the ratio of peaks at δ = 1.6 and 2.3 corresponding to the eight hydrogens of the methylene groups on the ADH to the singlet peak of the acetyl methyl protons in HA (δ = 1.88). HA-ADH (1.9 g) was reacted with N-acryloxysuccinimide (NHS-Ac) (1.33 g, 4.4 mmol) in HEPES buffer (10 mM HEPES, 150 mM NaCl, 10 mM EDTA, pH 7.2) overnight and purified through dialysis against a 100 mM to 0 mM salt gradient for 1 day, and then against DI water for 3-4 days before lyophilization. The degree of acrylation was determined to be ~10 % using 1H-NMR ($D_2O$) by taking the ratio of the multiplet peak at δ = 6.2 corresponding to the cis and trans acrylate hydrogens to the singlet peak of the acetyl methyl protons in HA (δ = 1.88).

### 5.2.3 Design template using PMMA microspheres

A PMMA microsphere template was used to generate porous hydrogels as previously described[154]. Briefly, approximately 24 mg polymethyl methacrylate (PMMA) microspheres (53–63 μm, Cospheric, Santa Barbara, CA) were resuspended in a solution of 1 % acetone in 70 % acetone at 0.4444 mg/μl into each PDMS well (6 mm x 2 mm, D x H) adhered to a sigmacoted glass slide. The templates were placed in an incubator at 37 °C for 1 h to create a dry, uniformly packed mold.

### 5.2.4 Hydrogel formation

#### 5.2.4.1 Porous hyaluronic acid hydrogel (μ)

Hydrogels were formed by Michael-type addition of acrylate functionalized HA (HA-Ac) with bis-cysteine containing MMP peptide cross-linkers at pH 7.6–7.8. Prior to reaction, a hydrogel precursor solution was made by mixing HA-Ac with a lyophilized aliquot of cell adhesion peptide, RGD, for 30 min at 37 °C. After incubation, HA-RGD was mixed with the remaining HA-Ac and 0.3 M triethanolamine (TEOA) at pH 8.8 for a final gel concentration of 3.5 w/v% HA and 100 μM RGD. Finally, lyophilized aliquots of the cross-linker (HS-MMP-SH) were diluted in TEOA buffer pH 8.8 immediately before addition to the rest of the mixture. For porous hydrogels, 20 μl of gel solution was then added directly on top of a PMMA microsphere template and perfused into the template by centrifugation at 700 g for 12 min at 4 °C. The slide was then incubated at 37 °C for 30–45 min to induce polymerization. Once complete, the gels were removed from the PDMS wells and placed directly into 100 % acetone for 48 h to dissolve the PMMA microsphere template. The acetone solution was replaced 2–3 times during this incubation. The gels were then serially hydrated into sterile phosphate buffered saline (PBS) and left in PBS + 1 % penicillin streptomycin (P/S) until ready for use.

#### 5.2.4.2 Fibrin gel formation (F)

Fibrin gels were formed by mixing a solution of fibrinogen (10 mg/ml) with thrombin (2U/ml, Sigma Aldrich, St. Louis, MO) with calcium chloride (5mM). A final volume of 30 μl was gelled in situ.

5.2.4.3 Composite hydrogel formation

Porous hydrogels were generated as described above in 5.2.4.1. The hydrated hydrogels were dabbed with a sterile kimwipe to remove excess fluid and allowed to air dry for an additional 10 min in a sterile hood. The hydrogels were then hydrated with fibrinogen (10 mg/ml) and submerged in a solution of thrombin (Tb, 2 U/ml) and $CaCl_2$ (5mM) to form a porous HA/fibrin composite hydrogel (μ/F). For μ/F/nV composite gels, VEGF nanocapsules (100 % degradable (L) at 50 ng, 25 % degradable (L) at 150 ng) were mixed within the fibrinogen hydration solution prior to submersion into thrombin/$CaCl_2$.

5.2.5 VEGF nanocapsule synthesis

VEGF nanocapsules ($_n$V) were formed as previously described [156] by buffering vascular endothelial growth factor-A (VEGF 165, Genentech, San Francisco, CA) with N-(3-aminopropyl) methacrylamide (APM) and acrylamide (AAm), positively charged and neutral monomers, respectively, and bisacrylated KNRVK peptide crosslinker to surround the protein with the monomers and crosslinkers. A thin polymer layer was formed around the protein by in-situ free-radical polymerization initiated by ammonium persulfate (APS) and tetramethylethyldiamine (TEMED). Protein nanocapsules were dialyzed against 10 mM phosphate buffer pH 7.4 (MWCO 10,000, Thermo Scientific). Encapsulated VEGF concentration was assayed via NanoOrange (Life Technologies, Grand Island, NY), a protein quantification kit per manufacturer's instructions.

5.2.6 Splinted wound healing model

All *in vivo* studies were conducted in compliance with the NIH Guide for Care and Use of Laboratory Animals and UCLA ARC standards. 4 to 6-week old female balb/C mice each 14-20 grams were used. Porous or composite hydrogels were formed as described above and cut to 4

mm in diameter using a sterile biopsy punch, for final overall dimensions of 4mm x 1 mm, D x H. In fabricating the hydrogels, the starting reagents were sterilized through filtering with a 0.22 μm filter. After scaffold fabrication, the hydrogels were washed with sterile PBS and kept in PBS with 1 % P/S. Immediately prior to surgery, mice were anesthetized with 3-3.5 % isoflurane through a nose cone inhaler. After anesthesia induction, the isoflurane concentration was lowered to 1.5-2 % for the remainder of the surgery. The back of the mouse was subsequently shaved and all remaining hair was removed with Nair (≤ 1 min total exposure time). The back of the mouse was sterilized with povidone-iodine (Betadine, Stamford, CT) and 70 % alcohol in three iterations. Two symmetric full-thickness wounds were generated using a through-and-through punch with a 4 mm biopsy punch and the hydrogels were placed directly into the wounds. Sterilized silicon rings (6 x 0.5 mm, DxH) sandwiched between two sterile pieces of Tegaderm (i.e. splints with non-stick, clear windows) were fixed to the outside of the wound using a combination of tissue adhesives, Mastisol and Vetbond. The splints were then lightly pressed down to contact the hydrogel and adhere to the skin bordering the wound. Six to eight interrupted sutures (5-0 Prolene, Ethicon, Somerville, NJ) were also utilized to hold the splint in place. Finally, additional adhesive (Tegaderm, Baxter, Deerfield, IL) was placed around the outer edges of the splints and the mice were wrapped in an elastic gauze (VetRap, 3M, St. Paul, MN) to further prevent splint removal for the duration of the study. All animals were observed daily for signs of pain and distress. In addition, buprenorphine injections (0.015 mg/ml) were administered every 12 h for the first 48 h post survival surgery. At the end of the study (7 days), animals (n=4) were sacrificed with isoflurane overdose and cervical dislocation. Pieces of tissue (8 mm diameter) were collected from each mouse containing the implant and the surrounding tissue and skin using a biopsy punch and preserved in OCT cryoblocks.

### 5.2.7 *In vivo* quantification and analysis

#### 5.2.7.1 Wound closure

Digital images of wounds at designated time points were used to assess wound closure. A ruler and/or the known diameter of the splint was used as a reference.

#### 5.2.7.2 Immunohistochemistry and immunofluorescence analysis

OCT embedded sections (14 μm thick) were thawed and fixed with cold acetone for 10 min. Sections were then washed with PBS and incubated in blocking buffer (1 % goat serum (Jackson Immuno Research Labs, West Grove, PA) + 0.05 % Tween-20 in PBS) for 1 h at RT before being incubated in primary antibody solution (1:100 rat anti-mouse CD31 (BD Pharmingen, San Diego, CA) and 1:200 rabbit anti-mouse NG-2 (Millipore, Billerica, MA)) overnight at 4 °C. Sections were again washed with PBS and incubated in blocking buffer for 10 min at RT before being incubated for 2 h at RT in secondary antibody solution (1:100 goat anti-rat Alexa 568, and 1:100 goat anti-rabbit Alexa 488 (Invitrogen, Grand Island, NY), and DAPI nuclear stain (1:400 dilution, Invitrogen, Grand Island, NY). Sections were then washed twice in PBS, mounted and imaged using a Nikon C2 confocal microscope. CD31-, NG2-, and DAPI-positive area fractions (%) reported were determined by normalizing the positively stained area to overall image area using ImageJ. All hematoxylin and eosin (H&E) staining of sections was conducted by the Translational Pathology Core Laboratory (TPCL) at UCLA. For each condition (n=4), five images were quantified over three different sections, each ≥ 140 μm apart.

#### 5.2.7.3 Histology evaluation

Cryosections (14 μm thick) were H&E stained and used to assess various aspects of wound healing. Three to four different sections ≥ 140 μm apart were used for histological

analysis of each condition. Re-epithelialization, granulation tissue formation and vascularization, collagen deposition and fibrosis/fibroplasia (early scar formation), and inflammation scores were evaluated by a modified 12-point scoring system [157]. The scores and criteria are listed in **Tables 5.1-4**.

**Table 5.1** Scoring of epidermis/re-epithelialization

| Score | Criteria |
|---|---|
| 0 | No migration. |
| 1 | Minimal re-epithelialization (<10%). |
| 2 | Partial re-epithelialization (incomplete closure). |
| 3 | Complete re-epithelialization without keratin layer formation. |
| 4 | Complete/thick re-epithelialization with keratin layer formation. |

**Table 5.2** Scoring of granulation tissue/vascularization

| Score | Criteria |
|---|---|
| 0 | No granulation tissue. |
| 1 | Early granulation tissue, no vascularization. |
| 2 | Mature granulation tissue, early vascularization. |
| 3 | Mature granulation tissue with mature blood vessel formation |

**Table 5.3** Scoring of collagen deposition/fibroplasia

| Score | Criteria |
|---|---|
| 0 | No collagen deposition/fibroplasias. |
| 1 | Fibroblast proliferation/no collagen deposition. |
| 2 | Fibroblast proliferation with minimal collagen deposition. |
| 3 | Fibroblast proliferation with extensive haphazard collagen deposition. |
| 4 | Extensive organized collagen deposition or complete replacement of dermis with fibrous tissue (mature scar). |

**Table 5.4** Scoring of inflammation

| Score | Criteria |
|---|---|
| 0 | No inflammatory cells. |
| 1 | 1-50 leukocytes per high power field. |
| 2 | 51-100 leukocytes per high power field. |
| 3 | 101-250 leukocytes per high power field. |
| 4 | ≥250 leukocytes per high power field or microabscesses or abscesses present. |

5.2.8 Statistical analysis

Statistical analyses were performed using Prism (GraphPad, San Diego, CA). All data were analyzed using t-tests and represented as mean ± SEM. Single asterisks represent $p<0.05$. A p value<0.05 was considered statistically significant.

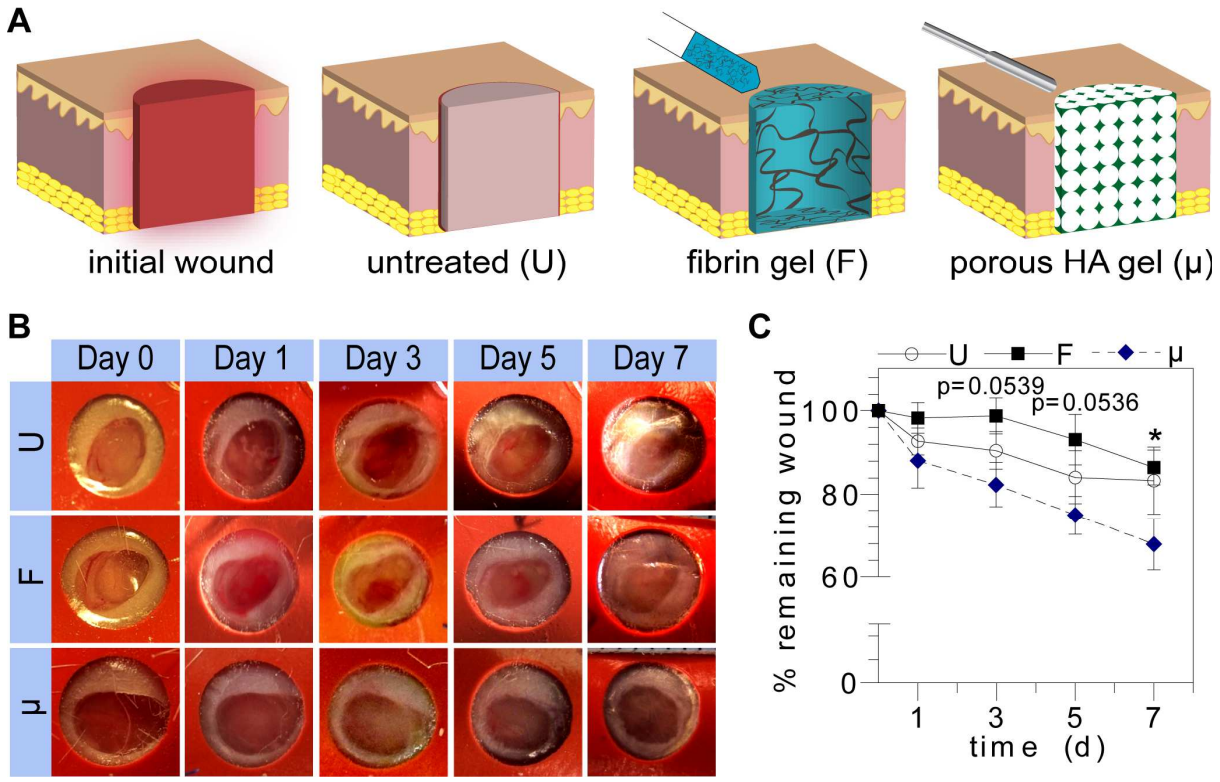


**Figure 5.1 Evaluation of solely conductive natural scaffolds in vivo.** (**A**) Schematic representation of untreated (U), fibrin (F), and microporous HA (μ) filled wounds following initial wound creation. Digital images of wounds were taken at regular time intervals for wound closure analysis (**B**, **C**).

## 5.3. Results and Discussion

5.3.1 Effect of conductive scaffolds on wound closure

Following creation of a full-thickness dermal wound, the splinted wound bed was either left untreated (U) or treated with a fibrin gel formed in situ (F) or pre-cast porous HA gel (μ) (**Figure 5.1A**). Digital images taken of each wound at regular time intervals demonstrated

wounds treated with μ gels close 1.3 fold more rapidly than U or F treated wounds by day 7 post-injury (**Figure 5.1, C**). Dramatic differences between μ and F treated wounds were realized as early as day 3 post-injury and carried on through day 7, where wound closure was significantly improved with μ treated wounds. Notably, F treated wounds closed more slowly than untreated wounds. This indicates that despite fibrin's intrinsic capacity to stimulate angiogenesis and cellular migration, it is not robust enough to encourage rapid wound closure as compared to a porous hydrogel structure (μ). Although fibrin in general is considered porous due to its fibril structure, we hypothesize that the reason for the decreased wound closure is that at 10 mg/ml of fibrin, the scaffold is too dense and acts as a barrier to overall wound closure.

### 5.3.2 Pathological findings of conductive scaffolds

Sections of skin demonstrate the effect of scaffold architecture on granulation tissue formation (**Figure 5.2A**). Under normal circumstances, complete healing from a full thickness wound results in a depressed fibrotic scar, about 60 % the size of the original wound due to wound contracture. As expected, 7 days after wounding, U wounds demonstrated early signs of this type of scar-healing with the commencement of re-epithelialization, granulation tissue with a modest inflammatory response and early angiogenesis/revascularization. As expected, wounds treated with F demonstrate a similar, large depression, and a similar caliber of granulation tissue formation with early angiogenesis. Healing in the U and F wounds was associated with extensive fibroplasia/fibroblast proliferation, consistent with early scar formation, in the wounded area. Histologically, the presence of μ gels better preserved dermal volume/ tissue architecture and minimizing depression formation. Gross images of U treated wounds depict the gradual wound healing that mimics human healing by re-epithelialization and granulation tissue formation rather than contraction. Wounds treated with F gels indicate similar structure to U treated gels. Histological scoring of the tissues reveal similar re-epithelialization, granulation

tissue, angiogenesis, and inflammatory response in the U, F, and μ wounds, but demonstrated a trend towards deceased fibroplasia and increased angiogenesis/more mature blood vessel formation when compared to U wounds (**Figure 5.2A**). Although fibrin and HA are generally regarded as biocompatible materials with little to no immunogenicity, evaluation of host-material immune response was conducted in good practice.

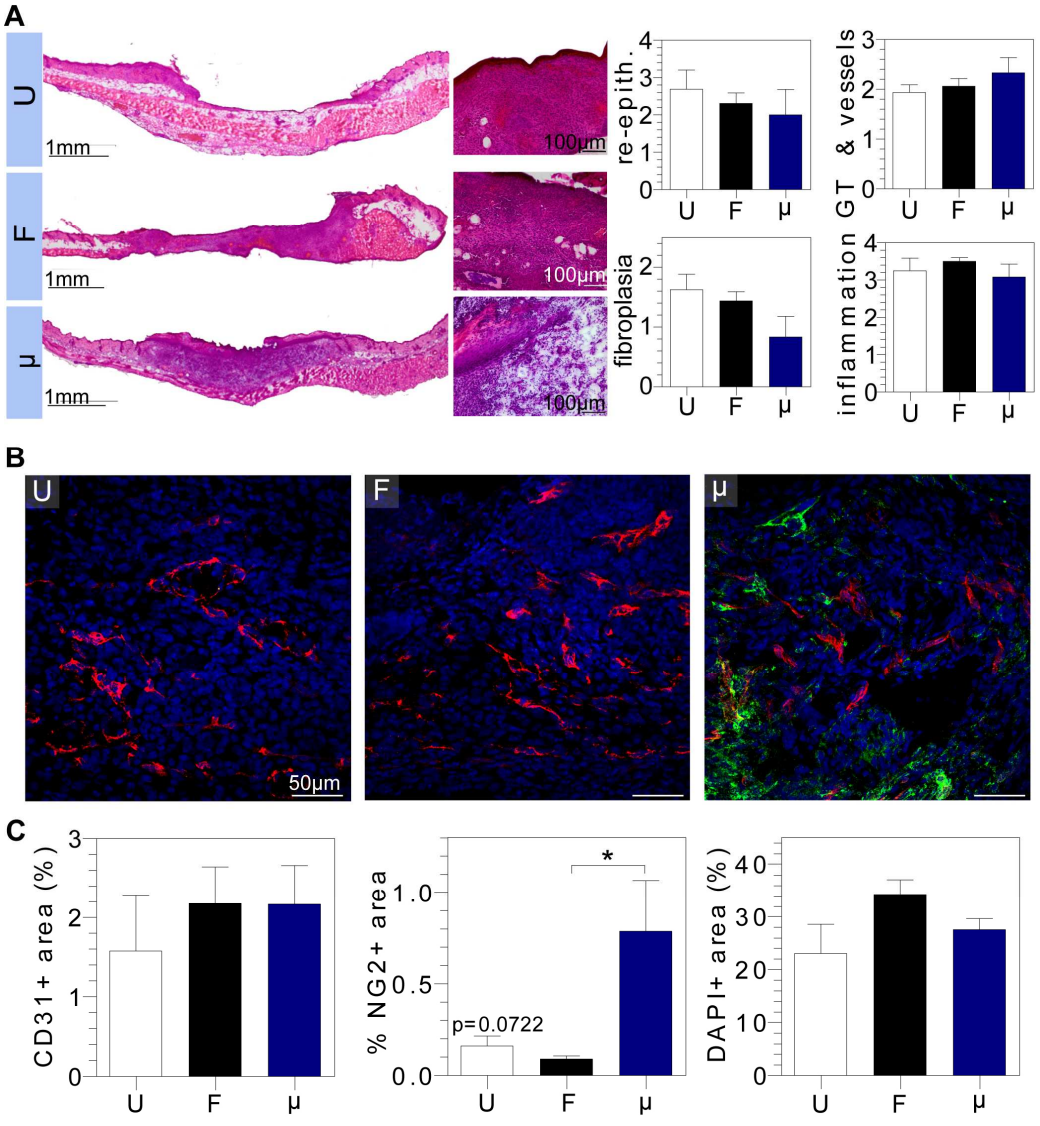


**Figure 5.2 Evaluation of solely conductive natural scaffolds in vivo.** H&E stained wounds depict granulation tissue formation and were scored by a pathologist for re-epithelialization, granulation tissue/vessel formation, fibroplasias, and inflammation (**A**). OCT embedded sections were stained for vascular cell populations (**B**), where CD31+, NG2+, and nuclei imaged in red, green, and blue, respectively, and quantified via imageJ (**C**).

5.3.3 Blood vessel characterization of conductive scaffolds

The effect of conductive scaffolds on vascular ingrowth was evaluated by immunofluorescence (IFC) staining for CD31- and NG2-positive cells in the granulation tissue. IFC staining revealed that blood vessels were present throughout each wound at day 7 regardless of treatment (**Figure 5.2B**). Quantification of CD31-positive endothelial cells show that F and μ treated wounds had an increased number of CD31+ cells (2.18 ± 0.47 %, 2.17 ± 0.50 %, respectively), although not statistically significant when compared to U treated wounds (1.58 ± 0.71 %) (**Figure 5.2C**). Quantification of NG2-positive pericytes demonstrated that μ treated wounds had a marked and statistically significant increase of NG2+ cells when compared to F and U treated wounds, with a 5- and 9-fold increase in NG2+ cells, respectively (**Figure 5.2C**). NG2 is a proteoglycan found on mural cell surfaces of neovascular structures and a marker for pericytes [158]. Its increased presence in μ treated wounds may be attributed to combination of factors that include inherent properties of HA and scaffold porous architecture. Utilizing HA as a scaffold mimics a more native environment since one of the highest concentrations of HA is naturally found in skin [159]. Moreover, HA is one of the most abundant components of the ECM, facilitating cell proliferation and migration [38, 159]. This capacity paired with a porous structure likely allowed for better cell infiltration, including pericyte populations, for more mature vasculature. Quantification of DAPI+ area to assess cell quantity in newly formed granulation tissue formation showed similar cell presence across groups.

5.3.4 Effect of composite gel on wound closure

The effect of scaffold porosity on enhancing wound closure from μ gels was paired with fibrin's natural, protein matrix to investigate the effect of a composite μ/F gel on wound closure in vivo (**Figure 5.3A**). Digital images of the wounds demonstrated that the presence of pores in

the composite gel allow for more rapid healing similar to μ gels when compared to F treated gels alone (**Figure 5.3B, C**). Interestingly, the effect on wound closure rate was not additive despite fibrin's inherent pro-angiogenic qualities being coupled with a porous gel structure to allow for more rapid tissue invasion. This further supports the inclusion of pores as a critical component of scaffold architecture for tissue repair.

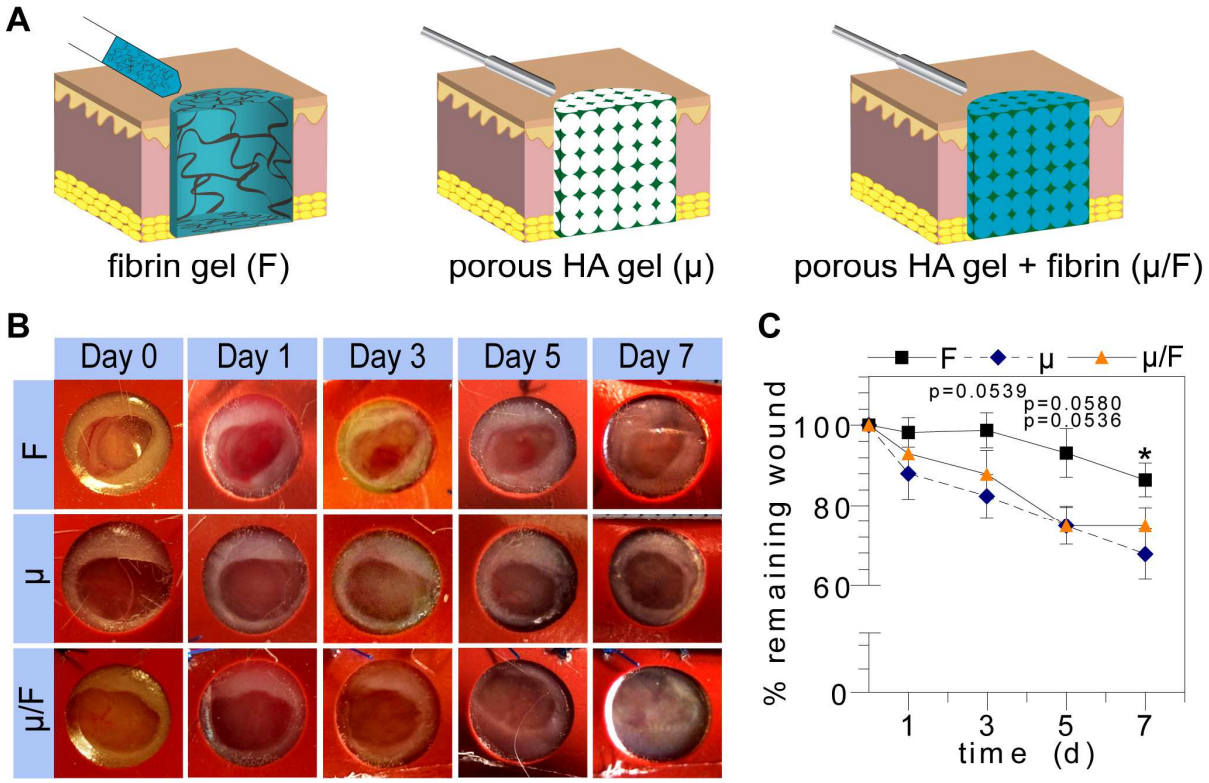


**Figure 5.3 Evaluation of composite natural scaffolds *in vivo*.** (**A**) Schematic representation of wound treated with fibrin (F), microporous HA (μ), or composite (μ/F) hydrogels. Digital images of wounds were taken at regular time intervals for wound closure analysis (**B**, **C**).

### 5.3.5 Pathological findings of composite gel

Histologically, sections of wounded skin demonstrate that the presence of pores in the μ/F gel also maintained the native skin structure for subsequent tissue ingrowth (**Figure 5.4A**). Similar to μ gels, μ/F composite gels demonstrated a trend towards decreased fibroplasia and increased mature angiogenesis within the granulation tissue, with no effects on re-

epithelialization and no increased inflammatory response (**Figure 5.4A**). Fibrin was not observed within the pores of the composite (μ/F) gels at day 7. This suggests that despite being encapsulated by the porous HA gel, components of the wound environment were able to penetrate the pores and degrade the fibrin gel.

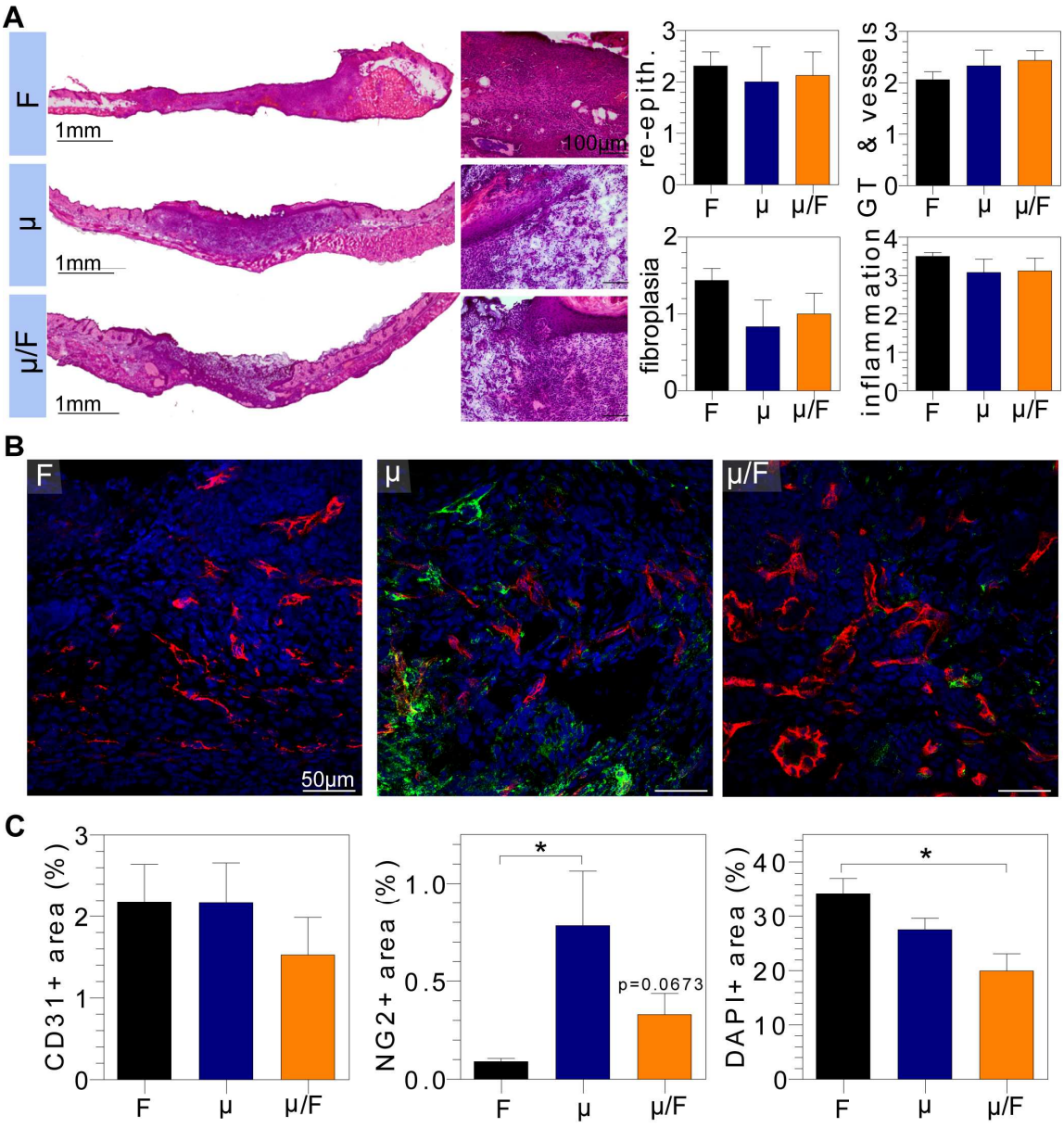


**Figure 5.4 Evaluation of composite natural scaffolds *in vivo*.** H&E stained wounds depict granulation tissue formation and were scored by a pathologist for re-epithelialization, granulation tissue/vessel formation, fibroplasias, and inflammation (**A**). OCT embedded sections were stained for vascular cell populations (**B**), where CD31+, NG2+, and nuclei imaged in red, green, and blue, respectively, and quantified via imageJ (**C**).

### 5.3.6 Blood vessel characterization of composite gels

Immunofluorescence staining of CD31- and NG2-positive cells indicated that blood vessels were present throughout each scaffold-treated wound with and without a porous architecture (**Figure 5.4B**). This suggests that the pro-angiogenic effect of a degradable porous HA hydrogel is comparable to fibrin's natural protein matrix with regard to recruitment of CD31+ endothelial cells. Quantification of CD31+ endothelial cells confirmed that there was no statistical difference among the groups (**Figure 5.4C**). Notably, quantification of NG2+ pericytes demonstrate that the presence of pores in μ and μ/F gels resulted in a significant increase in NG2+ cells, namely a 9- and 4-fold increase for μ and μ/F gels, respectively. Moreover, quantification of DAPI+ area indicated a significant difference between F and μ/F treated wounds, where μ/F gels experienced less cell number within the newly formed tissue, suggesting that the conductive composite gel (μ/F) achieved a higher vascular density, with more mural cell covered vessels than fibrin alone.

### 5.3.7 Effect of inductive composite scaffold on wound closure

To increase the therapeutic potential of the implanted scaffold for wound healing, plasmin-degradable nanocapsules encapsulating VEGF were utilized [160]. VEGF was bound to a cocktail of charged and neutral monomers in addition to peptide crosslinkers via electrostatic and hydrogen-bonding interactions to create nanocapsules, $_{n}$V (**Figure 5.5A**). Variation of these components allows tunable, controlled degradation of the nanocapsules. Since generation of the μ gel requires an organic solvent to dissolve the PMMA microspheres, incorporation of $_{n}$V must occur following μ gel formation. To this end, $_{n}$V was incorporated in the fibrin phase of the μ/F gel to create an inductive composite gel, μ/F/$_{n}$V (**Figure 5.5B**).

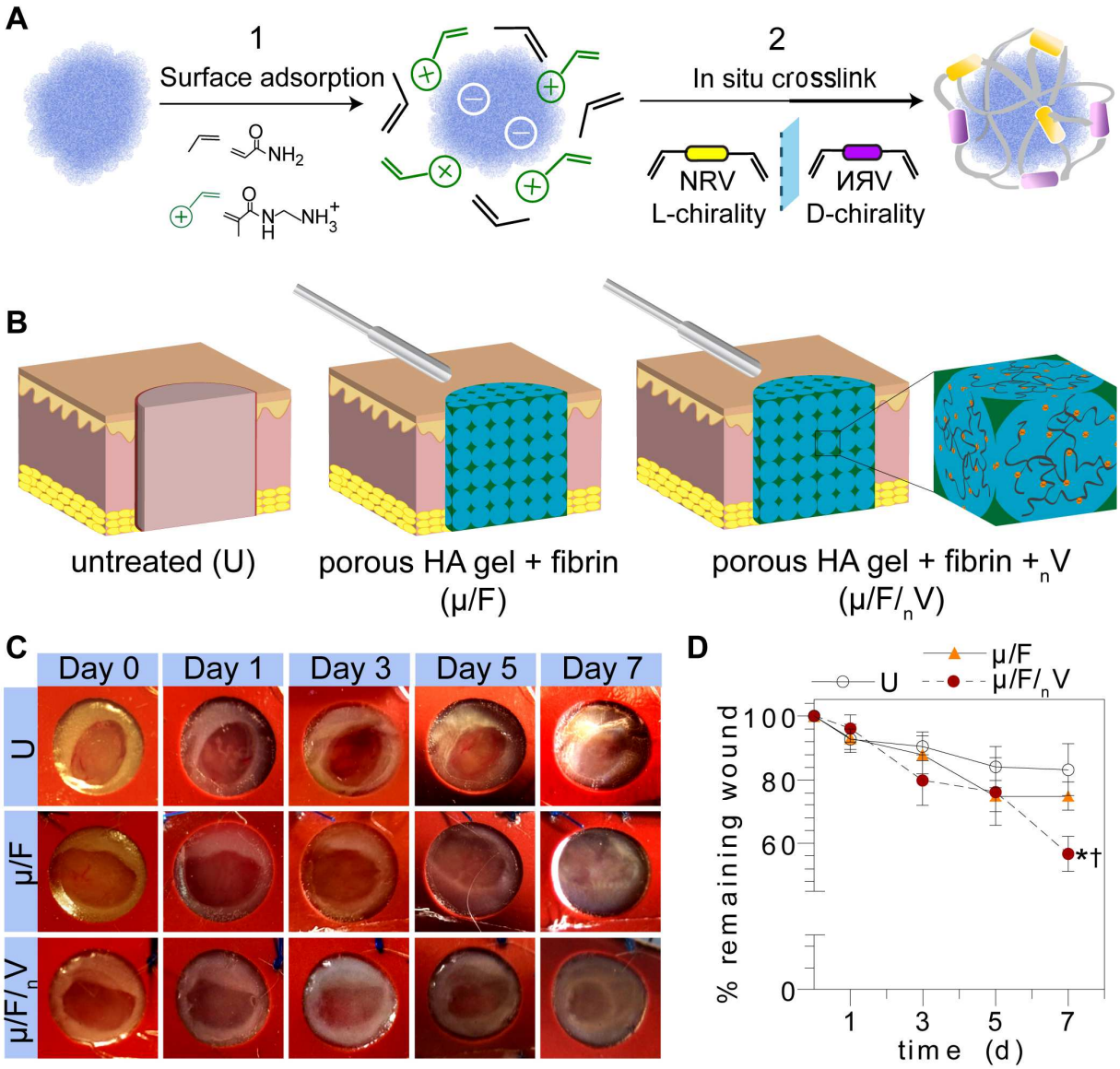


**Figure 5.5 Evaluation of inductive scaffolds *in vivo*.** (**A**) Schematic representation of ₙV synthesis. (**B**) Schematic representation of wounds with various treatments. Digital images of wounds were taken at regular time intervals for wound closure analysis (**C**, **D**).

Digital images of wounds treated with a conductive composite gel, μ/F, was compared to wounds treated with an inductive composite gel, μ/F/ₙV, to evaluate the effect of the VEGF nanocapsules on wound closure (**Figure 5.5C**). Analysis of wound closure demonstrated μ/F/ₙV gels resulted in the significant wound closure by day 7 at 56.75 ± 5.43 % remaining wound, compared to μ/F and U gels at 74.86 ± 4.56 % and 87.23 ± 2.48 %, respectively (**Figure 5.5D**). This degree of wound closure is comparable to full-thickness dermal wounds in C57BL/6 mice

treated with daily topical applications of 10 µg VEGF per wound six days post-injury [43], a total dosage that is 300-fold higher than the amount incorporated in the implanted µ/F/$_n$V gels. Wounds treated with µ/F/$_n$V gels significantly decreased wound size at day 7 by 1.3- and 1.5-fold when compared to µ/F treated and untreated (U) wounds, respectively.

### 5.3.8 Pathological findings of inductive composite scaffolds

Sections of H&E-stained wounds show µ/F/$_n$V treated wounds were integrated similarly to wounds treated with µ/F gels (**Figure 5.6A**). Histological scores indicated partial re-epithelialization, early signs of granulation tissue formation and vascularization, and fibroplasia were similar across groups, although there was a trend towards decreased fibroplasia in the µ/F and µ/F/$_n$V gels, consistent with previous experiments. Although VEGF is regarded as a pro-inflammatory cytokine through its role in increasing vascular permeability and promoting monocyte migration and adhesion of leukocytes to endothelial cells [161], µ/F/$_n$V treated wounds had a decreased inflammatory response when compared U wounds, and to its conductive counterpart, µ/F treated wounds. This diminished inflammatory response may be attributed to the slow release of VEGF from the degradable nanocapsules, $_n$V, as compared to the observed effects in response to bolus dosages reported in literature. Additionally, the slow release of VEGF may result in a more rapid resolution of the inflammatory response due to the continued presence of an inflammatory agent (i.e. immune tolerance mechanism [162]).

### 5.3.9 Blood vessel characterization of inductive composite scaffolds

Immunofluorescence staining of CD31- and NG2-positive cells demonstrated that blood vessels were present throughout the wounds in all groups (**Figure 5.6B**). Quantification of CD31+ endothelial cells confirmed that there was no statistical difference between U, µ/F, and µ/F/$_n$V treated wounds (**Figure 5.6C**). Quantification of NG2+ pericytes showed that wounds

treated with μ/F/$_n$V had increased numbers of NG2+ cells when compared to U and μ/F treated wounds. Wounds treated with μ/F/$_n$V had a 2-fold increase in NG2+ cells compared to μ/F treated wounds while there was a significant difference compared to U treated wounds at a 5-fold increase in NG2+ cells. Quantification of DAPI+ area demonstrated similar cell presence in newly formed granulation tissue where wounds received U, μ/F, and μ/F/$_n$V treatment.

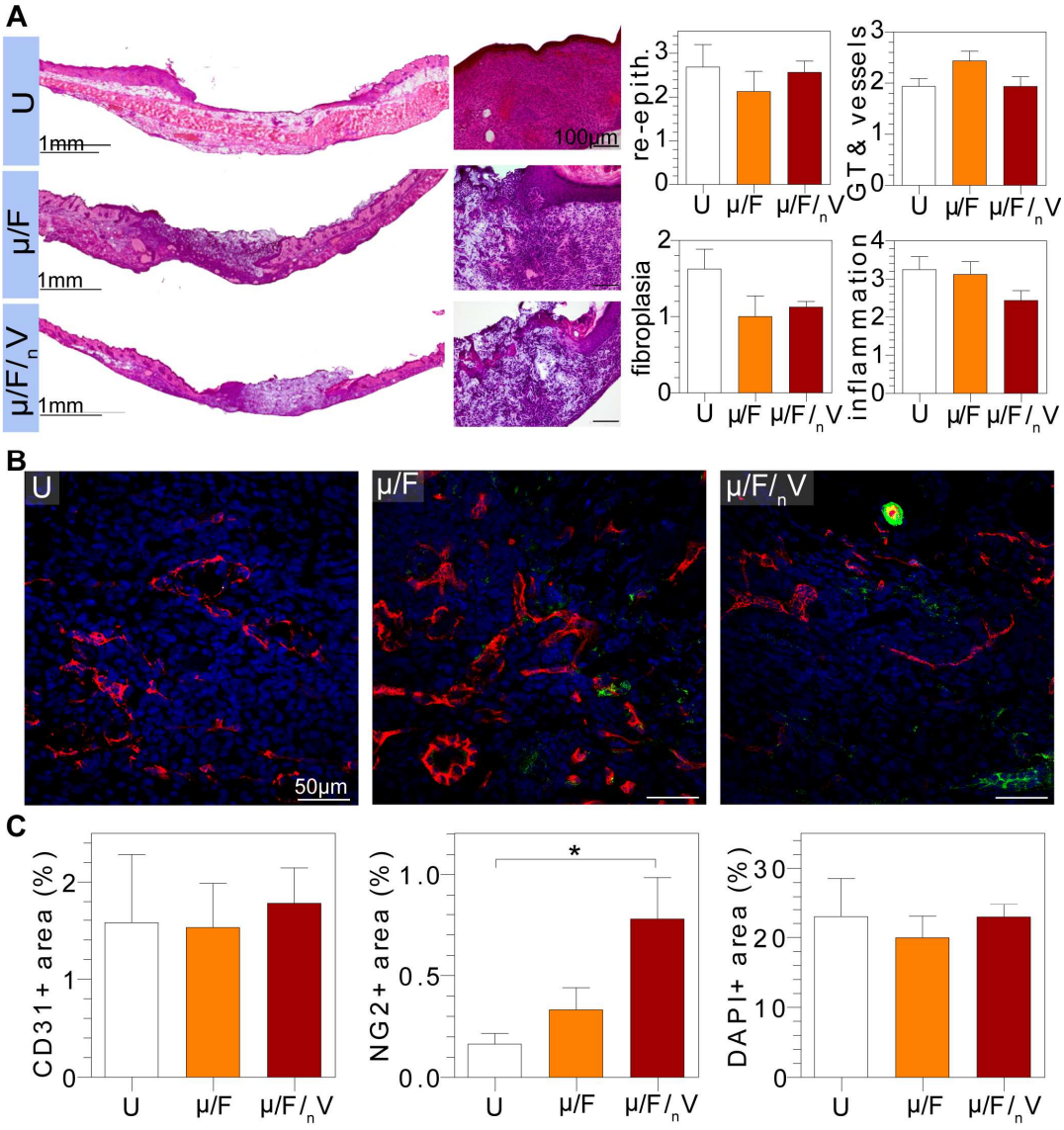


**Figure 5.6 Evaluation of inductive scaffolds *in vivo*.** H&E stained wounds depict granulation tissue formation and were scored by a pathologist for re-epithelialization, granulation tissue/vessel formation, fibroplasias, and inflammation (**A**). OCT embedded sections were stained for vascular cell populations (**B**), where CD31+, NG2+, and nuclei imaged in red, green, and blue, respectively, and quantified via imageJ (**C**).

## 5.4. Conclusions

In this chapter, an *in vivo* splinted wound healing model was utilized to systematically assess the effect of various scaffolds on tissue repair. It is widely accepted that material choice significantly affects host-material interactions, therefore we investigated one of the most commonly used scaffolds, fibrin, and compared it to another naturally found biopolymer, hylauronic acid in the form of a porous hydrogel to evaluate its role in wound healing. Despite its intrinsic pro-angiogenic activity and contribution to wound homeostasis, fibrin alone did not accelerate wound closure. The natural effect of fibrin was enhanced with the addition of VEGF nanocapsules to recapitulate what was observed with a basic empty porous HA scaffold. Although similar vascularization among the various treatments was observed, only wounds implanted with a porous scaffold resulted in increased wound closure and a tissue structure more similar to native skin with significantly more mature vasculature (pericyte coverage) and a trend towards a decreased fibrotic response. These observations were more pronounced with the addition of plasmin-degradable VEGF nanocapsules to create an inductive composite hydrogel.

# CHAPTER 6

# ENHANCED TRANSFECTION FROM DNA-LOADED POROUS HYALURONIC ACID HYDROGELS

## 6.1 Introduction

Gene delivery is an attractive therapeutic approach as it bypasses the complicated process of recombinant protein expression, purification and refolding and can be used to delivery any type of protein (e.g. extracellular, intracellular, membrane bound). Although gene delivery was originally conceived to treat genetic disorders [163-165], it quickly expanded to the treatment of cancer and tissue healing applications. For tissue healing applications, a scaffold is often required in order to provide structural support to the growing tissue while the native tissue regenerates as observed in Chapter 5. Thus, the combination of gene delivery and scaffolds is an ideal approach to provide mechanical support and the bioactive signals needed for tissue regeneration.

The development of materials for nonviral gene delivery has been driven by the promise to provide a safer alternative than the use of viral gene delivery vectors [166]. These approaches have focused on the development of novel nanocondensation or nanoencapsulation strategies that can overcome delivery barriers associated with nonviral gene delivery such as nanoparticle stability, targeted cellular internalization, endosomal escape, nuclear entry and expression [64, 66, 67, 88]. Ultimately these approaches have led to the development of more efficient gene transfer agents for the systemic delivery of genes. However, these same approaches have not been successful in the delivery of genetic material from

scaffolds for localized therapies. Recent scaffold-mediated nonviral gene delivery efforts have primarily focused on surface adsorption of complexed DNA nanoparticles onto electrospun polymer composites [167, 168] or collagen sponges [169, 170] for *in vivo* transfection, where large amounts of DNA are needed (50 – 170 μg DNA per scaffold). Other groups, including ours, have studied the encapsulation of these condensed DNA nanoparticles within a scaffold to achieve more controlled transgene expression mediated by scaffold degradation *in vivo*. Huang et al. demonstrated long-term (15 weeks) *in vivo* transfection from porous PLGA scaffolds loaded with 200 μg condensed DNA with: (i) a reporter plasmid system and (ii) a therapeutic plasmid in a rat cranial defect model [133, 171]. However, this large quantity of condensed DNA did not achieve significant transfection over uncondensed DNA within a scaffold or a bolus injection until 8 weeks post-implantation, suggesting that scaffold material choice dramatically influences DNA availability for transfection. This was clearly illustrated by Meilander-Lin et al. and Trentin et al., where agarose and fibrin gels loaded with only 25 and 10 μg condensed pDNA, respectively, achieved transfection soon after implantation with healing effects when a therapeutic plasmid was used [63, 102]. Moreover, we have recently shown that porous HA hydrogels loaded with 20 μg reporter (pGFPluc) via caged nanoparticle encapsulation (CnE) are able to transfect endogenous cells when implanted in a murine diabetic wound healing model [33]. However at two weeks, the angiogenic response was not enhanced when a proangiogenic plasmid was employed, suggesting that the polyplex availability and/or delivery can be improved.

We hypothesized that gene delivery from our porous hyaluronic acid (HA) hydrogels would be considerably enhanced by an approach that could initiate degradation of our scaffold while retaining our DNA payload, allowing for improved infiltration of endogenous cell populations to release the DNA for transfection via cell-mediated degradation of the matrix. Here we show that pre-treating our DNA loaded porous HA gels with various concentrations of

hyaluronidase (HAase) results in jumpstarting gel degradation without significant loss of DNA in gels loaded via caged nanoparticle encapsulation. This HAase pre-treatment resulted in significant *in vitro* transfection independent of resultant changes in bulk gel stiffness. Moreover, these observations of enhanced transfection was confirmed *in vivo* with a murine wound healing model with a reporter plasmid encoding for green fluorescent protein (pGFP). Enhanced transgene expression motivated our application of this approach to deliver a therapeutic plasmid encoding for vascular endothelial growth factor (pVEGF) in our wound healing model. This substantial improvement in transfection translated to more rapid wound closure, cellular infiltration, and vascularization, offering this approach as a useful tool for tissue repair, and a promising approach for *in vivo* transfection, as a whole.

## 6.2 Materials and methods

### 6.2.1 Materials

Peptides Ac-GCRDGPQGIWGQDRCG-NH2 (HS-MMP-SH) and Ac-GCGYGRGDSPG-NH2 (RGD) were purchased from Genscript (Piscataway, NJ). Sodium hyaluronan (HA) was a gift from Genzyme Corporation (60 kDa, Cambridge, MA). All other chemicals were purchased from Fisher Scientific (Pittsburgh, PA) unless otherwise noted.

### 6.2.2 Hyaluronic acid-acrylate modification

Sodium hyaluronan was modified to contain acrylate functionalities as previously described [154]. Briefly, hyaluronic acid (2.0 g, 5.28 mmol, 60 kDa) was reacted with 18.0 g (105.5 mmol) adipic acid dihydrazide (ADH) at pH 4.75 in the presence of 4.0 g (20 mmol) 1-ethyl-3-[3-dimethylaminopropyl] carbodiimide hydrochloride (EDC) overnight and purified through dialysis (8000 MWCO) in deionized (DI) water for two days. The purified intermediate

(HA-ADH) was lyophilized and stored at -20 °C until used. Approximately 60 % of the carboxyl groups were modified with ADH, which was determined using 1H-NMR ($D_2O$) by taking the ratio of peaks at δ = 1.6 and 2.3 corresponding to the eight hydrogens of the methylene groups on the ADH to the singlet peak of the acetyl methyl protons in HA (δ = 1.88). HA-ADH (1.9 g) was reacted with N-acryloxysuccinimide (NHS-Ac) (1.33 g, 4.4 mmol) in HEPES buffer (10 mM HEPES, 150 mM NaCl, 10 mM EDTA, pH 7.2) overnight and purified through dialysis against a 100 mM to 0 mM salt gradient for 1 day, and then against DI water for 3-4 days before lyophilization. The degree of acrylation was determined to be ~10% using 1H-NMR ($D_2O$) by taking the ratio of the multiplet peak at δ = 6.2 corresponding to the cis and trans acrylate hydrogens to the singlet peak of the acetyl methyl protons in HA (δ = 1.88).

### 6.2.3 DNA/PEI polyplex formation

DNA and PEI (linear, 25 kDa) (N/P=7) were mixed to form nanoparticles through vortexing for 15 s and incubating for 15 min at room temperature before hydrogel formation. Polyplexes were found to be ~140 nm (z-average, diameter) with polydispersity indexes (PDI) ~0.09-0.1.

### 6.2.4 CnE, polyplex lyophilization

For caged nanoparticle encapsulation (CnE), plasmid DNA (100 μg) and L-PEI (91.3 μg) [N/P=7] were mixed in 3.5 ml water in the presence of 35 mg (0.10 mmol) sucrose and incubated at room temperature for 15 min. Following incubation, 1.5 ml low-melting point agarose (0.67 mg/ml) was added prior to lyophilization. Each aliquot was intended for 100 μl hydrogel with DNA at 1 μg/ul.

### 6.2.5 PMMA microsphere template for porous hydrogel formation

Microsphere templates for porous hydrogels were prepared via chemical sintering as previously described [154]. Briefly, commercially acquired PMMA microspheres (53-63 μm dia.) were re-suspended in 1 % acetone in 70 % ethanol at 0.4444 mg/ml. Microspheres (21 mg/well) were pipetted into PDMS wells generated via punching out discs (6mm, dia.) in PDMS sheets (5mm thick) and adhered onto sigmacoted glass slides. The microsphere suspension was incubated at 37 °C for ~1 h to evaporate the acetone/ethanol to leave a neatly packed microsphere template. For CnE, the molds were heat sintered briefly for 1-2 h at 150 °C.

### 6.2.6 Porous hydrogel formation

Hydrogels were formed by Michael-type addition of acrylate-functionalized hyaluronic acid (HA-Ac) with bis-cysteine containing MMP peptide cross-linkers at pH 7.6-7.8. Prior to reaction, a hydrogel precursor solution was generated by mixing HA-Ac with a lyophilized aliquot of cell adhesion peptide, RGD, for 30 min at 37 °C. Following incubation, HA-Ac-RGD was mixed with the remaining HA-Ac and TEOA (0.3 M, pH 8.8) for a final gel concentration of 3.5% w/v% HA. For in vitro and in vivo experiments, the final RGD/HA cluster ratio was 1.17, with 100 μM RGD. Finally, lyophilized aliquots of the cross-linker were dissolved in TEOA (0.05 mg/μl) immediately before addition to a mixture of lyophilized (CnE) or fresh polyplexes and the hydrogel precursor solution. For porous hydrogels, 20 μl of gel solution was then added directly onto the PMMA microsphere template and perfused into the template via centrifugation at 750 g for 10 min at 4 °C. The molds were then incubated at 37 °C for 30 min to induce polymerization. Following polymerization, the gels were submerged in acetone for 48 h with periodic acetone changes to dissolve out remaining PMMA microspheres. The porous hydrogels were hydrated in PBS+1% penicillin-streptomycin (P/S) (pH=7.4) as needed.

### 6.2.7 Polyplex visualization

To visualize the polyplex distribution, hydrated gels with encapsulated DNA via CnE were stained with 1x SYBR Green (Life Technologies, Grand Island, NY) for 2 h. Following a PBS wash, the porous hydrogels were imaged via confocal (Nikon C2) microscopy. The hydrogels were then exposed to HA-ase (5000 U/ml) for 2 h and imaged at the initial exposure settings to visualize the effect of hyaluronidase on DNA release. To better visualize the distribution of the polyplexes throughout the hydrogel, multiple z-stacks were taken for each image and presented as maximum intensity projections.

### 6.2.8 Radiolabeled DNA

#### 6.2.8.1 Radiolabeling and purification

Plasmid DNA was radiolabeled with 32P-dCTP (250 μCi) using a Nick translation kit (Roche, Indianapolis, IN) as per instructed by the manufacturer's protocol. Briefly, an equimolar mixture of dATP, dGTP, dTTP, and 32P-dCTP was prepared and added to the DNA (12.5 μg) solution. Once the enzyme solution was added to the mixture, the final solution was gently mixed by pipetting and incubated for 35 min at 15 °C. The reaction was stopped by addition of 12.5 μl 0.5 M EDTA (pH=8.0) and heating to 65 °C for 10 min. The DNA was purified using the DNA Clean & Concentrator-5 kit (Zymo Research, Irvine, CA) following manufacturer instructions. The hot DNA was diluted to contain 0.15 % radiolabeled DNA.

#### 6.2.8.2 DNA loading and release

Radiolabeled DNA was used in place of naked pDNA to study the DNA loading and release from porous hydrogels as a result of hyaluronidase exposure. The porous hydrogel formation method was the same as previously described for direct encapsulation of fresh

polyplexes (-A/S) and CnE (+A/S). For porous hydrogels with direct encapsulation of fresh polyplexes, a final concentration of 0.12 μg/μl DNA was used per 20 μl hydrogel. For porous hydrogels with CnE, a final concentration of 1 μg/μl DNA was used per 20μl hydrogel. Porous hydrogels with CnE or direct encapsulation of fresh polyplexes ($n \geq 3$) were hydrated in PBS and then exposed to 500 μl HA-ase (0, 100, or 5000 U/ml) for 2 h at 37 °C. The hydrogels were then washed in 500 μl PBS for 10 min at RT to remove any residual HA-ase. Following the wash, all hydrogels were exposed to 500 μl collagenase type I (Col I, 1 U/ml) at 37 °C. At each step, 500 μl of the solution was collected for later analysis. At each indicated time point, 500 μl of the solution was collected and replaced with 500 μl of fresh Col I. Following the final solution collection time point, the hydrogels were collected to be read in order to complete the mass balance. DNA amounts were measured using a scintillation counter at the UCLA Chemistry core facility where each sample (100 μl) was added to 2 ml scintillation cocktail fluid. DNA loading experiments were conducted on porous gels loaded with DNA -A/S or +A/S. Whole gels were read following hydration (0 U/ml HA-ase) and following 2 h HA-se exposure at 100 and 5000 U/ml HA-ase. The readout was analyzed using a standard curve.

6.2.9 *In vitro* transfection

Plasmid encoding for Gaussia luciferase (pCMV-GLuc) was used to study the transfection from porous hydrogels exposed to HAase. The porous hydrogel formation method was the same as previously described for direct encapsulation of fresh polyplexes (-A/S) and CnE (+A/S). The porous hydrogels were hydrated in PBS + 1 % P/S to maintain sterility then exposed to 500 μl HAase (0, 100, or 5000 U/ml) for 2 h at 37 °C. The hydrogels were then washed in 500 μl PBS for 10 min at RT to remove any residual HA-ase. Mouse MSCs were seeded on the surface of the hydrogels by suspending cells (250 μl cells/gel, 1x106 cells/ml) in a 1.5ml tube with 3-4 hydrated porous hydrogels. Surface coating was achieved by inverting

and gently flicking the tube with cells and gels every 20 min for 3 h. Following 3 h, the gels were washed with sterile PBS to remove non-adherent cells and then plated individually in a non-tissue culture treated 48-well plate with fresh 500 µl cDMEM/well. The conditioned media was collected daily and frozen immediately at -20°C for later analysis; each well was replaced with fresh medium.

### 6.2.10 Gaussia luciferase assay

To quantify secreted Gaussia luciferase levels in the media, the collected samples were thawed on ice and assayed using a Biolux Gaussia Luciferase Assay Kit (New England BioLabs, Ipswich, MA) as instructed by the manufacturer's protocol. Briefly, 20 µl of each sample was mixed with 50 µl 1x substrate solution, pipette/mixed for 2-3 s, and read for luminescence with 5 sec integration. Values from the Gaussia luciferase assay were expressed as relative light units (gRLU).

### 6.2.11 Mechanical Characterization

To study the effect of HA-ase pre-treatment on the mechanical stiffness on the gels, porous hydrogels were formed as previously described for 32 µl hydrogels (40 mg microspheres/ 8 mm dia. well). Once hydrated, the gels were exposed to 0, 100, 5000, or 10,000 U/ml HA-ase for 2 h at 37 °C. Following a PBS wash to remove residual HA-ase, the storage and loss moduli were measured using a plate-to-plate rheometer (Physica MCR, Anton Paar, Ashland, VA) with an 8 mm (dia.) plate under a constant strain of 0.1 % and angular frequency ranging from 0.1 to 10 Hz. Hydrogels were generated as described above and cut to 8 mm in diameter using an 8 mm biopsy punch. To prevent the hydrogel from drying, a humidity hood was utilized and the stage was set to 37 °C.

6.2.12 Engineering pEF1α-eGFP-2A-VEGF, biscistronic vector

Preparation of pEF1α-eGFP-2A-VEGF was performed using ligation-free overlap extension PCR cloning with the Gibson assembly mix (New England BioLabs, Ipswich, MA) according to the manufacturer's instructions, a technique adapted from Szymczak-Workman et al [172]. The overlapping gene inserts and linearized backbone were amplified by PCR using Phusion High-Fidelity polymerase (New England BioLabs, Ipswich, MA). DpnI (New England BioLabs, Ipswich, MA) was used to digest the template remaining in the PCR product. Primers were designed to have 20-30 bp of overlap between the insert and the vector.

First, to enable bicistronic, stoichiometric expression of two genes with one promoter, a two-gene insert was prepared with a short, self-cleaving 2A peptide sequence from porcine teschovirus-1 incorporated between the two genes (5'-GGATCCGGAGCCACGAACTTCTCTCTGTTAAAGCAAGCAGGAGACGTGGAAGAAAACCCC GGTCCT-3'). This was done via overlap extension PCR; gene inserts were amplified with overlapping primers containing part of the 2A sequence to produce a (gene A)-2A-(gene B) insert with ends that overlap with the linearized vector. Insertion of this recombinant PCR product into the linearized vector was performed with Gibson assembly. Confirmation of correct vector construction was achieved by performing colony PCR and sequencing of the amplified plasmids.

6.2.13 Splinted wound healing model

All *in vivo* studies were conducted in compliance with the NIH Guide for Care and Use of Laboratory Animals and UCLA ARC standards. Female balb/C mice each aged 4-6 weeks and weighing 16-20 grams were used. Porous hydrogels containing pEF1α-eGFP-2A-VEGF were formed as described above and cut to 4 mm in diameter using a sterile biopsy punch, for final overall dimensions of 4mm x 1 mm, D x H. In fabricating the hydrogels, the starting reagents

were sterilized through filtering with a 0.22 μm filter. After scaffold fabrication, the hydrogels were stored in acetone until surgery day. On the day of surgery, the hydrogels were hydrated and exposed to various HA-ase treatments for 2 h, then washed with sterile PBS and kept in PBS with 1 % P/S. Immediately prior to surgery, mice were anesthetized with 3-3.5 % isoflurane through a nose cone inhaler. After anesthesia induction, the isoflurane concentration was lowered to 1.5-2 % for the remainder of the surgery. The back of the mouse was subsequently shaved with all remaining hair was removed with Nair (≤ 1 min), and finally sterilized with povidone-iodine (Betadine, Stamford, CT) and 70 % ethanol. Two full-thickness wounds were then generated using a 4 mm biopsy punch and the hydrogels were placed directly into the wounds. Sterilized silicon rings (6 mm dia., 0.5 mm thick) sandwiched between two sterile pieces of Tegaderm (i.e. splints with non-stick, clear windows) were fixed to the outside of the wound using tissue adhesives, Mastisol and Vetbond. The splints were then lightly pressed down to generate contact with the hydrogel and skin bordering the wound. Eight interrupted sutures (5-0 Prolene, Ethicon, Somerville, NJ) were also utilized to hold the splint in place. Finally, additional adhesive (Tegaderm, Baxter, Deerfield, IL) was placed around the outer edges of the splints and the mice were wrapped in an elastic gauze (VetRap, 3M, Saint Paul, MN) to further prevent the splint removal for the duration of the study. All animals were observed daily for signs of inflammation and pain. Buprenorphine injections were administered every 12 h for the first 48 h post survival surgery. At each time point (5 and 10 days, n=4-6), animals were sacrificed with isoflurane overdose and cervical dislocation. 8 mm diameter pieces of tissue were collected from each mouse containing the implant and the surrounding tissue and skin using a biopsy punch and preserved in OCT cryoblocks.

6.2.14 Wound closure

Digital images of wounds at designated time points were used to assess wound closure. A ruler and/or the known diameter of the splint were used as a reference.

6.2.15 Immunofluorescence and Immunohistochemistry

OCT embedded sections (25 μm thick) were thawed and fixed with cold acetone for 10 min. Sections were then washed with PBS and incubated in blocking buffer (5% normal goat serum (Jackson Immuno Research Labs, West Grove, PA) + 0.05% Tween-20 in PBS) for 1 h at RT before being incubated in primary antibody solution (1:100 rat anti-mouse CD31 (BD Pharmingen, San Diego, CA), 1:200 rabbit anti-mouse NG-2 (Millipore), 1:100 rat anti-mouse Ly6G, 1:100 mouse anti-mouse fibroblasts) overnight at 4 °C. Sections were again washed with PBS and incubated in blocking buffer for 10 min at RT before being incubated for 2 h at RT in secondary antibody solution (1:100 goat anti-rat Alexa 568, 1:100 goat ant-mouse Alexa 555, and 1:100 goat anti-rabbit Alexa 488 (Invitrogen, Grand Islands, NY), and DAPI nuclear stain (1:500 dilution, Invitrogen, Grand Island, NY). Sections were then washed twice in PBS, mounted and imaged using a Nikon C2 confocal microscope. All hematoxylin and eosin (H&E) staining of sections was conducted by the Translational Pathology Core Laboratory (TPCL) at UCLA.

6.2.16 Quantification and characterization of transfection and immune response in vivo

Three separate sections (25 μm thick) at least 150 μm apart were analyzed for each sample to obtain representative data. Five areas (one at each wound edge, three along the wound) were imaged on each vertical cross-section at 40X magnification with a water immersion lens, with 15 images total per animal. GFP+ and Ly6G+ area was quantified by

using ImageJ software. A threshold was applied to capture positive signal based on fluorescence intensity; positively stained areas were normalized to the total imaged area.

6.2.17 Quantification and characterization of cellular infiltration and blood vessels in vivo

Three separate sections (25 μm thick) at least 150 μm apart were analyzed for each sample to obtain representative data. For blood vessel characterization, three areas (one at each wound edge, one in the center) were imaged on each vertical cross-section at 20X magnification, with 9 images total per animal. CD31+, NG2+, and DAPI+ area was quantified by using ImageJ software. A threshold was applied to capture positive signal based on fluorescence intensity; positively stained areas were normalized to the total imaged area.

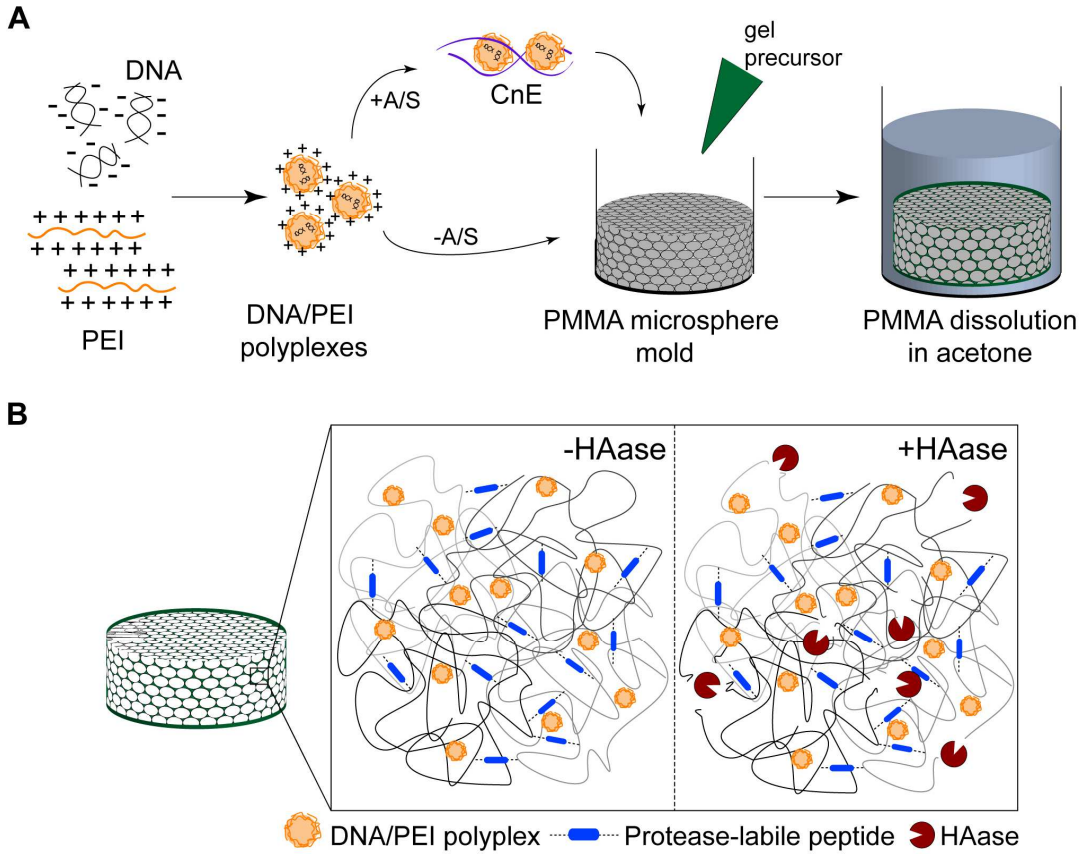


**Figure 6.1. Approach for releasing DNA/PEI polyplexes for enhanced transfection.** (**A**) Schematic of DNA loading, porous hyaluronic acid (HA) gel formation, and the effect of hyaluronidase (HAase) (**B**).

## 6.3 Results and Discussion

### 6.3.1 Effect of HAase on DNA loading and release

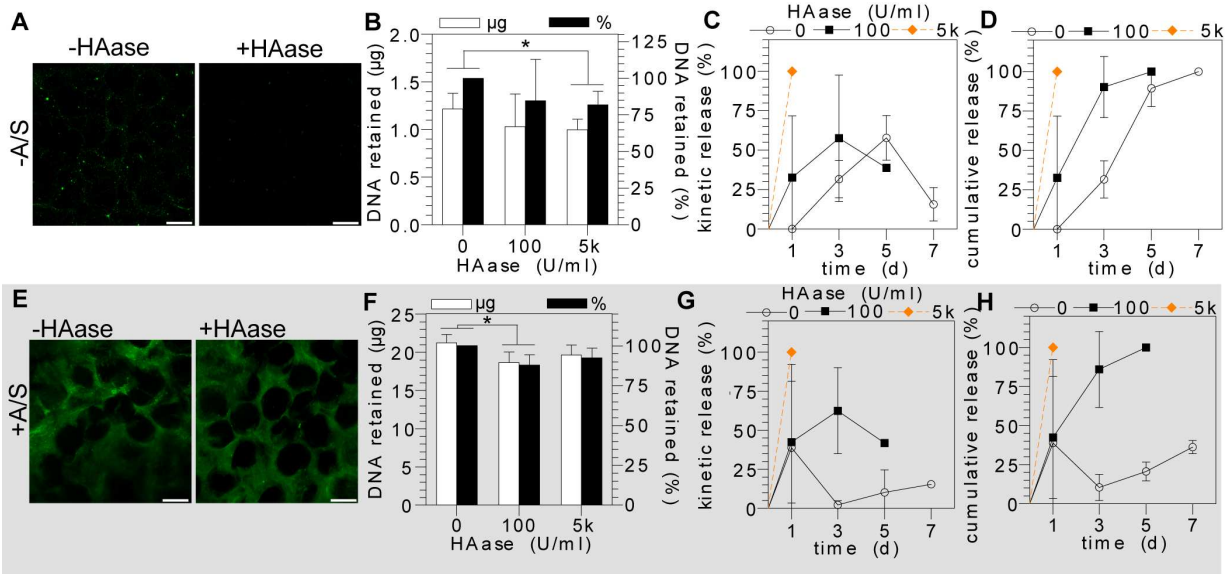


**Figure 6.2 DNA/PEI polyplexes release as a function of HAase concentration.** DNA loaded porous HA gels via direct encapsulation (-A/S) were imaged via fluorescent microscopy to evaluate stained DNA intensity before and after 5 kU/ml HAase treatment (**A**), and DNA retention (*p<0.05, t-test; **B**) and release due to enzymatic degradation (**C**, **D**) was quantified with radiolabeled DNA as a result of various HAase treatments. Similarly, DNA loaded porous HA gels via caged nanoparticle encapsulation (+A/S) were (**E**) imaged via fluorescent microscopy to evaluate stained DNA intensity before and after 5 kU/ml HAase treatment, and DNA retention (*p<0.05, t-test; **F**) and release due to enzymatic degradation (**G**, **H**) was quantified with radiolabeled DNA. Data represent the mean±SD. Scale bars, 50 µm.

To validate our previously developed technique to achieve high DNA loading within our porous HA gels, we generated DNA loaded hydrogels via two approaches in parallel and studied DNA retention, enzyme-mediated release, and in vitro transfection as a result of exposure to various concentrations of HAase, ranging from 0 to 5 kU/ml (**Figure 6.1A, B**). In the first commonly used approach (-A/S), nonviral plasmid DNA was complexed to linear polyethyleneimine (PEI) to form DNA/PEI polyplexes to be directly encapsulated within the gel precursor to form a porous HA hydrogel. In the second approach (+A/S), caged nanoparticle encapsulation (CnE) was employed where the DNA/PEI polyplexes were lyophilized in the presence of agarose and sucrose prior to porous gel formation to achieve higher DNA loading

with minimal aggregation within the gel [31, 113, 173]. DNA retention was visually evaluated by fluorescence imaging of DNA loaded gels stained for DNA before and after exposure to HAase at 5 kU/ml (**Figure 6.2A, E**). The significant decrease in fluorescence intensity (stained DNA) in gels loaded with direct DNA encapsulation (-A/S) was confirmed with radiolabeled DNA retention studies where 18 % of DNA was lost due to the HAase treatment (**Figure 6.2B**). Conversely, porous gels loaded via CnE (+A/S) maintained high fluorescence intensity and experienced a moderate loss of DNA at 7.64 % due to HAase exposure (**Figure 6.2F**). Notably, gels generated +A/S were able to achieve 18-fold higher DNA loading than its counterpart, -A/S, making it an attractive delivery system for localized, sustained transfection.

We hypothesized that HAase would degrade fragments of hyaluronic acid to increase the physical availability of our MMP-degradable peptide crosslinks for cell-mediated enzymatic degradation and ultimate release of polyplexes for transfection. We tested radiolabeled DNA/PEI polyplex release from DNA loaded porous gels. Following exposure to various HAase concentrations for 2 h, the porous gels were submerged in collagenase I (1 U/ml) and DNA release was monitored daily. In both DNA loaded systems, -A/S and +A/S, we observed that an increased concentration of HAase pre-treatment resulted in more rapid DNA release and gel degradation (**Figure 6.2C, D -A/S; Figure 6.2G, H +A/S**). More specifically, DNA loaded gels pre-treated with 5k and 100 U/ml HAase degraded within 24 h and 5 d, respectively, following exposure to collagenase I. This confirms that HAase does indeed initiate HA gel degradation and the degree of degradation is dependent on HAase concentration and further enhanced following exposure to matrix metalloproteinases (MMPs).

### 6.3.2 HAase pre-treatment enhances *in vitro* transfection

The effect of HAase pre-treatment on *in vitro* transfection was investigated by generating porous gels loaded with a secreted reporter plasmid encoding for gaussia luciferase, via -A/S or

+A/S. Following exposure to various concentrations of HAase (2 h) and sterile PBS rinses, porous gels were thoroughly coated with mouse mesenchymal stem cells (mMSCs) and assayed for transfection from daily collections of media (**Figure 6.3A**). Transfection was similar in gels loaded with direct encapsulation of DNA (-A/S) regardless of HAase treatment (**Figure 6.3B, C**). Conversely, DNA loaded porous gels +A/S experienced significant differences in transfection as a result of HAase pre-treatment concentration (**Figure 6.3E, F**). Exposure of DNA loaded gels to moderate HAase (100 U/ml) resulted in 7- to 16-fold increase in transfection when compared to gels with no HAase treatment (0 U/ml) (**Figure 6.3E**). This increase in transfection was more striking when compared to DNA loaded gels pre-treated with a high concentration of HAase (5k U/ml), where differences ranged from 30- to 59-fold (**Figure 6.3E**). Notably, *in vitro* transfection is sustained over 7 d with porous gels loaded +A/S (**Figure 6.3E**) as compared to gels loaded with direct encapsulation (-A/S, **Figure 6.3B**). This may be attributed to the total amount of DNA loaded within the gels; gels loaded with direct encapsulation (-A/S) have approximately 18-fold less DNA than +A/S gels. Cumulative transfection from gels loaded with direct encapsulation (-A/S) with various HAase treatments were low and similar to untreated gels +A/S (**Figure 6.3C**). HAase pre-treatment significantly increased cumulative transfection in gels loaded +A/S by 1 and 2 orders of magnitude for gels pre-treated with 100 and 5k U/ml HAase, respectively (**Figure 6.3F**). This demonstrates the necessity of gels loaded with DNA to employ CnE (+A/S) to increase the DNA payload in a gel for sustained transgene expression, and the significant impact of HAase pre-treatment in enhancing transfection in vitro. Moreover, the level of transfection was 1-2 orders of magnitude higher than previously achieved in our lab [31], demonstrating the effect of HAase on enhancing *in vitro* transfection.

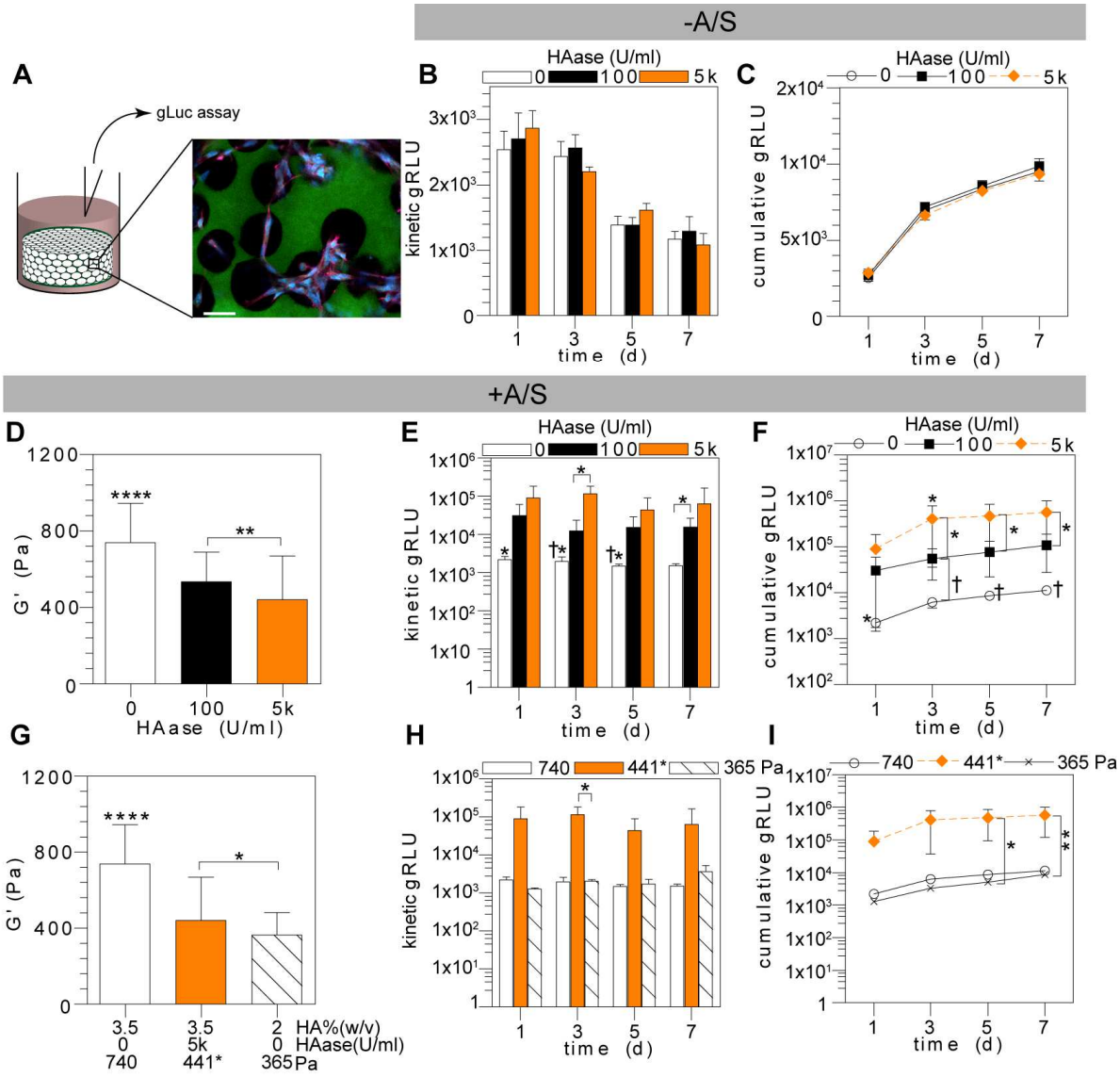


**Figure 6.3 HAase improves *in vitro* transfection with gels containing high DNA payload**. (**A**) Schematic of gaussia luciferase assay conducted to test in vitro transfection with fluorescent image of mMSCs migrating within the porous hyaluronic acid hydrogel. Gel, green; phalloidin, red; nuclei, blue. DNA loaded porous HA gels via direct encapsulation (-A/S) were assayed for gaussia luciferase and transfection was represented in kinetic relative light units (RLU) (**B**), and cumulative RLU (**C**) DNA loaded porous HA gels via caged nanoparticle encapsulation (+A/S) were evaluated for changes in mechanical properties due to HAase treatment (****p<0.0001, t-test; **p<0.01, t-test; **D**) and similarly assayed for gaussia luciferase, where transfection was represented in kinetic RLU (*p<0.05, t-test; †p<0.01, t-test; **E**) and cumulative RLU (*p<0.05, t-test; †p<0.01, t-test; **F**). To decouple the effect of stiffness from HAase treatment, softer gels were generated and confirmed with rheology, where the asterisk by 441Pa denotes the gel with HAase treatment (****p<0.0001, t-test; *p<0.05, t-test; **G**) and employed to test transfection of plasmid encoding for gaussia luciferase (*p<0.05, t-test; **H**, *p<0.05, t-test; **p<0.01, t-test; **I**). Data represent the mean±SD. Scale bar, 50 μm.

Since HAase degrades the porous HA hydrogel, it was important to study its effect on gel mechanical properties. Rheological analyses of DNA loaded porous gels +A/S were

performed following various HAase treatments for 2 h demonstrate that bulk gel stiffness significantly decreased with increasing HAase treatment concentration (**Figure 6.3D**). To decouple the effect of bulk gel stiffness from HAase treatment on transfection, we generated 2 % (w/v) HA porous gels with a lower initial storage modulus (365 Pa), where the gels were significantly softer than 3.5 % (w/v) HA porous gels without (740 Pa), and with 5k U/ml HAase treatment (441 Pa) (**Figure 6.3G**). Transfection from the 365 Pa gels without HAase treatment was significantly lower than a 441 Pa gels with HAase treatment, and similar to gels with higher moduli without HAase treatment (740 Pa) (**Figure 6.3H, I**). This demonstrates that enhanced transfection can be attributed HAase treatment of the gels and not simply due to low bulk mechanical stiffness.

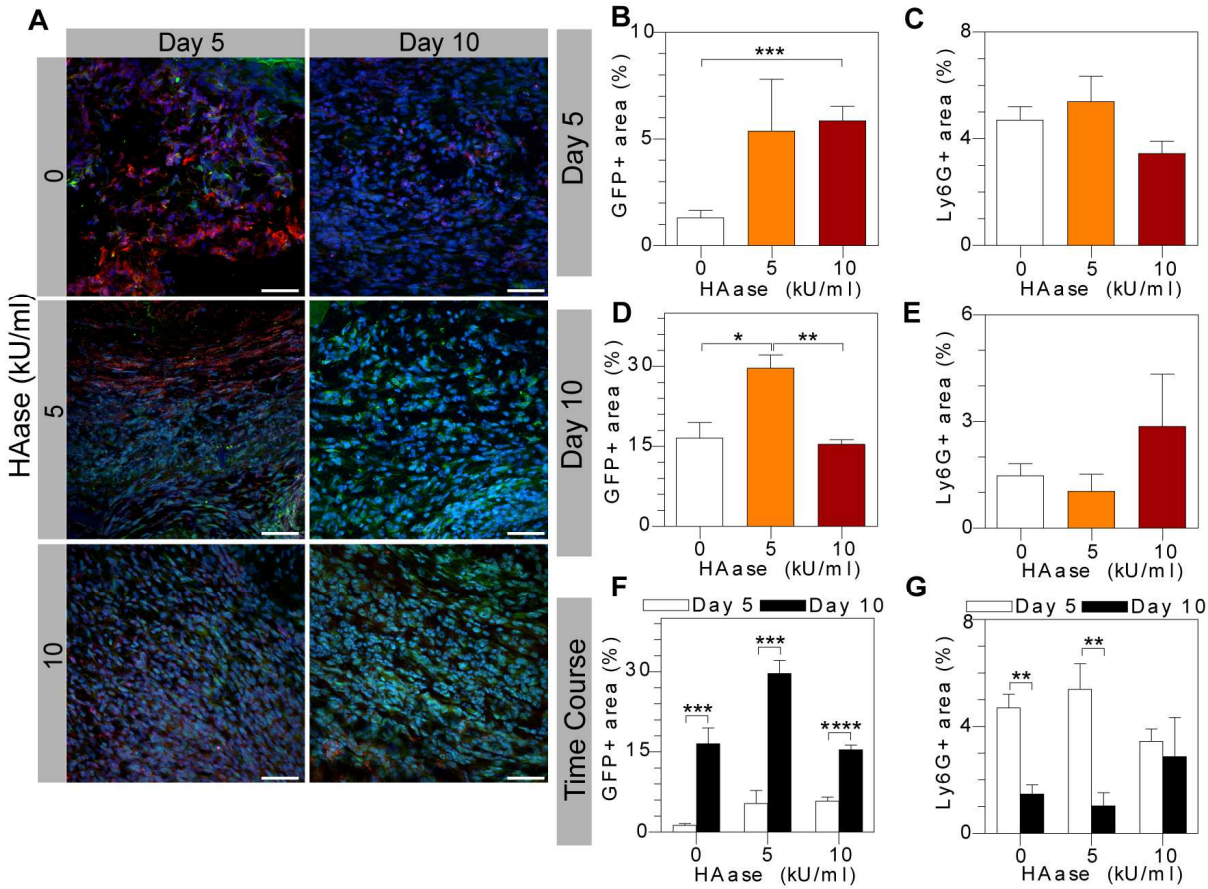


**Figure 6.4 HAase pre-treatment enhances transfection *in vivo* in murine wound healing model.** (**A**) Representative staining of tissue cross sections for GFP (green), Ly6G (red), and nuclei (blue) of wounds 5 and 10 days post-implantation with DNA loaded porous HA gels following various HAase treatment. Quantification of GFP+ and Ly6G+ area was evaluated at day 5 (***p<0.001, t-test; **B**, **C**) and day 10 (*p<0.05, t-test; **p<0.01, t-test; **D**, **E**) by measuring area from 5 random regions per tissue section across three different sections at least 150 μm apart (n=4-6). GFP transfection increased over time (***p<0.001, t-test; ****p<0.0001, t-test; **F**) while the immune response became quiescent (**p<0.01, t-test; **G**). Data represent the mean±SEM. Scale bars, 50 μm.

### 6.3.3 HAase pre-treatment enhances transfection *in vivo*

Due to the enhanced in vitro transfection from gels loaded with DNA +A/S as compared to direct encapsulation (-A/S), we decided to employ DNA loaded gels +A/S as our delivery system for our in vivo studies. We performed a human-relevant murine splinted wound healing model where full-thickness dermal wounds were created in the backs of balb/c mice and splinted open to allow for re-epithelialization and granulation, rather than skin contraction, as the primary mode of healing.[174] Porous gels loaded with a plasmid encoding for a reporter

protein, GFP, were treated with various HAase concentrations and implanted in the wounds to study transfection 5 and 10 days post-injury. HAase pre-treatment concentrations were selected to be 0 and 5 kU/ml to reflect our in vitro transfection observations. We also investigated DNA loaded porous gels pre-treated with 10 kU/ml HAase to assess whether a higher HAase concentration would result in even more enhanced transfection as compared to 5 kU/ml. Tissue sections were stained for GFP+ and Ly6G+ cells, indicative of the presence of transfected cells and neutrophils/immune cells, respectively (**Figure 6.4A**). At day 5, we observed a 4-fold increase in transfection (GFP+ area) in wounds implanted with DNA loaded gels pre-treated with HAase when compared to the control (0 kU/ml) suggesting that the HAase pre-treatment is necessary for enhanced in vivo transfection (**Figure 6.4B**). Analysis of Ly6G+ area demonstrates similar immune response to the scaffolds at day 5 (**Figure 6.4C**). Transfection persisted through 10 days, where DNA loaded porous gels pre-treated with 5 kU/ml HAase resulted in highest transfection when compared to 0 and 10 kU/ml HAase treated gels (**Figure 6.4D**). Again, similar immune response was observed across groups by day 10 (**Figure 6.4E**). This study demonstrates that transfection from DNA loaded porous gels significantly increases over time as endogenous cells infiltrate the gel, and the overall transfection is enhanced with pre-treatment of the gel with HAase (**Figure 6.4F**). Moreover, since untreated (0 kU/ml) gels resulted in eventual increased transfection, this investigation suggests that the degree of transfection can be temporally shifted by tuning the concentration of the HAase pre-treatment prior to implantation. Additionally, it is important to note that the immune response to these implanted DNA loaded porous gels aligned with a response expected for an acute wound, where neutrophil presence is high at the onset of the inflammatory phase in response to injury and diminishes within several days for tissue remodeling to occur (**Figure 6.4G**) [175].

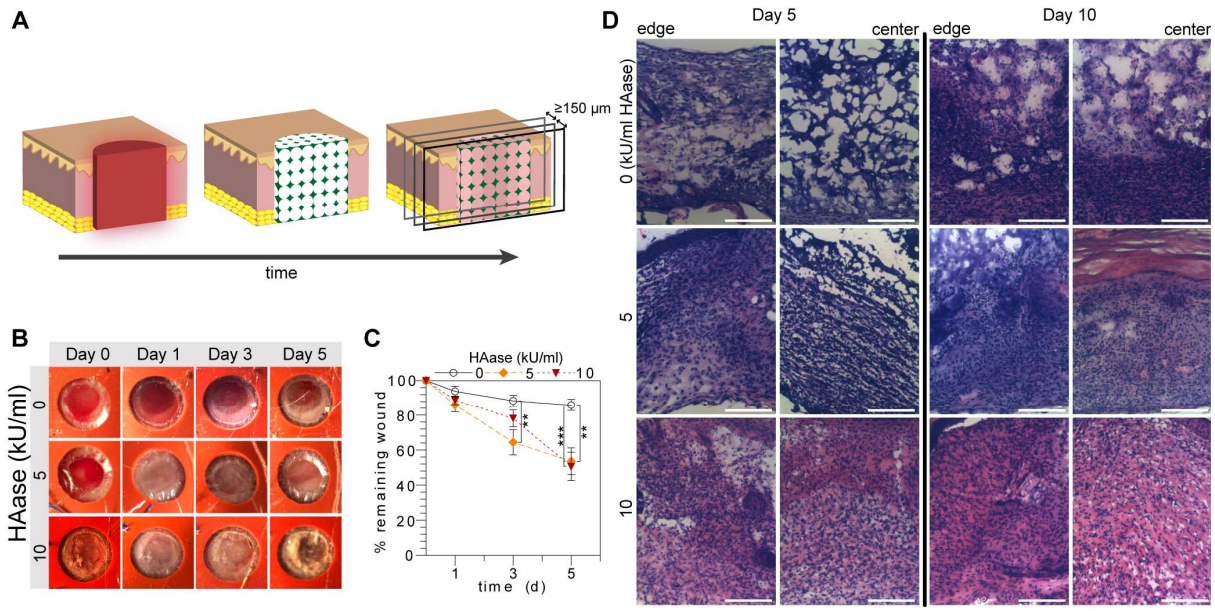


**Figure 6.5 HAase pre-treatment of porous HA gels loaded with therapeutic proangiogenic plasmid leads to more rapid wound closure in a murine wound healing model.** (**A**) Schematic of initial wound, implantation with DNA loaded porous HA gel, and newly formed tissue over time. (**B**) Wound closure was visually observed via digital photography over time and wound area was quantified to assess the effect of HAase-mediated transfection with a therapeutic plasmid (n=10-11) (**p<0.01, t-test; ***p<0.001, t-test; **C**). (**D**) Representative H&E stained wound cross sections show the degree of cellular infiltration from the edge to the center at day 5 and 10 as a result of various HAase pre-treatments. Scale bars, 125 µm (**D**)

### 6.3.4 *In vivo* transfection with a therapeutic plasmid encoding for VEGF

To evaluate *in vivo* transfection with a therapeutic plasmid, we employed porous hydrogels loaded with plasmid encoding for vascular endothelial growth factor (VEGF), a potent regulator of angiogenesis, and assessed wound closure, cellular infiltration, and vascularization within the newly formed granulation tissue. Digital images taken of wounds implanted with DNA loaded porous gels treated with various HAase concentrations demonstrate substantial wound closure with HAase pre-treatment by day 5 (**Figure 6.5B**). Differences in wound closure was confirmed with quantification of wound area over time, where wound area was significantly smaller with wounds implanted with gels pre-treated with 5 kU/ml HAase (53.64 ± 7.12 %) and 10 kU/ml HAase (50.64 ± 8.04 %) as compared to untreated gels (0 kU/ml, 85.97 ± 3.23 %) suggesting that wound healing was improved with enhanced transfection of the pro-angiogenic plasmid (**Figure 6.5C**). Moreover, evaluation of histological staining of wound cross sections

showed that gels with increasing HAase concentration pre-treatment resulted in a greater degree of cellular infiltration from the edge of the implanted gel through the center (**Figure 6.5D**). This increased cellular infiltration may be attributed to a variety of reasons that include bulk stiffness and transfection. Decreased bulk mechanical stiffness of the gels as a result of HAase degrading the HA polymer chains increases the physical availability of infiltrating cells to enzymatically degrade the MMP-sensitive crosslinkers. This in turn allows cells to more easily migrate and degrade the surrounding gel, creating more routes for infiltration. Additionally, successful transfection and resultant VEGF expression alone may also increase cellular infiltration since VEGF induces endothelial cell migration and proliferation [176, 177]. Immunofluorescence staining for vascularization focused on CD31+ and NG2+ cell populations within the newly formed granulation tissue, indicative of endothelial and mural cells, respectively (**Figure 6.6A**). At day 5 post-injury, newly formed granulation tissue in wounds treated with DNA loaded gels had a positive trend in CD31+ endothelial cells with increasing HAase pre-treatment concentrations, where gels pre-treated with 5 and 10 kU/ml HAase had 24- and 55-fold increase, respectively, in CD31+ area compared to its untreated counterpart (0 kU/ml) (**Figure 6.5B**). NG2+ staining demonstrated increased mural cell populations in wounds implanted with gels pre-treated with 5 kU/ml HAase (**Figure 6.5C**). Quantification of DAPI+ area to evaluate cell populations within the newly formed granulation tissue as a result of various HAase pre-treatments in DNA loaded porous gels confirmed histological observations (**Figure 6.5D**), where HAase pre-treated (5 and 10 kU/ml, respectively) gels had a marked and significant increase in cell populations ranging from 2.73- and 4.16- fold greater than untreated gels at day 5 (**Figure 6.6D**). At day 10, CD31+ stained endothelial cell area was sustained where DNA loaded porous gels pre-treated with 10 kU/ml HAase had the greatest population of endothelial cells (**Figure 6.6E**). Quantification of NG2+ and DAPI+ area was similar among the groups (**Figure 6.6F, G**). This evaluation of wound vascularization demonstrates that transgene expression of a potent

pro-angiogenic regulator can be enhanced with HAase pre-treatment and achieve sustained CD31+ and NG2+ cell populations over the course of 10 d (**Figure 6.6H, I, J**). This is especially significant since the proliferative stage of wound healing occurs 2-10 days post-injury [2, 178], when angiogenesis peaks, thus validating our system for improved wound healing in a clinically relevant time period.

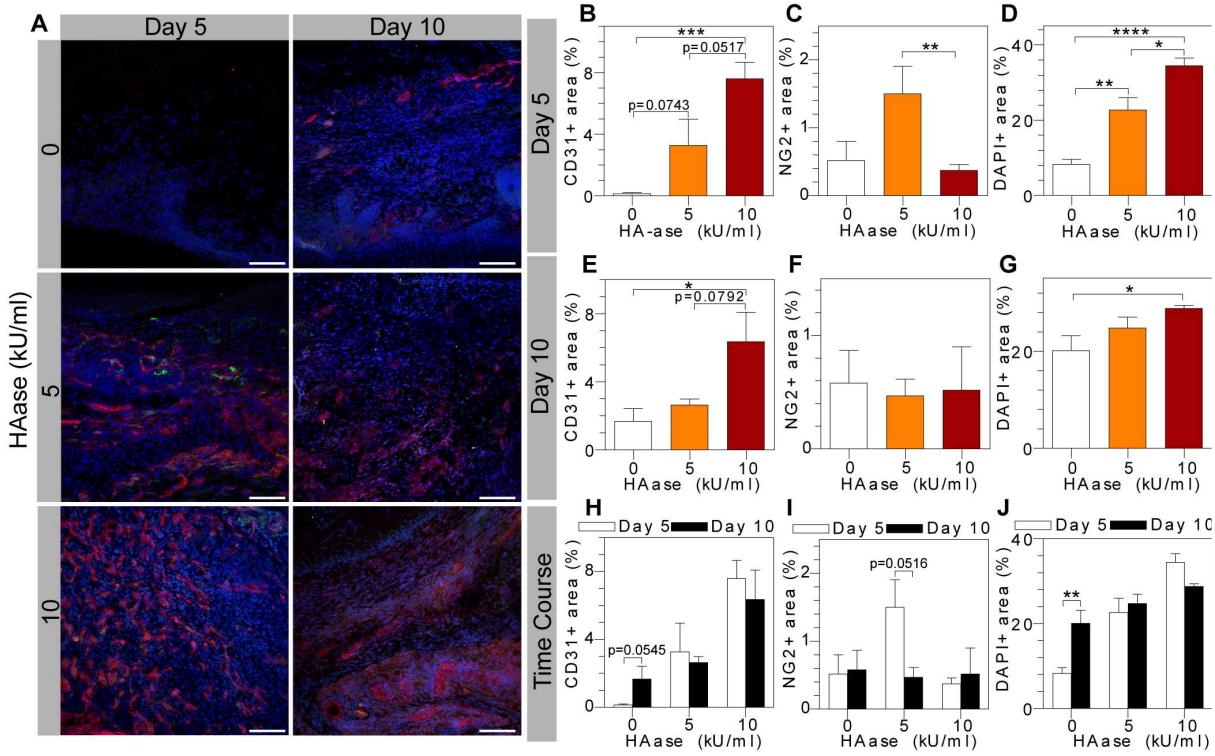


**Figure 6.6 HAase pre-treatment of porous HA gels loaded with therapeutic proangiogenic plasmid leads to more enhanced vascularization in a murine wound healing model.** (**A**) Representative images of granulation tissue stained for CD31 (red), NG2 (green), and nuclei (blue) show more vascularization as a result of HAase pre-treatments. Quantification of CD31+, NG2+, and DAPI+ area was evaluated at day 5 (***p<0.001, t-test; **B**, **p<0.01, t-test; **C**, *p<0.05, t-test; **p<0.01, t-test; ****p<0.0001, t-test; **D**) and day 10 (*p<0.05, t-test; **E**, **F**, *p<0.05, t-test; **G**) by measuring area from 3 random regions per tissue section across three different sections at least 150 μm apart (Figure 6.5A) (n=4-6). HAase pre-treated gels loaded with plasmid encoding for VEGF achieved sustained vascularization and larger cell populations in the newly formed granulation tissue, in general (**H**, **I**, **p<0.01, t-test; **J**). Data represent the mean±SEM. Scale bars, 100 μm (**A**).

## 6.4 Conclusions

Collectively, this chapter demonstrates an improved approach at achieving enhanced and sustained *in vivo* transfection in a human-relevant wound healing model. We validated use of caged nanoparticle encapsulation (CnE, +A/S) for high DNA loading into our porous HA hydrogels, resulting in enhanced and sustained transfection following HAase pre-treatment irrespective of mechanical stiffness. Furthermore, following confirmation of *in vivo* transfection with a reporter plasmid, we applied our approach to a system delivering a therapeutic plasmid encoding for VEGF and demonstrated substantial improvement on wound closure, cell infiltration, and vascularization in a wound healing model. In this chapter, we primarily focused on enhancing *in vivo* transfection and subsequently applied it to a model for tissue repair; however we believe that this promising approach is highly tunable for the delivery of any nonviral plasmid DNA to achieve successful, localized therapies.

# CHAPTER 7

# DUAL GENE DELIVERY FROM TWO HYDROGEL SYSTEMS: SURFACE COATED VS. TWO PHASE HYDROGELS

## 7.1 Introduction

In Chapter 6, we discussed a novel approach to achieve enhanced transfection from porous HA hydrogels by employing hyaluronidase pre-treatment to better facilitate transfection via cell-mediated gel degradation and DNA release. Moreover, we employed our porous hydrogel system to deliver only one gene, namely plasmids encoding for GFP or VEGF, to explore transfection as a whole, and a basic investigation of its therapeutic, pro-angiogenic potential. However, angiogenesis is a complex process that is critically dependent on multiple factors at each step [14]. Therefore, despite achieving rapid vascular ingrowth from pVEGF delivery alone, the delivery of multiple factors from our porous hydrogels may be required to improve the quality of vascularization for improved wound healing.

Vascular endothelial growth factor (VEGF) is an important pro-angiogenic bioactive cue that induces endothelial cell migration and proliferation [179] for blood vessel formation, while platelet derived growth factor (PDGF) assists in the recruitment and proliferation of smooth muscle cells and perictyes, aiding in vessel maturation [180]. For this reason, there have been several studies conducted on the dual delivery of VEGF and PDGF from alginate [181], PLG [182, 183], PELCL [184], PEG [185], and polyurethane [186] scaffolds. However, *in vitro* release studies often show a burst release of growth factors within the first 24 h which does not simulate a normal physiological response to injury. Maximal VEGF activity occurs approximately

between 3-7 days following injury, within the proliferative stage of wound healing when new tissue is formed [2, 178], and expression of αvβ3, an integrin associated with VEGF activity, disappears by day 7 as VEGF returns to baseline levels [179]. Moreover, the role of PDGF may extend to the later stages of wound healing where PDGF can stimulate fibroblasts to produce and secrete collagenase [187], an event in remodeling that occurs much later at 2-3 weeks following injury [2]. Thus to combat the concerns of growth factor cost, storage, and burst release from scaffolds, many groups have investigated dual or multiple gene delivery. The advantages include bioactivity preservation for longer time periods and potential for prolonged protein expression levels at therapeutically relevant values, as well as synergistic cell-mediated protein expression for enhanced tissue repair. Dual gene delivery has been investigated *in vivo* in collagen-nanohydroxyapatite and electrospun PELA fibrous scaffolds for bone regeneration and subcutaneous vascularization, respectively, demonstrating the powerful and therapeutic effect of combinatorial gene therapy [188, 189].

. Herein, we discuss our efforts to simulate the physiological development of blood vessels by considering the specific role of growth factors and its order of delivery to aid in tissue repair. In this chapter, we describe an investigation of two different gene delivery systems for sequential gene delivery (with HAase treatment as described in Chapter 6) *in vitro*: (i) a porous hydrogel encapsulated and surface coated with two distinct genes, respectively, and (ii) a two phase hydrogel system with two different genes within each respective phase. Knowledge gained from our *in vitro* transfection studies with reporter plasmids led us to design a hybrid of our initially proposed systems to deliver plasmids encoding for VEGF and PDGF in a humanized splinted murine wound healing model to investigate its therapeutic and pro-angiogenic capacity *in vivo*.

## 7.2 Materials and methods

### 7.2.1 Materials

Peptides Ac-GCRDGPQGIWGQDRCG-NH2 (HS-MMP-SH) and Ac-GCGYGRGDSPG-NH2 (RGD) were purchased from Genscript (Piscataway, NJ). Sodium hyaluronan (HA) was a gift from Genzyme Corporation (60 kDa, Cambridge, MA). All other chemicals were purchased from Fisher Scientific (Pittsburgh, PA) unless otherwise noted.

### 7.2.2 Hyaluronic acid-acrylate modification

Sodium hyaluronan was modified to contain acrylate functionalities as previously described8b. Briefly, hyaluronic acid (2.0 g, 5.28 mmol, 60 kDa) was reacted with 18.0 g (105.5 mmol) adipic acid dihydrazide (ADH) at pH 4.75 in the presence of 4.0 g (20 mmol) 1-ethyl-3-[3-dimethylaminopropyl] carbodiimide hydrochloride (EDC) overnight and purified through dialysis (8000 MWCO) in deionized (DI) water for two days. The purified intermediate (HA-ADH) was lyophilized and stored at -20 °C until used. Approximately 71 % of the carboxyl groups were modified with ADH, which was determined using 1H-NMR ($D_2O$) by taking the ratio of peaks at δ = 1.6 and 2.3 corresponding to the eight hydrogens of the methylene groups on the ADH to the singlet peak of the acetyl methyl protons in HA (δ = 1.88). HA-ADH (1.9 g) was reacted with N-acryloxysuccinimide (NHS-Ac) (1.33 g, 4.4 mmol) in HEPES buffer (10 mM HEPES, 150 mM NaCl, 10 mM EDTA, pH 7.2) overnight and purified through dialysis against a 100 mM to 0 mM salt gradient for 1 day, and then against DI water for 3-4 days before lyophilization. The degree of acrylation was determined to be ~13% using 1H-NMR ($D_2O$) by taking the ratio of the multiplet peak at δ = 6.2 corresponding to the cis and trans acrylate hydrogens to the singlet peak of the acetyl methyl protons in HA (δ = 1.88).

### 7.2.3 DNA/PEI polyplex formation and surface coating

DNA and L-PEI (N/P=7) were mixed to form nanoparticles through vortexing for 15 s and incubating for 15 min at room temperature before hydrogel formation. To surface coat porous hydrogels, gels placed in a 1.5 ml tube with a solution of polyplexes (0.2 µg/ul, 50 µL/gel) were inverted and gently flicked every 20 min for 2 h at RT. Following the coating procedure, the gels were rinsed with PBS three times to remove any unbound polyplexes.

### 7.2.4 CnE, polyplex lyophilization

For caged nanoparticle encapsulation (CnE), plasmid DNA (100 µg) and L-PEI (91.3 µg) [N/P=7] were mixed in 3.5 ml water in the presence of 35 mg (0.10 mmol) sucrose and incubated at room temperature for 15 min. Following incubation, 1.5 ml low-melting point agarose (0.67 mg/ml) was added prior to lyophilization. Each aliquot was intended for 100 µl hydrogel with DNA at 1 µg/ul.

### 7.2.5 PMMA microsphere template for surface-coated and two phase hydrogel formation

Microsphere templates for surface-coated porous hydrogels were prepared via chemical sintering as previously described [154]. Briefly, commercially acquired PMMA microspheres (53-63 µm dia.) were re-suspended in 1 % acetone in 70 % ethanol at 0.4444 mg/ml [cite chemical sintering]. Microspheres (21 mg/well) were pipetted into PDMS wells generated via punching out discs (6mm, dia.) in PDMS sheets (5mm thick) and adhered onto sigmacoted glass slides. For two phase hydrogels, each 6 mm diameter well contained an additional 2 mm diameter PDMS post in the center and was filled with 15 mg PMMA microspheres (0.4444 mg/ml re-suspension). The microsphere suspension was incubated at 37 °C for ~1 h to evaporate the acetone/ethanol to leave a neatly packed microsphere template. For CnE, the molds were heat sintered briefly for 1-2 h at 150 °C.

### 7.2.6 Hydrogel formation

Hydrogels were formed by Michael-type addition of acrylate-functionalized hyaluronic acid (HA-Ac) with bis-cysteine containing MMP peptide cross-linkers at pH 7.6-7.8. Prior to reaction, a hydrogel precursor solution was generated by mixing HA-Ac with a lyophilized aliquot of cell adhesion peptide, RGD, for 30 min at 37 °C. Following incubation, HA-Ac-RGD was mixed with the remaining HA-Ac and TEOA (0.3 M, pH 8.8) for a final gel concentration of 3.5% w/v% HA. For in vitro and in vivo experiments, the final RGD/HA cluster ratio was 1.17, with 100 μM RGD. Finally, lyophilized aliquots of the cross-linker were dissolved in TEOA (0.05 mg/μl) immediately before addition to a mixture of lyophilized polyplexes (CnE) and the hydrogel precursor solution. For surface-coated porous hydrogels, 20 μl of gel solution was then added directly onto the PMMA microsphere template and perfused into the template via centrifugation at 750 g for 10 min at 4 °C. The molds were then incubated at 37 °C for 30 min to induce polymerization. For two phase hydrogels, 15 μl of gel precursor was added onto the PMMA microsphere template and centrifuged. Once polymerized, the 2 mm PDMS post was removed and an additional 5 μl of another gel precursor was added to the central void volume. For gels with a homogenous two phase composition, the PDMS post was removed immediately following heat sintering and a total of 20 μl of gel precursor was added to the entire mold. Following polymerization, the gels were submerged in acetone for 48 h with periodic acetone changes to dissolve out remaining PMMA microspheres. The porous hydrogels were hydrated in PBS+1 % penicillin-streptomycin (P/S) (pH=7.4) as needed.

### 7.2.7 Hydrogel composition and mechanical characterization

#### 7.2.7.1 Visual characterization via confocal microscopy and SEM

To visualize polyplex distribution in surface coated porous hydrogels, hydrated gels before and after surface coating were stained with NHS-Alexa 350 (Invitrogen, Grand Island, NY) and 1xSYBR green (Invitrogen, Grand Island, NY) for 1-2 h, when DNA was present. Following PBS washes, the gels were imaged via confocal (Nikon C2) microscopy and represented by maximum intensity projections of multiple z-stacks. Two phase gels formed with two separate polymerizations (μ-pore, then n-pore post) were visualized with scanning electron microscopy (SEM) and fluorescent microscopy. SEM imaging was performed on hydrated two phase hydrogels that were halved with the vertical cross section facing up and placed onto a dry carbon tape-covered holder. Samples were imaged under low vacuum at 50 Pa, 10 kV, and spot size of 3.0 using an FEI Nova Nano 230 SEM in the UCLA Molecular & Nano Archaeology (MNA) facility. Confocal microscopy allowed visualization of two phase gels composed of gel phases that were polymerized separately; the distinct gel phases were tagged with Alexa Fluor 555 C2 Maleimide and Alexa Fluor 350 Maleimide (Life Technologies, Grand Island, NY).

#### 7.2.7.2 Mechanical characterization

To investigate the bulk mechanical properties of the two phase hydrogel, rheological studies were conducted to compare the moduli of two phase gels to non-porous and porous hydrogels. Nonporous gels were formed by similar methods as described as above, and instead of perfusing it through a microsphere mold, 30 μl of the gel solution was sandwiched between two sigmacoted slides using 1 mm thick plastic spacers and incubated at 37 °C for 30–45 min to induce polymerization. Once complete, the gels were placed directly into sterile PBS and left in PBS until ready for use. Porous and two phase hydrogels were formed as previously described. Once hydrated and trimmed to 8 mm (diameter), the storage and loss moduli were measured

using a plate-to-plate rheometer (Physica MCR, Anton Paar, Ashland, VA) with an 8 mm (dia.) plate under a constant strain of 0.1% and angular frequency ranging from 0.1 to 10 Hz. To prevent the hydrogel from drying, a humidity hood was utilized and the stage was set to 37 °C.

### 7.2.8 Radiolabeled DNA

#### 7.2.8.1 Radiolabeling and purification

Plasmid DNA was radiolabeled with 32P-dCTP (250 μCi) using a Nick translation kit (Roche, Indianapolis, IN) as per instructed by the manufacturer's protocol. Briefly, an equimolar mixture of dATP, dGTP, dTTP, and 32P-dCTP was prepared and added to the DNA (12.5 μg) solution. Once the enzyme solution was added to the mixture, the final solution was gently mixed by pipetting and incubated for 35 min at 15 °C. The reaction was stopped by addition of 12.5 μl 0.5M EDTA (pH=8.0) and heating to 65 °C for 10 min. The DNA was purified using the DNA Clean & Concentrator-5 kit following manufacturer instructions. The hot DNA was diluted to contain 0.15% radiolabeled DNA.

#### 7.2.8.2 DNA release

Radiolabeled DNA was used in place of naked pDNA to study the DNA release from surface coated and two phase hydrogels as potential sequential gene delivery systems. The surface coated porous gel system would consist of encapsulated DNA and polyplexes adhered to the surface of the pores as the two presentations of DNA. Since 32P was the only isotope used to radiolabel the DNA, we deconstructed our system to two basic release studies: (i) 20 μl porous hydrogels loaded with 1 μg/μl hot DNA via CnE (referred to as encapsulated) and (ii) 20 μl porous hydrogels surface coated with polyplexes as described previously with hot DNA (referred to as surface). Similarly, the two phase hydrogel system was deconstructed to reflect

the two different regions: (i) the first gel system contained 15 µl hot DNA loaded via CnE in the porous region, with 5 µl normal gel in the center and (ii) the second system contained a normal 15 µl gel within the porous region with 5 µl hot DNA loaded via CnE at 1 µg/µl. Following polymerization, PMMA microsphere dissolution was achieved as previously described. Once hydrated, the hydrogels were exposed to 500 µl hyaluronidase (5,000 U/ml, HAase) for 2 h at 37 °C. The hydrogels were then washed in 500 µl PBS for 10 min at RT to remove any residual HA-ase. Following the wash, all hydrogels were exposed to fresh PBS at 37 °C. At each step, 500 µl of the solution was collected for later analysis. All of the supernatant was collected daily and refreshed with PBS for 10 d. Following the final solution collection time point, the hydrogels were collected to be read in order to complete the mass balance. DNA amounts were measured using a scintillation counter at the UCLA Chemistry core facility where each sample (100 µl) was added to 2 ml scintillation cocktail fluid (Bio-safe II, RPI Corp., Mount Prospect, IL).The readout was analyzed using a standard curve.

7.2.9 *In vitro* transfection

Plasmids encoding for Gaussia luciferase (pCMV-GLuc) and secreted alkaline phosphatase (pCMV-SEAP) were used to study the transfection from the different delivery systems. The surface coated porous system consisted of a 20 µl porous gel loaded with 20 µg pGLuc via CnE and surface coated with pSEAP polyplexes. The two phase hydrogel system comprised of 15 µg pGLuc in the 15 µl porous region while the 5 µl nonporous center contained 5 µg pSEAP, all loaded via CnE. The porous hydrogels were hydrated in PBS + 1% P/S to maintain sterility then exposed to 500 µl HA-ase (5000 U/ml) for 2 h at 37 °C. The hydrogels were then washed in 500 µl PBS for 10 min at RT to remove any residual HAase. Mouse MSCs were seeded on the surface of the hydrogels by suspending cells (250 µl cells/gel, 1x106 cells/ml) in a 1.5ml tube with 3-4 hydrated porous hydrogels. Surface coating was achieved by

inverting and gently flicking the tube with cells and gels every 20 min for 3 h. Following 3 h, the gels were washed with sterile PBS to remove non-adherent cells and then plated individually in a non-tissue culture treated 48-well plate with 500 µl fresh cDMEM/well. Since pSEAP and pGLuc inherently have different transgene expression profiles, it was necessary to obtain a scaling factor. This was achieved by exposing seeded mSCs (25,000 cells/well) in a 48 well plate to a bolus mixture of pSEAP and pGLuc polyplexes (0.4 µg each) for 4 h. Following 4h, the media and any remaining polyplexes were collected and the wells were refreshed with fresh media. The conditioned media was collected daily and frozen immediately at -20°C for later analysis; each well was replaced with fresh medium.

### 7.2.10 Gaussia luciferase assay

To quantify secreted Gaussia luciferase levels in the media, the collected samples were assayed using a Biolux Gaussia Luciferase assay kit (New England Biolabs, Ipswich, MA) as instructed by the manufacturer's protocol. Briefly, 20 µl of each sample was mixed with 50 µl 1x substrate solution, pipette/mixed for 2-3 s, and read for luminescence with 5 s integration. Values from the Gaussia luciferase assay were expressed as relative light units (gRLU).

### 7.2.11 SEAP assay

To quantify SEAP levels in the media, the collected samples were assayed using a Phospha-Light SEAP assay kit (Life Technologies, Grand Island, NY) as instructed by the manufacturer's protocol. Briefly, 25 µl of each sample was added to 75 µl 1x dilution buffer and heated for 30 min at 65 °C. Once the samples were cooled, 100 µl assay buffer was added and incubated for 5 min at RT. Lastly, 100 µl of reaction buffer was added to each sample and luminescence was read 20 min later with 1 s integration time. Values from the SEAP assay were expressed as RLU.

7.2.12 Cell proliferation

An alamarBlue® assay (AbD Serotec, Raleigh, NC) was used to quantify cell proliferation rate. Surface coated and two phase hydrogels were constructed and seeded with cells as previously described for in vitro transfection. 50 µl alamarBlue reagent with 500 µl cDMEM was added to each well containing a hydrogel seeded with cells in a 48-well plate and incubated at 37 °C for 4 h. The solutions were transferred to a new plate and absorbance was measured at 570 nm and 600 nm using a standard plate reader. Four gels for each condition were analyzed at each time point and proliferation rate was calculated following the manufacturer's instructions.

7.2.13 Splinted wound healing model

All *in vivo* studies were conducted in compliance with the NIH Guide for Care and Use of Laboratory Animals and UCLA ARC standards. Female balb/C mice each aged 4-6 weeks and weighing 15-20 grams were used. Hydrogels were formed as described above with final overall dimensions of 6mm x 1 mm, D x H. In fabricating the hydrogels, the starting reagents were sterilized through filtering with a 0.22 µm filter. After scaffold fabrication, the hydrogels were stored in acetone until surgery day. On the day of surgery, the hydrogels were hydrated and exposed to 10 kU/ml HAase treatment for 2 h, then washed with sterile PBS and kept in PBS with 1 % P/S. Immediately prior to surgery, mice were anesthetized with 3-3.5 % isoflurane through a nose cone inhaler. After anesthesia induction, the isoflurane concentration was lowered to 1.5-2 % for the remainder of the surgery. The back of the mouse was subsequently shaved, all remaining hair was removed with Nair (≤ 1 min), and finally sterilized with povidone-iodine (Betadine, Stamford, CT) and 70 % ethanol. Two full-thickness wounds were then

generated using a 6 mm biopsy punch and the hydrogels were placed directly into the wounds. Sterilized silicon rings (8 mm dia., 0.5 mm thick) sandwiched between two sterile pieces of Tegaderm (i.e. splints with non-adhesive, clear windows) were fixed to the outside of the wound using a tissue adhesive, Mastisol and Vetbond. The splints were then lightly pressed down to generate contact with the hydrogel and skin bordering the wound. Eight interrupted sutures (5-0 Prolene, Ethicon, Somerville, NJ) were also utilized to hold the splint in place. Finally, additional adhesive (Tegaderm, Baxter, Deerfield, IL) was placed around the outer edges of the splints and the mice were wrapped in an elastic gauze (VetRap, 3M, St. Paul, MN) to further prevent the splint removal for the duration of the study. For animals evaluated with bioluminescence (n=6), four wounds were created in the mice backs and two Tegaderm bandages were fabricated where a rectangular strip of Tegaderm (~10 x 20 mm) had its central region made non-adhesive by applying another smaller strip of Tegaderm (~8 x 18 mm). Each Tegaderm bandage was large enough to cover two wounds and still able to adhere to the skin. All animals were observed daily for signs of inflammation and pain. Buprenorphine injections were administered every 12 h for the first 48 h post survival surgery. At day 7, animals (n=6) were sacrificed with isoflurane overdose and cervical dislocation. 8 mm diameter pieces of tissue were collected from each mouse containing the implant and the surrounding tissue and skin using a biopsy punch and preserved in OCT cryoblocks.

### 7.2.14 Bioluminescence Imaging

To study *in vivo* transfection from our two phase gene delivery system, we again deconstructed our system to three basic hydrogels containing plasmid encoding for firefly luciferase (pCMV-GFP-FLuc) as previously described: (i) a two phase hydrogel with 15 μg DNA in the porous phase only with surface coated polyplexes, (ii) a two phase hydrogel with 5 μg DNA in the n-pore post only, and (iii) a two phase hydrogel with DNA in both μ-pore and n-pore

phase with a total of 20 μg DNA. All DNA loaded in the respective phases were incorporated via CnE and the hydrogels were pre-treated with 10 kU/ml HAase for 2 h at 37 °C prior to implantation. The animals were imaged on day 1 and every two days thereafter for 21 d. In vivo luciferase expression was monitored using an IVIS imaging system (Xenogen Corp., Alameda, CA). For imaging, the animals received 10 μl injections of D-luciferin (30 mg/ml, Gold Biotechnology, St. Louis, MO) into each wound bed by inserting a 29 1/2G through the Tegaderm bandage. The animals were placed in a ventilated, dark chamber and bioluminescence images were acquired (every 5 min for a total of 20-25 min) until the peak light emission was confirmed. With gray scale and bioluminescence images superimposed, a constant size region of interest (ROI) was drawn over each wound site to measure total flux (photons/s) using the Living Image software (Xenogen Corp., Alameda, CA). Reported data represent the maximum total flux detected for each animal over the course of image acquisition. Bioluminescence imaging data is represented as total flux normalized to background total fluxes obtained by quantifying and averaging three random ROIs within the superimposed image at each time point.

### 7.2.15 Engineering biscistronic vectors

Preparation of pEF1α-eGFP-2A-VEGF and pEF1α-mCherry-2A-PDGF was performed using ligation-free overlap extension PCR cloning with the Gibson assembly mix (New England BioLabs, Ipswich, MA) according to the manufacturer's instructions, a technique adapted from Szymczak-Workman et al [172]. The overlapping gene inserts and linearized backbone were amplified by PCR using Phusion High-Fidelity polymerase (New England BioLabs). DpnI (New England BioLabs) was used to digest the template remaining in the PCR product. Primers were designed to have 20-30 bp of overlap between the insert and the vector.

First, to enable bicistronic, stoichiometric expression of two genes with one promoter, a two-gene insert was prepared with a short, self-cleaving 2A peptide sequence from porcine teschovirus-1 incorporated between the two genes (5'-GGATCCGGAGCCACGAACTTCTCTCTGTTAAAGCAAGCAGGAGACGTGGAAGAAAACCCC GGTCCT-3'). This was done via overlap extension PCR; gene inserts were amplified with overlapping primers containing part of the 2A sequence to produce a (gene A)-2A-(gene B) insert with ends that overlap with the linearized vector. Insertion of this recombinant PCR product into the linearized vector was performed with Gibson assembly. Confirmation of correct vector construction was achieved by performing colony PCR and sequencing of the amplified plasmids.

7.2.16 Wound closure

The two phase gene delivery system was utilized in the murine wound healing model with biscistronic vectors encoding for pro-angiogenic proteins (VEGF and PDGF) in addition to reporter proteins (GFP and mCherry). To study the effect of spatial plasmid presentation, we employed two gene delivery systems: (i) a two phase hydrogel with 15 µg pEF1α-eGFP-2A-VEGF in the porous phase and 5 µg pEF1α-mCherry-2A-PDGF in the n-pore post with surface coated polyplexes (pEF1α-eGFP-2A-VEGF, 0.2 µg/µl), and (ii) a two phase hydrogel with homogenous distribution of pEF1α-eGFP-2A-VEGF and pEF1α-mCherry-2A-PDGF (10 µg each), and surface coated polyplexes (pEF1α-eGFP-2A-VEGF and pEF1α-mCherry-2A-PDGF, equal volumes at 0.2 µg/µl). The first two phase gel system described will be referred to as V→P hereafter, and the second, V/P; both two phase gene delivery systems were compared to a control, splinted untreated wounds (U). Digital images of wounds at designated time points were used to assess wound closure. A ruler and/or the known diameter of the splint was used as a reference. Only images where wounds have a distinct border were used for analysis.

7.2.17 Immunofluorescence and Immunohistochemistry

OCT embedded sections (20 μm thick) were thawed and fixed with cold acetone for 10 min. Sections were then washed with PBS and incubated in blocking buffer (5 % normal goat serum (Jackson Immuno Research Labs, West Grove, PA) + 0.05 % Tween-20 in PBS) for 1 h at RT before being incubated in primary antibody solution (1:100 rat anti-mouse CD31 (BD Pharmingen, San Diego, CA), 1:200 rabbit anti-mouse NG-2 (Millipore), 1:100 rat anti-mouse Ly6G, 1:100 mouse anti-mouse fibroblasts) overnight at 4 °C. Sections were again washed with PBS and incubated in blocking buffer for 10 min at RT before being incubated for 2 h at RT in secondary antibody solution (1:100 goat anti-rat Alexa 568, 1:100 goat ant-mouse Alexa 555, and 1:100 goat anti-rabbit Alexa 488 (Invitrogen, Grand Islands, NY), and DAPI nuclear stain (1:500 dilution, Invitrogen, Grand Island, NY). Sections were then washed twice in PBS, mounted and imaged using a Nikon C2 confocal microscope. All hematoxylin and eosin (H&E) staining of sections was conducted by the Translational Pathology Core Laboratory (TPCL) at UCLA.

7.2.18 Quantification and characterization of cellular infiltration and blood vessels *in vivo*

Three separate sections (20 μm thick) at least 150 μm apart were analyzed for each sample to obtain representative data. For blood vessel characterization, three areas (one at each wound edge, one in the center) were imaged on each vertical cross-section at 20X magnification, with 9 images total in per animal. CD31+, NG2+, and DAPI+ area was quantified by using ImageJ software. A threshold was applied to capture positive signal based on fluorescence intensity; positively stained areas were normalized to the total imaged area.

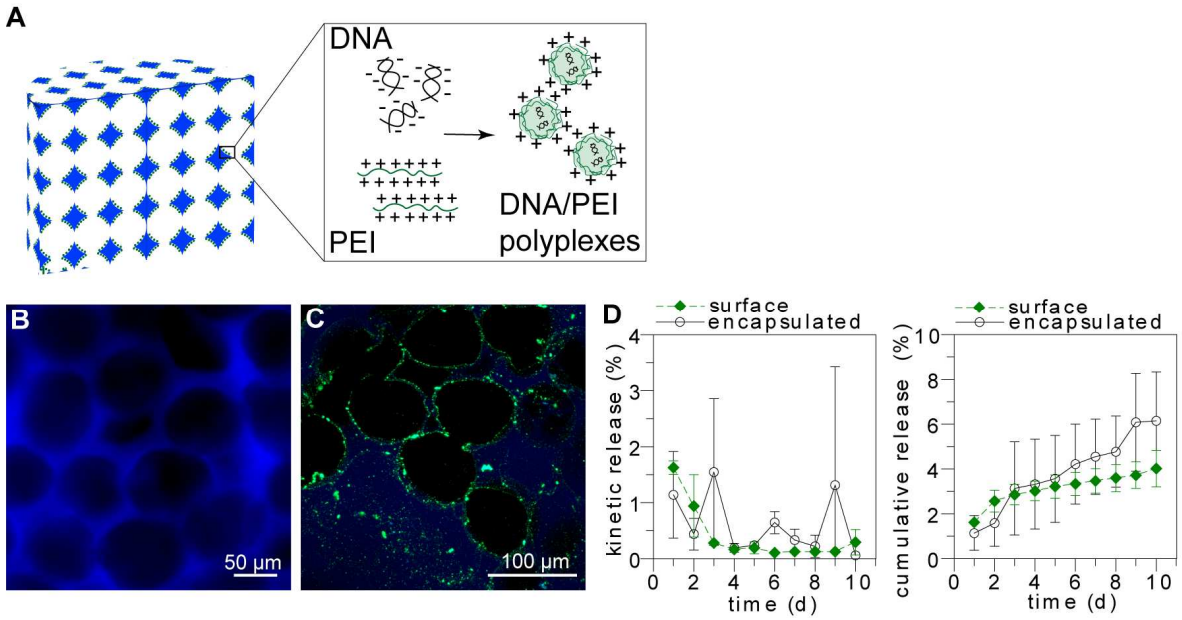


**Figure 7.1 Surface coated gene delivery system** (A) Schematic representation of the surface coated gene delivery system where condensed polyplexes are encapsulated and coated on the surface of the pores. Porous hydrogels before (B) and after (C) surface coating with DNA polyplexes; HA gel = blue, DNA = green. (D) Minimal DNA release was observed from surface coated or encapsulated polyplexes in this delivery system.

## 7.3 Results and discussion

### 7.3.1 Characterization of surface coated vs. two phase gene delivery systems

In this report, we aimed to develop a sequential gene delivery system with the capacity to achieve distinct transgene expression profiles *in vitro* and *in vivo*. Our investigation began with two different approaches: (i) a porous HA hydrogel with DNA encapsulated and coated on the surface of the pores (**Figure 7.1A**) and (ii) a two phase HA hydrogel system where a non-porous (n-pore) hydrogel post is centered in a porous HA gel, with each phase capable of DNA loading (**Figure 7.2A**). In the first approach, surface coating of porous HA hydrogels was visualized and confirmed via confocal fluorescence microscopy where the gels following coating had a uniform distribution of stained polyplexes along each pore surface (**Figure 7.1B, C**). DNA release from the surface coated hydrogel system was evaluated by comparing release profiles of radiolabeled DNA encapsulated in porous hydrogels via CnE to porous HA hydrogels with

radiolabeled surface coated polyplexes following HAase treatment and passive diffusion (**Figure 7.1D**). Minimal DNA release was observed from either porous hydrogels encapsulated or surface coated with DNA, suggesting that the electrostatic interactions are strong enough to immobilize the polyplexes onto the HA hydrogel with high retention.

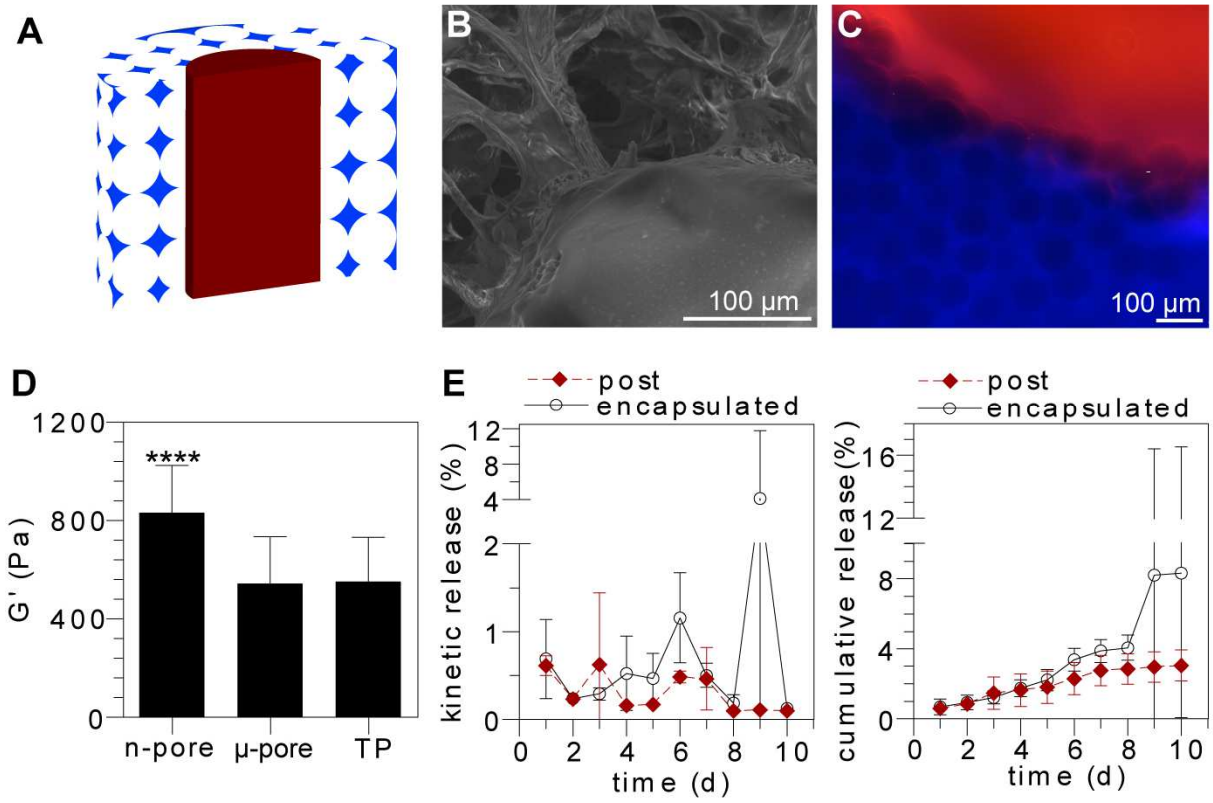


**Figure 7.2 Two phase gene delivery hydrogel system.** (**A**) Schematic representation of the proposed two phase hydrogel system for sequential gene delivery. (**B**) SEM and (**C**) fluorescent images demonstrate a mated interface between gel phases following separate polymerization. (**D**) Mechanical characterization shows that the two phase (TP) gel has a bulk modulus similar to porous HA gels. (**E**) DNA polyplex release from each respective phase is minimal.

In the second approach, a two phase hydrogel gene delivery system was employed where a homogenous two phase gel could be generated in a single gelation event or each gel phase could be polymerized separately. Rheological studies demonstrate that a two phase hydrogel possesses a bulk modulus more similar to porous HA hydrogels of the same composition (**Figure 7.2D**). Scanning electron micrographs (SEM) and fluorescence microscopy demonstrate that a single two phase hydrogel comprised of two distinct gel architectures can be

formed from two gelation events resulting in a single complete hydrogel with a mated interface between the phases (**Figure 7.2 B, C**). This suggests that this system is highly tunable to form two phase gels with a variety of combinations of compositions and mechanical properties with the capacity to deliver multiple bioactive agents in each gel phase. Similar radiolabeled DNA release was observed for the two phase gel system, where minimal release was observed in either two phase gels containing DNA encapsulated within the porous region or the n-pore post (**Figure 7.2E**).

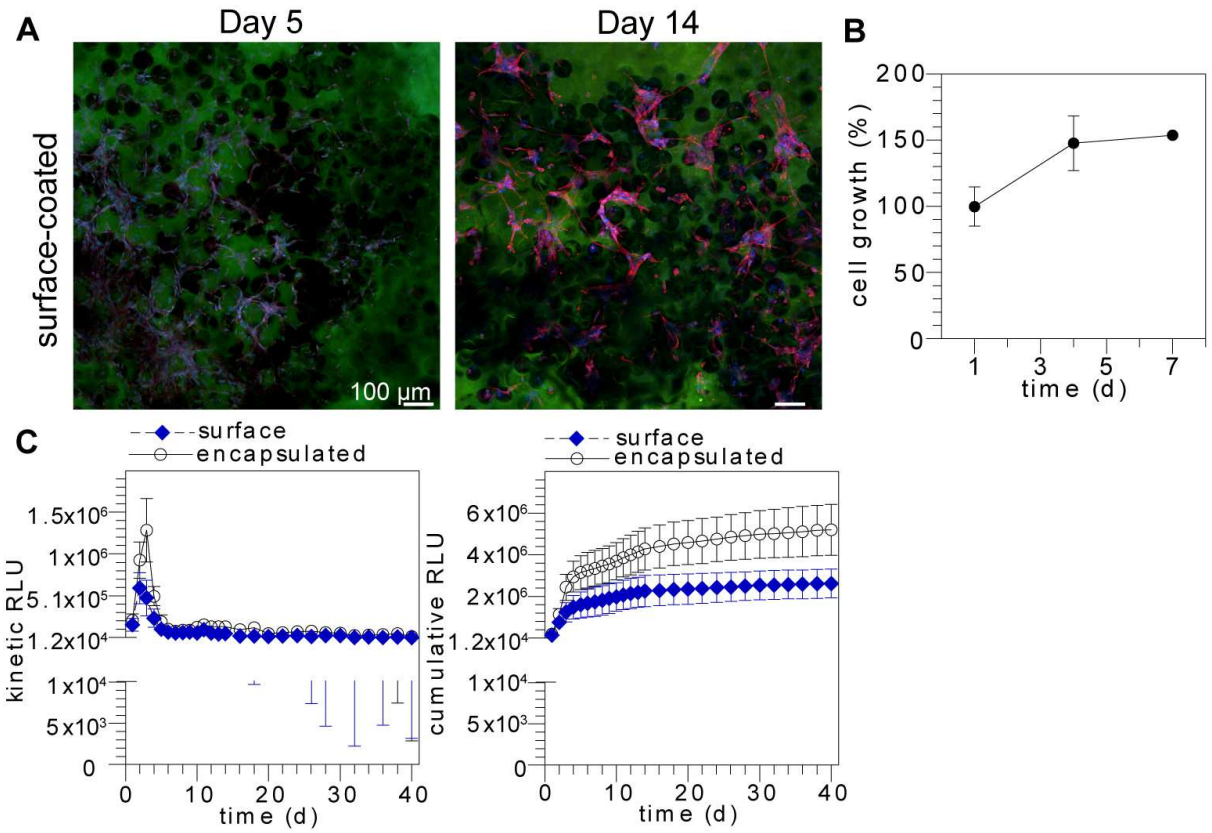


**Figure 7.2 *in vitro* evaluation of surface coated hydrogels as a gene delivery system.** (**A**) mMSCs exhibited spreading throughout the porous HA gels at day 5 and 14 of culture; HA gel = green, F-actin = red, nuclei = blue. (**B**) Cell health monitored by an alamarBlue® assay demonstrated that the DNA loaded gels were not cytotoxic. (**C**) Transfection from two secreted plasmids incorporated within each region (encapsulated vs. surface coated) was monitored for 40 days and showed similar transgene expression profiles.

7.3.2 *In vitro* evaluation of surface coated vs. two phase gene delivery systems

Cell-matrix interactions were evaluated by seeding mMSCs on porous and two phase HA gels to observe cell spreading and proliferation over time. Confocal fluorescence microscopy confirmed successful cell seeding in both platforms with observed cell migration and spreading at 5 and 14 d of culture throughout each hydrogel system (**Figure 7.3A, Figure 7.4A**). An alamarBlue® assay utilized to monitor cell health and proliferation over 7 days demonstrated that both gene delivery systems, surface coated and two phase, were not cytotoxic despite the high DNA payload (~20 μg) (**Figure 7.3B, Figure 7.4B**). This suggests that the HA hydrogel serves as a depot, slowly releasing complexed DNA at an acceptable level for cell survival that is below the threshold for *in vitro* toxicity which has been observed to be approximately 0.2-0.3 μg/well in a 48-well plate [190].

The *in vitro* transgene expression profiles were investigated over the course of 40 days by generating both hydrogel gene delivery systems, surface coated and two phase, loaded with two different secreted reporter plasmids. Surface coated hydrogels loaded with plasmids encoding for gaussia luciferase (pGLuc) via CnE were treated with HAase, then coated with polyplexes containing plasmids encoding for secreted alkaline phosphatase (pSEAP). Encapsulated GLuc expression peaked at day 3, while peak surface coated SEAP expression was seen at day 2 (**Figure 7.3C**). This agrees with our expectations that the immediately available pSEAP polyplexes coated on the surface would facilitate more rapid transgene expression. Moreover, the kinetic transgene expression profiles suggest a peak in transfection at initial culture followed with sustained expression, suggesting that there is a burst release of DNA available for immediate transfection. Despite the average 2.2-fold increase in pGLuc transfection over pSEAP, the transgene expression profiles were similar between the encapsulated and surface coated polyplexes, rendering this system more suitable for dual gene delivery rather than sequential gene delivery. Two phase hydrogels had pSEAP loaded in the

non-porous post and pGLuc encapsulated within the porous region via CnE. Gluc expression was stable for 40 d of culture while pSEAP expression increased dramatically between days 6 and 18. This was clearly illustrated by the kinetic transgene expression profiles, where GLuc expression was on average 218-fold higher than pSEAP at days 1-5, and dropped to 46-fold greater between days 6-18, suggesting that the encapsulated pGLuc DNA was readily available and accessible for uptake while the cells migrated through the pores until reaching the central n-pore post containing pSEAP at a later time (**Figure 7.4C**).

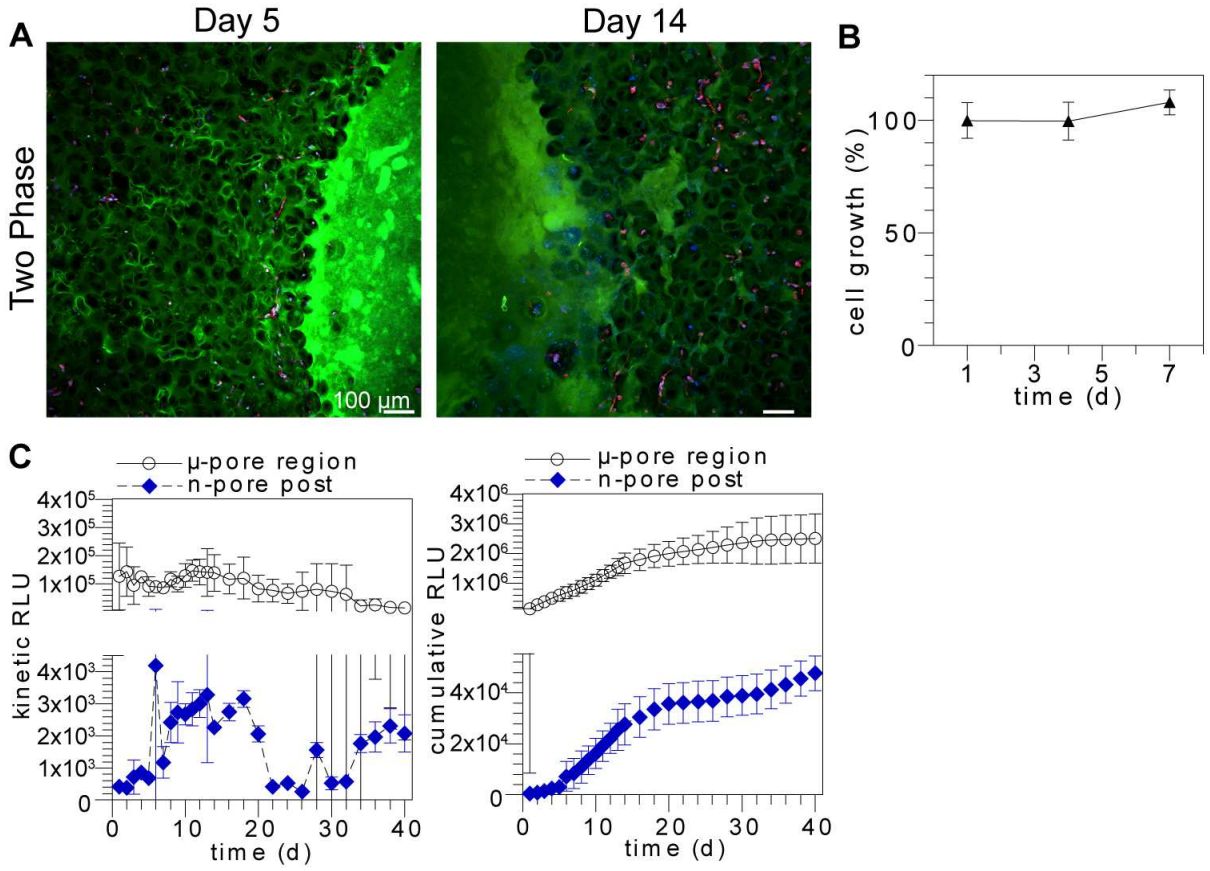


**Figure 7.4 *in vitro* evaluation of two phase hydrogels as a gene delivery system.** (**A**) mMSCs exhibited spreading throughout the porous HA gels at day 5 and 14 of culture; HA gel = green, F-actin = red, nuclei = blue. (**B**) Cell health monitored by an alamarBlue® assay demonstrated that the DNA loaded gels were not cytotoxic. (**C**) Transfection from two secreted plasmids incorporated within each region (µ-pore vs. n-pore) was monitored for 40 days and showed distinct transgene expression profiles.

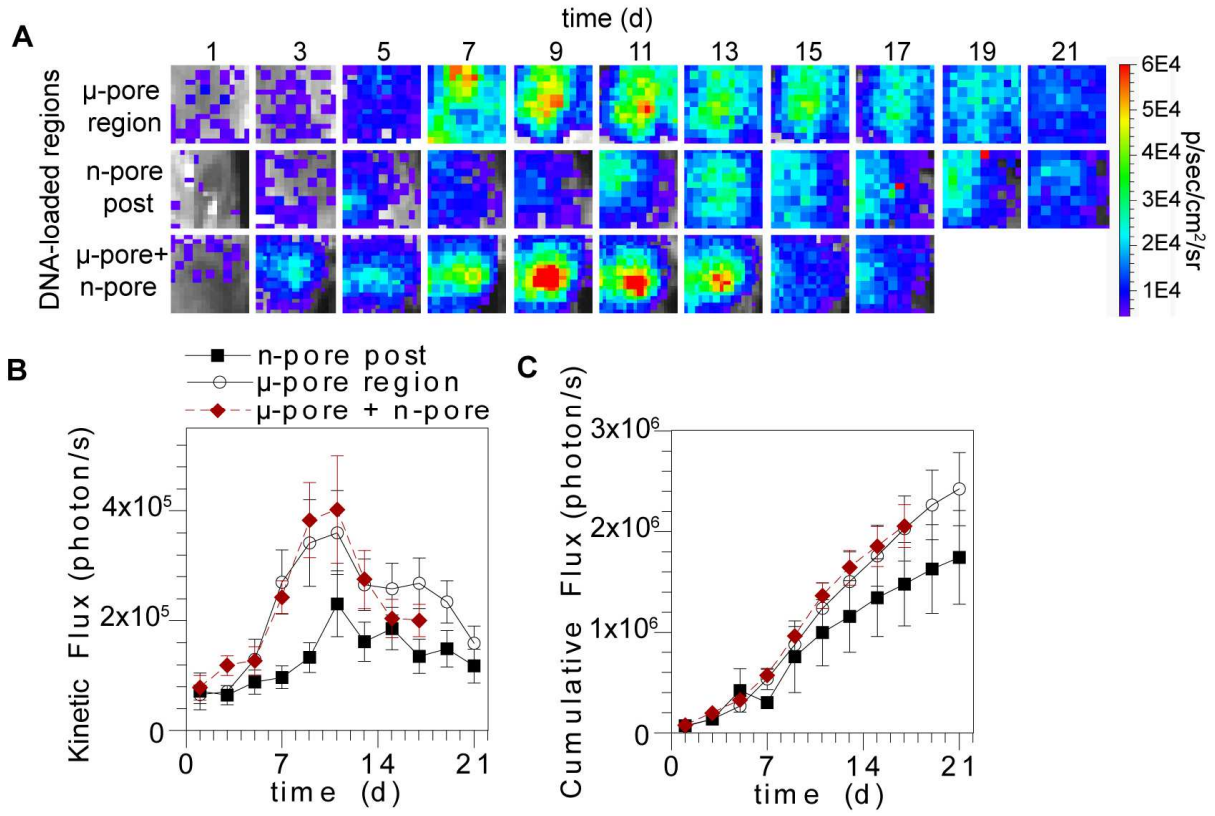


**Figure 7.5 Bioluminescence imaging of balb/c mice wounds implanted with two phase gels.** (**A**) Bioluminescence imaging was conducted regularly for 21 days to monitor transfection due to each region (μ-pore vs. n-pore) or in combination. (**B**, **C**) Quantification of total flux over time suggests that transgene expression profiles are similar and the signal is not additive. The μ-pore + n-pore condition was only imaged until day 17; the animals had removed their wound dressings thereafter.

### 7.3.3 *In vivo* transfection

Since two distinct transgene expression profiles were observed with the two phase hydrogels *in vitro*, we moved forward to employ this system *in vivo* as a potential approach for sequential gene delivery. In addition, since SEAP transgene expression from surface coated porous HA gels was on average equivalent to the GLuc expression from encapsulated polyplexes within the two phase gels, we chose to adopt surface coating of polyplexes onto the two phase gel system with the aim to enhance transfection with an additional source of immediately available polyplexes. To evaluate transfection *in vivo*, two phase gels were loaded with plasmid encoding for firefly luciferase (pFLuc) in three different presentations: (i) only in the μ-pore region with surface coated polyplexes, (ii) only in the n-pore post, and (iii) both μ-pore

and n-pore phases. We observed luciferin-induced light emission over 21 days via bioluminescence imaging and quantified total flux as our metric for transfection. Transgene expression increased with time and peaked around day 11 for all gels (**Figure 7.5A, B**), where gels with encapsulated and surface coated DNA within the porous region had 1.1 to 2.9-fold greater luciferase activity than gels with DNA only in the n-pore post with significant differences at day 7 and 9 (**Figure 7.5C**). Interestingly, two phase gels loaded with DNA in both porous and n-pore post regions resulted in luciferase activity similar to observed transfection in gels loaded within the μ-pore only, suggesting that there is an upper limit to transfection as a function of DNA loading. This may be attributed to several reasons that may include: (i) the amount of DNA polyplexes available at any given time via cell mediated release is similar when the amount loaded exceeds an upper limit, or (ii) the number of transfection events is limited to the number of endogenous cells present and available for polyplex uptake at a given time. Notably, despite the distinct regional (μ-pore vs. n-pore) transgene expression profiles observed *in vitro*, the *in vivo* transgene expression kinetics were similar between the groups, thus demonstrating the importance of *in vivo* investigations and oversimplification of *in vitro* transfection assays.

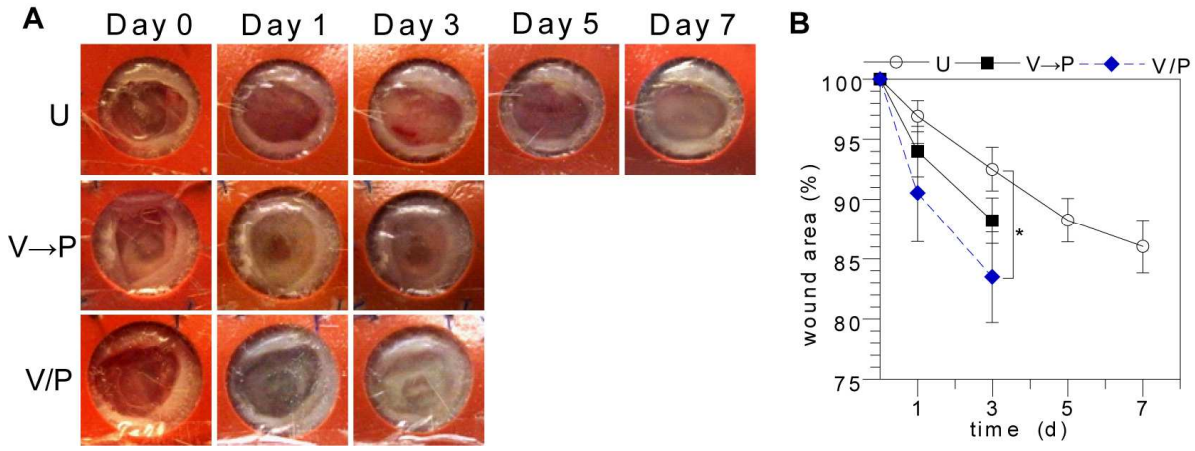


**Figure 7.6 Wound closure.** (**A**) Digital images of wounds taken at regular time intervals. (**B**) Quantification of wound area demonstrated that wounds treated with V/P and V→P gels closed more rapidly than untreated wounds (U).

Nevertheless, we subsequently investigated the delivery of pro-angiogenic plasmids from the two phase hydrogels in a murine splinted wound healing model. Two distinct gel systems were utilized to evaluate the effect of temporal and spatial presentation of pro-

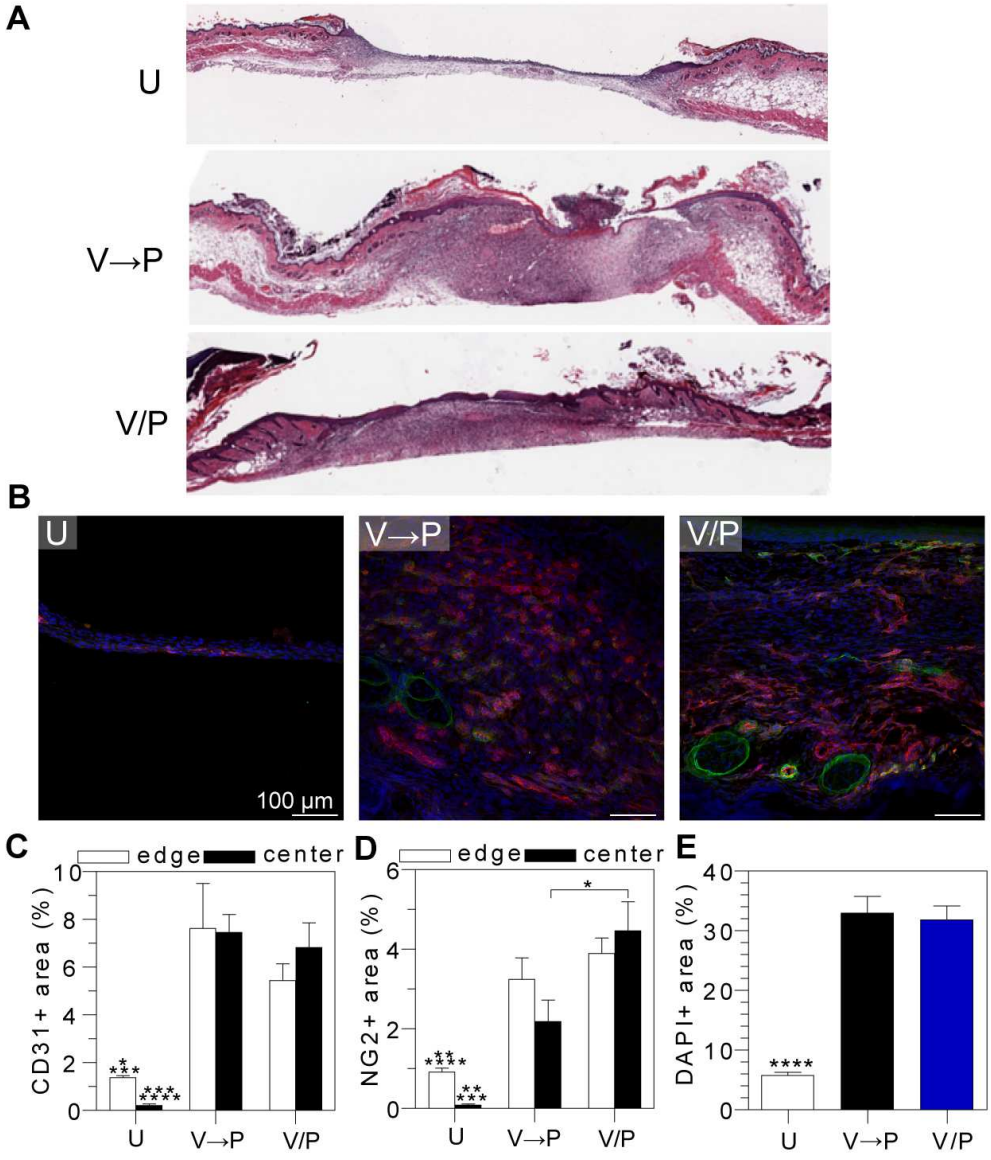


**Figure 7.7 Delivery of pro-angiogenic plasmids from two phase gels.** (**A**) H&E stained wound cross sections demonstrate untreated wounds with very little dermal volume by day 7. (**B**) Staining for endothelial and mural cell markers indicated significantly more positive staining in two phase gels when compared to untreated wounds; CD31= red, NG2=green, nuclei = blue. Quantification of CD31+, NG2+, and DAPI+ area (**C**, **D**, **E**) demonstrate that the two phase gels containing the pro-angiogenic plasmids significantly increase vascular cell populations within the newly formed tissue.

angiogenic plasmids on cutaneous wound healing: (i) a two phase gel comprised of pmCherry-2A-PDGF loaded in the n-pore post, while pGFP-2A-VEGF was encapsulated and surface coated in the μ-pore region (V→P), and (ii) a two phase gel with a homogenous equal distribution of pmCherry-2A-PDGF and pGFP-2A-VEGF polyplexes encapsulated and surface coated in the pores (V/P). VEGF and PDGF were selected due to their important roles in angiogenesis, where VEGF is a potent mediator in endothelial cell migration and proliferation while PDGF promotes vessel maturation. Digital images of wound closure taken at regular time intervals demonstrated the dramatic effect of wounds implanted with a two phase gel with the therapeutic plasmids as compared to untreated wounds (**Figure 7.6A**). By day 3, V→P and V/P treated wound areas were 88.35 ± 1.91 % and 83.50 ± 3.78 %, similar to the wound area present for untreated wounds several days later, at day 7 (86.06 ± 2.22 %) (**Figure 7.6B**). Due to rapid wound healing with the two phase gels containing pmCherry-2A-PDGF and pGFP-2A-VEGF, wound edges were difficult to distinguish to quantify wound closure following day 3. However, by day 3, wound closure was significantly improved with V/P gels when compared to untreated wounds. H&E stained tissue sections demonstrate granulation tissue formation following 7 days post-injury where untreated wounds exhibited very little dermal volume as compared to wounds treated with the two phase gels (**Figure 7.7A**). Moreover, the effect of spatio-temporal presentation of these pro-angiogenic plasmids was evaluated by immunfluorescence (IF) staining of CD31+ and NG2+ cells within the granulation tissue. IF staining confirmed histological observations where minimal cellular activity was observed in untreated wounds and CD31+, NG2+, and DAPI+ area fractions were significantly higher in wounds treated with the therapeutic two phase gels. It is worth noting that wound healing in an untreated wound naturally occurs with vascularization from the wound edge, going inward toward the center of the wound bed, as seen with the CD31+ area quantification plotted by region. Thus, it was clearly demonstrated that the two phase gels loaded with plasmids

encoding for pro-angiogenic factors, regardless of presentation, encouraged substantial blood vessel infiltration into the wound bed and newly formed tissue (**Figure 7.7B**). An investigation of the spatio-presentation of polyplexes demonstrates that the presence of pVEGF polyplexes either presented alone in the porous region or combined with pPDGF resulted in more CD31+ area, indicative of elevated populations of vascular endothelial cells (**Figure 7.7C**). Moreover, the presence of PDGF does not enhance CD31 activity, suggesting that the vascular endothelial activity is primarily dependent on VEGF presence by day 7. Interestingly, implantation of the V→P gels did not result in more NG2+ cells in the center of the wound (**Figure 7.7D**). Conversely, V/P gels resulted in more NG2+ area, with significantly more NG2 activity in the center when compared to V→P gels, indicative of more mature, mural cell-covered blood vessels. This may suggest that the PDGF polyplexes encapsulated only in the n-pore post of the V→P gels have not been released yet or the amount released was not high enough to yield a therapeutic effect by day 7.

### 7.4 Conclusions

In this chapter, we explored a hydrogel system with the aim to achieve sequential gene delivery. We designed two different hydrogel systems to study *in vitro* transfection where one system comprised of a porous hydrogel with two different genes were encapsulated and surface coated, respectively, and the other system was a two phase hydrogel with two different genes encapsulated within each respective phase (porous vs. non-porous). The two phase hydrogel system was able to achieve different transgene expression kinetics, thus it was selected to move forward to *in vivo* studies. However, since *in vitro* transfection from surface coated polyplexes achieved as high levels as encapsulated polyplexes within the two phase gels, surface coated polyplexes were adopted as an additional feature to the two phase gels. Bioluminescence imaging demonstrated that the two phase hydrogel system achieved similar

transgene expression profiles regardless of regional DNA loading, indicating that this system is capable of dual, rather than sequential gene delivery. To study the delivery of plasmids encoding for pro-angiogenic factors, the two phase hydrogel system was applied to a humanized wound healing model where spatio-temporal presentations of VEGF and PDGF polyplexes were investigated. Interestingly, homogenous distributions of VEGF and PDGF polyplexes encapsulated and surface coated on the two phase gels resulted in more NG2 activity, indicative of more mature vasculature despite the other system's localization of pPDGF to the central non-porous post. This result agrees with observations seen with dual VEGF and PDGF protein delivery in various models including subcutaneous implant, non-obese diabetic hindlimb ischemia, and myocardial infarction models in rodents, where the presence of both growth factors synergistically recruit more vessels overall, in addition to larger, more stable vessels [181, 182]. Despite not achieving sequential delivery in this investigation, we still believe that it can be made possible with modifications to several parameters. Since each gel phase can be polymerized separately, we can tailor each phase's mechanical properties or crosslink density to achieve different DNA polyplex release kinetics. Additionally, the number or diameter of the non-porous posts can be modified to elicit varied transgene expression as a result of various DNA polyplex presentations. With so many tunable parameters, we believe that this two phase gel system has great potential to achieve combinatorial gene delivery for a wide variety of therapies, including tissue repair.

# CHAPTER 8

# CONCLUSIONS AND FUTURE DIRECTIONS

## 8.1 Introduction

The goal of the research presented in this dissertation was to design a porous hyaluronic acid hydrogel for localized, controlled non-viral gene delivery to promote angiogenesis, cellular infiltration, and vascular ingrowth into the scaffold for improved cutaneous would healing. Despite reported strategies to promote angiogenesis within implanted scaffolds, there are limited reports on the strategic design of hydrogels, in particular, with or without the aid of bioactive signals to promote angiogenesis in a clinically relevant timeframe or with practical considerations. The following sections recall the proposed specific aims and hypotheses, describe the major conclusions, and discuss possible future directions.

## 8.2 Specific Aim 1 (Chapter 4)

This aim developed an improved technique with significantly reduced processing time to generate porous HA hydrogels for enhanced cellular infiltration *in vitro* and *in vivo*. Following rigorous *in vitro* characterization, a murine subcutaneous implant model was utilized to assess its performance *in vivo*.

*Hypothesis 1*: Resuspension of porogens in volatile solution will allow for easier liquid handling and reproducible sphere-templating to generate microporous HA hydrogels with greatly reduced manufacturing time.

Resuspension of PMMA microspheres in ethanol or acetone solutions to create a sphere template for porous hydrogel formation resulted in comparable hydrogel pore interconnectivity and swelling, with no cytotoxic effects *in vitro* when compared to the commonly used heat sintered PMMA microspheres. Moreover, following subcutaneous implantation in mice, endogenous cell infiltration and vascular ingrowth was similar among the groups. Thus, the process for sphere templating to generate porous HA hydrogels was optimized with resuspending the porogens in volatile solutions to reduce manufacturing time from 17-22 h to only 1-2 h. It is also important to note that n-pore gels implanted *in vivo* had minimal cellular infiltration with most degradation occurring at the periphery of the gel, supporting our design choice of scaffolds with porous structure. The chemical sintering technique developed in this Aim was applied to experiments featured in the remainder of this dissertation when porous hydrogels are discussed.

**8.3 Specific Aim 2** (Chapter 5)

This aim investigated the implantation of various conductive and inductive scaffolds to determine the effect of scaffold type on tissue repair in a murine splinted wound healing model over 7 days. The scaffold types used in this study was: fibrin, porous HA hydrogel, a composite of fibrin and porous HA, and an inductive composite gel with plasmin-degradable vascular endothelial growth factor (VEGF) nanocapsules embedded within the composite gel.

*Hypothesis 2*: The porous architecture of the HA hydrogel will better preserve the structure of skin for cellular infiltration when compared to fibrin.

*Hypothesis 3*: Incorporation of an inductive factor, plasmin-degradable nanocapsules delivering VEGF will enhance vascularization of the newly formed tissue.

Here, we demonstrate how scaffold choice significantly influences the effect of wound healing in a humanized murine splinted wound healing model over 7 days. Interestingly, despite fibrin's popularity as a scaffold, fibrin treated wounds resulted in slow wound closure and thin granulation tissue formation similar to untreated wounds. Since the density of the fibrin gel at 10 mg/ml may have been a physical barrier to wound closure, a future study may investigate wound closure as a function of fibrin gel concentration. Conversely, the porous architecture of the HA gel resulted in significantly rapid wound closure better preservation of the dermal volume and more mural-covered blood vessels. The inclusion of plasmin-degradable nanocapules delivering VEGF into composite gels resulted in more rapid wound closure, but not increased vascularization. This may be due to several reasons that include: (i) the amount of VEGF incorporated into the gels was not enough to result in an enhanced therapeutic response or (ii) the nanocapules did not degrade enough to release the payload. Future studies can be done to test both ideas; wound closure and vascularization can be studied as a function of VEGF nanocapsule concentration and hydrogels loaded with nanocapsules containing fluorescent or radiolabeled molecules are monitored for release *in vivo* to determine whether the harsh wound environment indeed can degrade the capsules for release.

**8.4 Specific Aim 3** (Chapter 6)

This aim tested an approach to treat DNA-loaded porous HA hydrogels with hyaluronidase to enhance DNA release for improved transfection. Two different techniques

(traditional vs. previously described technique by our lab [CnE]) to load DNA/poly(ethylene imine) polyplexes into the porous HA gels were discussed in this aim. Gene transfer and angiogenesis was evaluated *in vitro* and *in vivo* in a splinted murine wound healing model at days 5 and 10.

*Hypothesis 4*: Porous HA hydrogel mechanics and DNA release will be a function of hyaluronidase concentration.

*Hypothesis 5*: The large concentration of DNA loaded via caged nanoparticle encapsulation (CnE) will result in higher transgene expression as the polyplexes are released from the hydrogel.

*Hypothesis 6*: The incorporation of plasmids encoding for VEGF, a proangiogenic factor, into porous HA gels treated with hyaluronidase will enhance wound closure, angiogenesis, and cellular infiltration when compared to untreated porous HA gels.

Here we demonstrate that porous HA hydrogels degradation and mechanical properties are a function of hyaluronidase concentration, although encapsulated DNA polyplexes are well retained. We also validate the caged nanoparticle encapsulation (CnE) of the DNA polyplexes as a technique to load large amounts of DNA within a porous HA hydrogel with minimal aggregation. This technique paired with hyaluronidase treatment resulted in significantly higher transfection *in vitro* when compared to the traditional DNA polyplex loading technique. Moreover, the effect of mechanical properties was decoupled from HAase treatment to confirm that HAase was indeed responsible for the enhanced transfection. Application of HAase treated DNA-loaded porous HA gels agreed with *in vitro* studies where gels pre-treated with HAase

resulted in significantly higher transfection and improved wound healing, cellular infiltration, and vascular activity. Despite our confidence in HAase functioning to make MMP-degradable crosslinks more accessible and available for cell-mediated degradation and DNA polyplex release, a quantitative approach would provide stronger support. To do this, future studies can investigate the percolation threshold of porous hydrogels as a function of hyaluronidase concentration. Quantifying the shift where the crosslinked gel becomes more “liquid-like” due to various HAase treatments would be valuable information for tunable delivery. Regardless, the breakthrough in achieving transfection from our DNA loaded porous HA gels was very exciting, and HAase treatment of DNA-loaded gels was instituted following the studies described in Chapter 6.

**8.5 Specific Aim 4** (Chapter 7)

This aim utilized the hyaluronidase pre-treatment of DNA-loaded porous hydrogels described in Aim 3 (Chapter 6) towards a strategy for sequential gene delivery. Two different hydrogel designs were investigated *in vitro* before moving forward *in vivo* with one system. Full thickness dermal wounds in mice were implanted with the engineered hydrogels and transfection was monitored via optical imaging for 21 days. A splinted murine wound healing model was used to assess transfection, angiogenesis, and wound healing as a function of spatio-temporal presentations of polyplexes encoding for pro-angiogenic factors (VEGF and PDGF).

*Hypothesis 7*: Porous hydrogels with encapsulated and surface coated polyplexes (different plasmids for each presentation) will result in transfection from surface coated polyplexes first since they are more immediately available and accessible to infiltrating cells than encapsulated polyplexes.

*Hypothesis 8*: Cells will degrade non-porous gels slower thus a two phase hydrogel system containing a central non-porous post surrounded by a porous HA gel with different plasmids within each distinct phase will result in different transgene expression profiles.

*Hypothesis 9*: The spatio-temporal presentation of pro-angiogenic plasmids within the hydrogel will affect the number and type of vascular cells present within the newly formed tissue.

Here, we demonstrate an investigation of two hydrogel systems for sequential non-viral gene delivery *in vitro*. The first system described in Chapter 7 was a porous hydrogel composed of two different plasmids either encapsulated or electrostatically bound to the surface of the pores via surface coating. Surprisingly, *in vitro* transfection showed that the encapsulated polyplexes resulted in transgene expression similar to the surface coated polyplexes even at day 1. We had hypothesized that since polyplexes bound on the surface of the pores are more readily available for uptake, the surface coated polyplex transgene expression profile would be much higher than the encapsulated polyplexes. The other system investigated was a two phase hydrogel where a central non-porous post was surrounded by a second porous gel, with each phase containing different plasmids. In this two phase system, *in vitro* transfection showed very different transgene expression profiles as expected, where encapsulated polyplexes achieved high transfection first while transgene expression of the n-pore post polyplexes took about 6 days to ramp up. Application of a hybrid two phase hydrogel with surface coated polyplexes *in vivo* showed that transfection occurred during similar time frames, despite the distinctly different expression profiles observed *in vitro*. This highlights the importance of *in vitro* vs. *in vivo* studies; *in vivo* studies must be performed to investigate or validate *in vitro* findings that may have been oversimplified. Despite not being able to achieve sequential gene delivery in Chapter 7, we still

maintain that it is possible with this system if hydrogel properties were modified. For example, crosslinking density of the porous or n-pore post can be modified to allow for faster cell-mediated degradation and DNA polyplex release for transfection. Once different transgene expression profiles have been achieved, transfection could be further controlled with delivering vectors with inducible promoters to regulate and time protein expression.

Application of this two phase gene delivery system with pVEGF and pPDGF polyplexes did not result in differences in vascularization with regard to regions within the granulation tissue (edge vs. center). The observation that NG2+ area was not found to be higher in the wound center, as expected, with implanted V→P gels may be attributed to the time point (day 7) or perhaps the assumption that only VEGF should come first then PDGF is incorrect. It may be that a simultaneous presentation of both as in the V/P gels is necessary for angiogenesis in a wound healing model. That synergistic effect may explain the enhanced wound closure and NG2+ area in wounds treated with V/P gels. Future studies can be conducted to investigate vessel quality and function as a result of transfection with these pro-angiogenic plasmids. Doppler flow studies can be used to monitor vessel function in real time as wounds heal. Moreover perfusion of dye or fluorescent dyes would aid in determining vessel permeability and maturity. Likewise, micro-CT would be a valuable tool to obtain a three-dimensional view of wound vascularization.

# CHAPTER 9

# REFERENCES

[1] Hudson DM. Human anatomy & physiology. Portland, ME: Walch Pub.; 2006.

[2] Gurtner GC, Werner S, Barrandon Y, Longaker MT. Wound repair and regeneration. Nature. 2008;453:314-21.

[3] Sun BK, Siprashvili Z, Khavari PA. Advances in skin grafting and treatment of cutaneous wounds. Science. 2014;346:941-5.

[4] Swift ME, Burns AL, Gray KL, DiPietro LA. Age-Related Alterations in the Inflammatory Response to Dermal Injury. 2001;117:1027-35.

[5] Guo S, DiPietro LA. Factors Affecting Wound Healing. J Dent Res. 2010;89:219-29.

[6] Zhao M, Song B, Pu J, Wada T, Reid B, Tai GP, et al. Electrical signals control wound healing through phosphatidylinositol-3-OH kinase-gamma and PTEN. Nature. 2006;442:457-60.

[7] Ogawa R. The Most Current Algorithms for the Treatment and Prevention of Hypertrophic Scars and Keloids. Plastic and Reconstructive Surgery. 2010;125:557-68.

[8] Eaglstein WH. Moist Wound Healing with Occlusive Dressings: A Clinical Focus. Dermatologic Surgery. 2001;27:175-82.

[9] Halim AS, Khoo TL, Mohd. Yussof SJ. Biologic and synthetic skin substitutes: An overview. Indian Journal of Plastic Surgery : Official Publication of the Association of Plastic Surgeons of India. 2010;43:S23-S8.

[10] Vyas K, Vasconez H. Wound Healing: Biologics, Skin Substitutes, Biomembranes and Scaffolds. Healthcare. 2014;2:356-400.

[11] Snyder DL, Sullivan N, Schoelles KM. Skin Substitutes for Treating Chronic Wounds. 2012.

[12] Shevchenko RV, James SL, James SE. A review of tissue-engineered skin bioconstructs available for skin reconstruction2010.

[13] Bramfeldt H, Sabra G, Centis V, Vermette P. Scaffold Vascularization: A Challenge for Three-Dimensional Tissue Engineering. Current Medicinal Chemistry. 2010;17:3944-67.

[14] Carmeliet P, Jain RK. Molecular mechanisms and clinical applications of angiogenesis. Nature. 2011;473:298-307.

[15] Kannan RY, Salacinski HJ, Sales K, Butler P, Seifalian AM. The roles of tissue engineering and vascularisation in the development of micro-vascular networks: a review. Biomaterials. 2005;26:1857-75.

[16] Peirce SM, Skalak TC. Microvascular remodeling: a complex continuum spanning angiogenesis to arteriogenesis. Microcirculation. 2003;10:99-111.

[17] Jain RK, Au P, Tam J, Duda DG, Fukumura D. Engineering vascularized tissue. Nat Biotech. 2005;23:821-3.

[18] Singer AJ, Clark RAF. Cutaneous Wound Healing. New England Journal of Medicine. 1999;341:738-46.

[19] Eming SA, Krieg T, Davidson JM. Gene therapy and wound healing. Clin Dermatol. 2007;25:79-92.

[20] Rimann M, Hall H. Non-viral and local gene medicine for improvement of cutaneous wound healing. Gene Ther Mol Biol. 2009;13:53-63.

[21] Novosel EC, Kleinhans C, Kluger PJ. Vascularization is the key challenge in tissue engineering. Advanced Drug Delivery Reviews. 2011;63:300-11.

[22] Tremblay P-L, Hudon V, Berthod F, Germain L, Auger FA. Inosculation of Tissue-Engineered Capillaries with the Host's Vasculature in a Reconstructed Skin Transplanted on Mice. American Journal of Transplantation. 2005;5:1002-10.

[23] Laschke MW, Rucker M, Jensen G, Carvalho C, Mulhaupt R, Gellrich NC, et al. Improvement of vascularization of PLGA scaffolds by inosculation of in situ-preformed functional blood vessels with the host microvasculature. Ann Surg. 2008;248:939-48.

[24] Mikos AG, Sarakinos G, Lyman MD, Ingber DE, Vacanti JP, Langer R. Prevascularization of porous biodegradable polymers. Biotechnology and Bioengineering. 1993;42:716-23.

[25] Jang JH, Rives CB, Shea LD. Plasmid delivery in vivo from porous tissue-engineering scaffolds: transgene expression and cellular transfection. Mol Ther. 2005;12:475-83.

[26] Chiu YC, Larson JC, Isom A, Jr., Brey EM. Generation of porous poly(ethylene glycol) hydrogels by salt leaching. Tissue Eng Part C Methods. 2010;16:905-12.

[27] Galperin A, Long TJ, Ratner BD. Degradable, Thermo-Sensitive Poly(N-isopropyl acrylamide)-Based Scaffolds with Controlled Porosity for Tissue Engineering Applications. Biomacromolecules. 2010;11:2583-92.

[28] Kang JY, Chung CW, Sung JH, Park BS, Choi JY, Lee SJ, et al. Novel porous matrix of hyaluronic acid for the three-dimensional culture of chondrocytes. Int J Pharm. 2009;369:114-20.

[29] Madden LR, Mortisen DJ, Sussman EM, Dupras SK, Fugate JA, Cuy JL, et al. Proangiogenic scaffolds as functional templates for cardiac tissue engineering. Proc Natl Acad Sci U S A. 2010;107:15211-6.

[30] Chiu YC, Cheng MH, Engel H, Kao SW, Larson JC, Gupta S, et al. The role of pore size on vascularization and tissue remodeling in PEG hydrogels. Biomaterials. 2011;32:6045-51.

[31] Tokatlian T, Cam C, Siegman SN, Lei Y, Segura T. Design and characterization of microporous hyaluronic acid hydrogels for in vitro gene transfer to mMSCs. Acta Biomaterialia. 2012;8:3921-31.

[32] Tokatlian T, Cam C, Segura T. Non-viral DNA delivery from porous hyaluronic acid hydrogels in mice. Biomaterials. 2014;35:825-35.

[33] Tokatlian T, Cam C, Segura T. Porous Hyaluronic Acid Hydrogels for Localized Nonviral DNA Delivery in a Diabetic Wound Healing Model. Advanced Healthcare Materials. 2015:n/a-n/a.

[34] Okay O. General Properties of Hydrogels. 2009.

[35] Garg T, Singh O, Arora S, Murthy R. Scaffold: a novel carrier for cell and drug delivery. Crit Rev Ther Drug Carrier Syst. 2012;29:1-63.

[36] Slaughter BV, Khurshid SS, Fisher OZ, Khademhosseini A, Peppas NA. Hydrogels in regenerative medicine. Adv Mater. 2009;21:3307-29.

[37] Taylor KR, Trowbridge JM, Rudisill JA, Termeer CC, Simon JC, Gallo RL. Hyaluronan Fragments Stimulate Endothelial Recognition of Injury through TLR4. J Biol Chem. 2004;279:17079-84.

[38] Reitinger S, Lepperdinger G. Hyaluronan, a ready choice to fuel regeneration: a mini-review. Gerontology. 2013;59:71-6.

[39] Toole BP. Hyaluronan: from extracellular glue to pericellular cue. Nat Rev Cancer. 2004;4:528-39.

[40] Dechert TA, Ducale AE, Ward SI, Yager DR. Hyaluronan in human acute and chronic dermal wounds. Wound Repair and Regeneration. 2006;14:252-8.

[41] Slevin M, Krupinski J, Gaffney J, Matou S, West D, Delisser H, et al. Hyaluronan-mediated angiogenesis in vascular disease: Uncovering RHAMM and CD44 receptor signaling pathways. Matrix Biology. 2007;26:58-68.

[42] Slevin M, Kumar S, Gaffney J. Angiogenic Oligosaccharides of Hyaluronan Induce Multiple Signaling Pathways Affecting Vascular Endothelial Cell Mitogenic and Wound Healing Responses. J Biol Chem. 2002;277:41046-59.

[43] Gao F, Liu Y, He Y, Yang C, Wang Y, Shi X, et al. Hyaluronan oligosaccharides promote excisional wound healing through enhanced angiogenesis. Matrix Biology. 2010;29:107-16.

[44] Shu XZ, Liu Y, Luo Y, Roberts MC, Prestwich GD. Disulfide Cross-Linked Hyaluronan Hydrogels. Biomacromolecules. 2002;3:1304-11.

[45] Camci-Unal G, Nichol JW, Bae H, Tekin H, Bischoff J, Khademhosseini A. Hydrogel surfaces to promote attachment and spreading of endothelial progenitor cells. Journal of Tissue Engineering and Regenerative Medicine. 2012:n/a-n/a.

[46] Eng D, Caplan M, Preul M, Panitch A. Hyaluronan scaffolds: A balance between backbone functionalization and bioactivity. Acta Biomaterialia. 2010;6:2407-14.

[47] Burdick JA, Prestwich GD. Hyaluronic acid hydrogels for biomedical applications. Adv Mater. 2011;23:H41-56.

[48] Bulpitt P, Aeschlimann D. New strategy for chemical modification of hyaluronic acid: Preparation of functionalized derivatives and their use in the formation of novel biocompatible hydrogels. J Biomed Mater Res. 1999;47:152-69.

[49] Lei Y, Gojgini S, Lam J, Segura T. The spreading, migration and proliferation of mouse mesenchymal stem cells cultured inside hyaluronic acid hydrogels. Biomaterials. 2011;32:39-47.

[50] Kim J, Park Y, Tae G, Lee K, Hwang S, Kim I, et al. Synthesis and characterization of matrix metalloprotease sensitive-low molecular weight hyaluronic acid based hydrogels. J Mater Sci: Mater Med. 2008;19:3311-8.

[51] Gill SE, Parks WC. Metalloproteinases and their inhibitors: Regulators of wound healing. The International Journal of Biochemistry & Cell Biology. 2008;40:1334-47.

[52] Bowen-Pope DF, Malpass TW, Foster DM, Ross R. Platelet-derived growth factor in vivo: levels, activity, and rate of clearance. Blood. 1984;64:458-69.

[53] Edelman ER, Nugent MA, Karnovsky MJ. Perivascular and intravenous administration of basic fibroblast growth factor: vascular and solid organ deposition. Proc Natl Acad Sci U S A. 1993;90:1513-7.

[54] Eppler SM, Combs DL, Henry TD, Lopez JJ, Ellis SG, Yi JH, et al. A target-mediated model to describe the pharmacokinetics and hemodynamic effects of recombinant human vascular endothelial growth factor in humans. Clin Pharmacol Ther. 2002;72:20-32.

[55] Simons M, Annex BH, Laham RJ, Kleiman N, Henry T, Dauerman H, et al. Pharmacological treatment of coronary artery disease with recombinant fibroblast growth factor-2: double-blind, randomized, controlled clinical trial. Circulation. 2002;105:788-93.

[56] Simons M, Ware JA. Therapeutic angiogenesis in cardiovascular disease. Nat Rev Drug Discov. 2003;2:863-71.

[57] Henry TD, Annex BH, McKendall GR, Azrin MA, Lopez JJ, Giordano FJ, et al. The VIVA trial: Vascular endothelial growth factor in Ischemia for Vascular Angiogenesis. Circulation. 2003;107:1359-65.

[58] Gauglitz GG, Jeschke MG. Combined gene and stem cell therapy for cutaneous wound healing. Mol Pharm. 2011;8:1471-9.

[59] Agarwal A, Mallapragada SK. Synthetic sustained gene delivery systems. Curr Top Med Chem. 2008;8:311-0.

[60] Lee S, Chen TT, Barber CL, Jordan MC, Murdock J, Desai S, et al. Autocrine VEGF Signaling Is Required for Vascular Homeostasis. Cell. 2007;130:691-703.

[61] Huang M, Chen Z, Hu S, Jia F, Li Z, Hoyt G, et al. Novel minicircle vector for gene therapy in murine myocardial infarction. Circulation. 2009;120:S230-7.

[62] Wilber A, Frandsen JL, Wangensteen KJ, Ekker SC, Wang X, McIvor RS. Dynamic gene expression after systemic delivery of plasmid DNA as determined by in vivo bioluminescence imaging. Hum Gene Ther. 2005;16:1325-32.

[63] Meilander-Lin NJ, Cheung PJ, Wilson DL, Bellamkonda RV. Sustained in vivo gene delivery from agarose hydrogel prolongs nonviral gene expression in skin. Tissue Eng. 2005;11:546-55.

[64] Storrie H, Mooney DJ. Sustained delivery of plasmid DNA from polymeric scaffolds for tissue engineering. Adv Drug Deliv Rev. 2006;58:500-14.

[65] Chen RR, Mooney DJ. Polymeric growth factor delivery strategies for tissue engineering. Pharm Res. 2003;20:1103-12.

[66] De Laporte L, Shea LD. Matrices and scaffolds for DNA delivery in tissue engineering. Adv Drug Deliv Rev. 2007;59:292-307.

[67] Yamamoto M, Tabata Y. Tissue engineering by modulated gene delivery. Adv Drug Deliv Rev. 2006;58:535-54.

[68] Pannier AK, Shea LD. Controlled Release Systems for DNA Delivery. Mol Ther. 2004;10:19-26.

[69] Herweijer H, Wolff JA. Progress and prospects: naked DNA gene transfer and therapy. Gene Ther. 2003;10:453-8.

[70] Yew NS, Zhao H, Wu IH, Song A, Tousignant JD, Przybylska M, et al. Reduced Inflammatory Response to Plasmid DNA Vectors by Elimination and Inhibition of Immunostimulatory CpG Motifs. Mol Ther. 2000;1:255-62.

[71] Klinman DM, Yamshchikov G, Ishigatsubo Y. Contribution of CpG motifs to the immunogenicity of DNA vaccines. J Immunol. 1997;158:3635-9.

[72] Scheule RK. The role of CpG motifs in immunostimulation and gene therapy. Advanced Drug Delivery Reviews. 2000;44:119-34.

[73] Yew NS, Zhao H, Przybylska M, Wu IH, Tousignant JD, Scheule RK, et al. CpG-depleted plasmid DNA vectors with enhanced safety and long-term gene expression in vivo. Mol Ther. 2002;5:731-8.

[74] Darquet AM, Rangara R, Kreiss P, Schwartz B, Naimi S, Delaere P, et al. Minicircle: an improved DNA molecule for in vitro and in vivo gene transfer. Gene Ther. 1999;6:209-18.

[75] Chen ZY, He CY, Ehrhardt A, Kay MA. Minicircle DNA vectors devoid of bacterial DNA result in persistent and high-level transgene expression in vivo. Mol Ther. 2003;8:495-500.

[76] Papadakis ED, Nicklin SA, Baker AH, White SJ. Promoters and control elements: designing expression cassettes for gene therapy. Curr Gene Ther. 2004;4:89-113.

[77] Nguyen AT, Dow AC, Kupiec-Weglinski J, Busuttil RW, Lipshutz GS. Evaluation of Gene Promoters for Liver Expression by Hydrodynamic Gene Transfer. Journal of Surgical Research. 2008;148:60-6.

[78] Avilés MO, Lin C-H, Zelivyanskaya M, Graham JG, Boehler RM, Messersmith PB, et al. The contribution of plasmid design and release to in vivo gene expression following delivery from cationic polymer modified scaffolds. Biomaterials. 2010;31:1140-7.

[79] Gill DR, Pringle IA, Hyde SC. Progress and prospects: the design and production of plasmid vectors. Gene Ther. 2009;16:165-71.

[80] Thomas M, Klibanov AM. Non-viral gene therapy: polycation-mediated DNA delivery. Applied Microbiology and Biotechnology. 2003;62:27-34.

[81] Tros de Ilarduya C, Sun Y, Düzgüneş N. Gene delivery by lipoplexes and polyplexes. European Journal of Pharmaceutical Sciences. 2010;40:159-70.

[82] Luo D, Saltzman WM. Synthetic DNA delivery systems. Nat Biotech. 2000;18:33-7.

[83] Scholz C, Wagner E. Therapeutic plasmid DNA versus siRNA delivery: Common and different tasks for synthetic carriers. Journal of Controlled Release. 2012;161:554-65.

[84] des Rieux A, Shikanov A, Shea LD. Fibrin hydrogels for non-viral vector delivery in vitro. Journal of Controlled Release. 2009;136:148-54.

[85] Shepard JA, Huang A, Shikanov A, Shea LD. Balancing cell migration with matrix degradation enhances gene delivery to cells cultured three-dimensionally within hydrogels. J Control Release. 2010;146:128-35.

[86] Lei P, Padmashali RM, Andreadis ST. Cell-controlled and spatially arrayed gene delivery from fibrin hydrogels. Biomaterials. 2009;30:3790-9.

[87] Wegman F, Geuze RE, van der Helm YJ, Cumhur Öner F, Dhert WJA, Alblas J. Gene delivery of bone morphogenetic protein-2 plasmid DNA promotes bone formation in a large animal model. Journal of Tissue Engineering and Regenerative Medicine. 2012:n/a-n/a.

[88] He CX, Tabata Y, Gao JQ. Non-viral gene delivery carrier and its three-dimensional transfection system. Int J Pharm. 2010;386:232-42.

[89] Kwoh DY, Coffin CC, Lollo CP, Jovenal J, Banaszczyk MG, Mullen P, et al. Stabilization of poly-l-lysine/DNA polyplexes for in vivo gene delivery to the liver. Biochimica et Biophysica Acta (BBA) - Gene Structure and Expression. 1999;1444:171-90.

[90] Zhang X, Ma G-H, Su Z-G, Benkirane-Jessel N. Novel poly(L-lysine) particles for gene delivery. Journal of Controlled Release. 2011;152, Supplement 1:e182-e4.

[91] Merdan T, Kopeček J, Kissel T. Prospects for cationic polymers in gene and oligonucleotide therapy against cancer. Advanced Drug Delivery Reviews. 2002;54:715-58.

[92] Morille M, Passirani C, Vonarbourg A, Clavreul A, Benoit J-P. Progress in developing cationic vectors for non-viral systemic gene therapy against cancer. Biomaterials. 2008;29:3477-96.

[93] Pathak A, Patnaik S, Gupta KC. Recent trends in non-viral vector-mediated gene delivery. Biotechnology Journal. 2009;4:1559-72.

[94] Lavertu M, Méthot S, Tran-Khanh N, Buschmann MD. High efficiency gene transfer using chitosan/DNA nanoparticles with specific combinations of molecular weight and degree of deacetylation. Biomaterials. 2006;27:4815-24.

[95] Aillon KL, Xie Y, El-Gendy N, Berkland CJ, Forrest ML. Effects of nanomaterial physicochemical properties on in vivo toxicity. Advanced Drug Delivery Reviews. 2009;61:457-66.

[96] Gojgini S, Tokatlian T, Segura T. Utilizing Cell–Matrix Interactions To Modulate Gene Transfer to Stem Cells Inside Hyaluronic Acid Hydrogels. Molecular Pharmaceutics. 2011;8:1582-91.

[97] Kleemann E, Jekel N, Dailey LA, Roesler S, Fink L, Weissmann N, et al. Enhanced gene expression and reduced toxicity in mice using polyplexes of low-molecular-weight poly(ethylene imine) for pulmonary gene delivery. J Drug Target. 2009;17:638-51.

[98] Perevyazko IY, Bauer M, Pavlov GM, Hoeppener S, Schubert S, Fischer D, et al. Polyelectrolyte Complexes of DNA and Linear PEI: Formation, Composition and Properties. Langmuir. 2012;28:16167-76.

[99] Asuri P, Bartel MA, Vazin T, Jang J-H, Wong TB, Schaffer DV. Directed Evolution of Adeno-associated Virus for Enhanced Gene Delivery and Gene Targeting in Human Pluripotent Stem Cells. Mol Ther. 2012;20:329-38.

[100] Zhang Y, Wu C, Luo T, Li S, Cheng X, Miron RJ. Synthesis and inflammatory response of a novel silk fibroin scaffold containing BMP7 adenovirus for bone regeneration. Bone. 2012;51:704-13.

[101] Koria P. Delivery of Growth Factors for Tissue Regeneration and Wound Healing. BioDrugs. 2012;26:163-75.

[102] Trentin D, Hall H, Wechsler S, Hubbell JA. Peptide-matrix-mediated gene transfer of an oxygen-insensitive hypoxia-inducible factor-1alpha variant for local induction of angiogenesis. Proc Natl Acad Sci U S A. 2006;103:2506-11.

[103] Ginsburg DS, Thyagarajan, B., Phillips, J.E., Calos, M.P. Gene Delivery by Viruses. Encyclopedia of Life Sciences. 2005:1-5.

[104] Giacca M, Zacchigna S. Virus-mediated gene delivery for human gene therapy. Journal of Controlled Release. 2012;161:377-88.

[105] Curtin CM, Cunniffe GM, Lyons FG, Bessho K, Dickson GR, Duffy GP, et al. Innovative collagen nano-hydroxyapatite scaffolds offer a highly efficient non-viral gene delivery platform for stem cell-mediated bone formation. Adv Mater. 2012;24:749-54.

[106] Shin S, Shea LD. Lentivirus Immobilization to Nanoparticles for Enhanced and Localized Delivery From Hydrogels. Mol Ther. 2010;18:700-6.

[107] Shea LD, Smiley E, Bonadio J, Mooney DJ. DNA delivery from polymer matrices for tissue engineering. Nat Biotechnol. 1999;17:551-4.

[108] Kong H, Kim E, Huang Y-C, Mooney D. Design of Biodegradable Hydrogel for the Local and Sustained Delivery of Angiogenic Plasmid DNA. Pharmaceutical Research. 2008;25:1230-8.

[109] Kidd ME, Shin S, Shea LD. Fibrin hydrogels for lentiviral gene delivery in vitro and in vivo. Journal of Controlled Release. 2012;157:80-5.

[110] Raut SD, Lei P, Padmashali RM, Andreadis ST. Fibrin-mediated lentivirus gene transfer: Implications for lentivirus microarrays. Journal of Controlled Release. 2010;144:213-20.

[111] Saito T, Tabata Y. Preparation of gelatin hydrogels incorporating small interfering RNA for the controlled release. J Drug Target. 2012;20:864-72.

[112] Shepard JA, Wesson PJ, Wang CE, Stevans AC, Holland SJ, Shikanov A, et al. Gene therapy vectors with enhanced transfection based on hydrogels modified with affinity peptides. Biomaterials. 2011;32:5092-9.

[113] Lei Y, Rahim M, Ng Q, Segura T. Hyaluronic acid and fibrin hydrogels with concentrated DNA/PEI polyplexes for local gene delivery. J Control Release. 2011;153:255-61.

[114] Lei Y, Segura T. DNA delivery from matrix metalloproteinase degradable poly(ethylene glycol) hydrogels to mouse cloned mesenchymal stem cells. Biomaterials. 2009;30:254-65.

[115] Lei YG, Huang SX, Sharif-Kashani P, Chen Y, Kavehpour P, Segura T. Incorporation of active DNA/cationic polymer polyplexes into hydrogel scaffolds. Biomaterials. 2010;31:9106-16.

[116] Shepard JA, Virani FR, Goodman AG, Gossett TD, Shin S, Shea LD. Hydrogel macroporosity and the prolongation of transgene expression and the enhancement of angiogenesis. Biomaterials. 2012;33:7412-21.

[117] Kim HS, Yoo HS. MMPs-responsive release of DNA from electrospun nanofibrous matrix for local gene therapy: In vitro and in vivo evaluation. Journal of Controlled Release. 2010;145:264-71.

[118] Tokatlian T, Shrum CT, Kadoya WM, Segura T. Protease degradable tethers for controlled and cell-mediated release of nanoparticles in 2- and 3-dimensions. Biomaterials. 2010;31:8072-80.

[119] Segura T, Chung PH, Shea LD. DNA delivery from hyaluronic acid-collagen hydrogels via a substrate-mediated approach. Biomaterials. 2005;26:1575-84.

[120] Saul JM, Linnes MP, Ratner BD, Giachelli CM, Pun SH. Delivery of non-viral gene carriers from sphere-templated fibrin scaffolds for sustained transgene expression. Biomaterials. 2007;28:4705-16.

[121] Chang PC, Seol YJ, Cirelli JA, Pellegrini G, Jin Q, Franco LM, et al. PDGF-B gene therapy accelerates bone engineering and oral implant osseointegration. Gene Ther. 2009;17:95-104.

[122] Rose LC, Kucharski C, Uludag H. Protein expression following non-viral delivery of plasmid DNA coding for basic FGF and BMP-2 in a rat ectopic model. Biomaterials. 2012;33:3363-74.

[123] Chang SCN, Chung H-Y, Tai C-L, Chen PKT, Lin T-M, Jeng L-B. Repair of large cranial defects by hBMP-2 expressing bone marrow stromal cells: Comparison between alginate and collagen type I systems. Journal of Biomedical Materials Research Part A. 2010;94A:433-41.

[124] Tuinstra HM, Aviles MO, Shin S, Holland SJ, Zelivyanskaya ML, Fast AG, et al. Multifunctional, multichannel bridges that deliver neurotrophin encoding lentivirus for regeneration following spinal cord injury. Biomaterials. 2012;33:1618-26.

[125] Yang Y, Xia T, Chen F, Wei W, Liu C, He S, et al. Electrospun Fibers with Plasmid bFGF Polyplex Loadings Promote Skin Wound Healing in Diabetic Rats. Molecular Pharmaceutics. 2011;9:48-58.

[126] Guo R, Xu S, Ma L, Huang A, Gao C. Enhanced angiogenesis of gene-activated dermal equivalent for treatment of full thickness incisional wounds in a porcine model. Biomaterials. 2010;31:7308-20.

[127] Luo T, Zhang W, Shi B, Cheng X, Zhang Y. Enhanced bone regeneration around dental implant with bone morphogenetic protein 2 gene and vascular endothelial growth factor protein delivery. Clinical Oral Implants Research. 2012;23:467-73.

[128] Khormaee S, Ali OA, Chodosh J, Mooney DJ. Optimizing siRNA efficacy through alteration in the target cell-adhesion substrate interaction. J Biomed Mater Res A. 2012;100:2637-43.

[129] Orsi S, Guarnieri D, De Capua A, Netti PA. Gene-activated and cell-migration guiding PEG matrices based on three dimensional patterning of RGD peptides and DNA complexes. Acta Biomater. 2012;8:3228-40.

[130] Dhaliwal A, Maldonado M, Lin C, Segura T. Cellular Cytoskeleton Dynamics Modulates Non-Viral Gene Delivery through RhoGTPases. PLoS One. 2012;7:e35046.

[131] Dhaliwal A, Maldonado M, Han Z, Segura T. Differential uptake of DNA–poly(ethylenimine) polyplexes in cells cultured on collagen and fibronectin surfaces. Acta Biomaterialia. 2010;6:3436-47.

[132] Riddle KW, Kong HJ, Leach JK, Fischbach C, Cheung C, Anseth KS, et al. Modifying the proliferative state of target cells to control DNA expression and identifying cell types transfected in vivo. Mol Ther. 2007;15:361-8.

[133] Huang YC, Riddle K, Rice KG, Mooney DJ. Long-term in vivo gene expression via delivery of PEI-DNA condensates from porous polymer scaffolds. Hum Gene Ther. 2005;16:609-17.

[134] Nam YS, Yoon JJ, Park TG. A novel fabrication method of macroporous biodegradable polymer scaffolds using gas foaming salt as a porogen additive. J Biomed Mater Res. 2000;53:1-7.

[135] Huang X, Zhang Y, Donahue HJ, Lowe TL. Porous thermoresponsive-co-biodegradable hydrogels as tissue-engineering scaffolds for 3-dimensional in vitro culture of chondrocytes. Tissue Eng. 2007;13:2645-52.

[136] Iyer P, Walker KJ, Madihally SV. Increased matrix synthesis by fibroblasts with decreased proliferation on synthetic chitosan-gelatin porous structures. Biotechnol Bioeng. 2012;109:1314-25.

[137] Kang HW, Tabata Y, Ikada Y. Fabrication of porous gelatin scaffolds for tissue engineering. Biomaterials. 1999;20:1339-44.

[138] Van Vlierberghe S, Cnudde V, Masschaele B, Dubruel P, De Paepe I, Jacobs PJ, et al. Porous gelatin cryogels as cell delivery tool in tissue engineering. J Control Release. 2006;116:e95-8.

[139] Lanasa SM, Hoffecker IT, Bryant SJ. Presence of pores and hydrogel composition influence tensile properties of scaffolds fabricated from well-defined sphere templates. J Biomed Mater Res B Appl Biomater. 2011;96:294-302.

[140] Shelly R. Peyton ZIK, Joshua C. Cohen, Anne P. Runkle,, Krystyn J. Van Vliet DAL, Linda G. Griffith. Marrow-Derived Stem Cell Motility in 3D Synthetic Scaffold Is Governed by Geometry Along With Adhesivity and Stiffness. Biotechnology and Bioengineering. 2010;108:1181-93.

[141] Stachowiak AN, Bershteyn A, Tzatzalos E, Irvine DJ. Bioactive hydrogels with an ordered cellular structure combine interconnected macroporosity and robust mechanical properties. Advanced Materials. 2005;17:399-+.

[142] Ratner BD. A paradigm shift: biomaterials that heal. Polym Int. 2007;56:1183-5.

[143] Ghajar CM, George SC, Putnam AJ. Matrix metalloproteinase control of capillary morphogenesis. Crit Rev Eukaryot Gene Expr. 2008;18:251-78.

[144] Tokatlian T, Shrum CT, Kadoya WM, Segura T. Protease degradable tethers for controlled and cell-mediated release of nanoparticles in 2- and 3-dimensions. Biomaterials. 2010;31:8072-80.

[145] Schrementi ME, Ferreira AM, Zender C, DiPietro LA. Site-specific production of TGF-beta in oral mucosal and cutaneous wounds. Wound Repair Regen. 2008;16:80-6.

[146] Szpaderska AM, Zuckerman JD, DiPietro LA. Differential injury responses in oral mucosal and cutaneous wounds. J Dent Res. 2003;82:621-6.

[147] Engler AJ, Sen S, Sweeney HL, Discher DE. Matrix Elasticity Directs Stem Cell Lineage Specification. Cell. 2006;126:677-89.

[148] Marklein RA, Soranno DE, Burdick JA. Magnitude and presentation of mechanical signals influence adult stem cell behavior in 3-dimensional macroporous hydrogels. Soft Matter. 2012;8:8113-20.

[149] Sang Jin L, Anthony A. Scaffold technologies for controlling cell behavior in tissue engineering. Biomed Mater. 2013;8:010201.

[150] Langer R, Vacanti JP. Tissue engineering. Science. 1993;260:920-6.

[151] Cantu DA, Kao WJ. Combinatorial biomatrix/cell-based therapies for restoration of host tissue architecture and function. Adv Healthc Mater. 2013;2:1544-63.

[152] Breen A, O'Brien T, Pandit A. Fibrin as a delivery system for therapeutic drugs and biomolecules. Tissue engineering Part B, Reviews. 2009;15:201-14.

[153] Whelan D, Caplice NM, Clover AJP. Fibrin as a delivery system in wound healing tissue engineering applications. Journal of Controlled Release. 2014;196:1-8.

[154] Cam C, Segura T. Chemical sintering generates uniform porous hyaluronic acid hydrogels. Acta Biomater. 2014;10:205-13.

[155] Perng CK, Wang YJ, Tsi CH, Ma H. In vivo angiogenesis effect of porous collagen scaffold with hyaluronic acid oligosaccharides. J Surg Res. 2011;168:9-15.

[156] Zhu S, Nih L, Carmichael ST, Lu Y, Segura T. Enzyme-Responsive Delivery of Multiple Proteins with Spatiotemporal Control. Advanced Materials. in press.

[157] Greenhalgh DG, Sprugel KH, Murray MJ, Ross R. PDGF and FGF stimulate wound healing in the genetically diabetic mouse. Am J Pathol. 1990;136:1235-46.

[158] Ozerdem U, Grako KA, Dahlin-Huppe K, Monosov E, Stallcup WB. NG2 proteoglycan is expressed exclusively by mural cells during vascular morphogenesis. Dev Dynam. 2001;222:218-27.

[159] Anderegg U, Simon JC, Averbeck M. More than just a filler – the role of hyaluronan for skin homeostasis. Experimental Dermatology. 2014;23:295-303.

[160] Wen J, Anderson SM, Du J, Yan M, Wang J, Shen M, et al. Controlled Protein Delivery Based on Enzyme-Responsive Nanocapsules. Advanced Materials. 2011;23:4549-53.

[161] Takahashi H, Shibuya M. The vascular endothelial growth factor (VEGF)/VEGF receptor system and its role under physiological and pathological conditions. Clin Sci. 2005;109:227-41.

[162] Nasrabadi MH, Ebrahimi MT, Banadaki SD, Kajousangi MT, Zahedi F. Study of cutaneous wound healing in rats treated with Lactobacillus plantarum on days 1, 3, 7, 14 and 21. Afr J Pharm Pharmaco. 2011;5:2395-401.

[163] Goldspiel BR, Green L, Calis KA. Human gene therapy. Clin Pharm. 1993;12:488-505.

[164] Mitani K, Clemens PR, Moseley AB, Caskey CT. Gene Transfer Therapy for Heritable Disease: Cell and Expression Targeting1993.

[165] Blaese RM, Culver KW. Gene therapy for primary immunodeficiency disease. Immunodefic Rev. 1992;3:329-49.

[166] Gao X, Kim K-S, Liu D. Nonviral gene delivery: What we know and what is next. AAPS J. 2007;9:E92-E104.

[167] Kobsa S, Kristofik NJ, Sawyer AJ, Bothwell ALM, Kyriakides TR, Saltzman WM. An electrospun scaffold integrating nucleic acid delivery for treatment of full-thickness wounds. Biomaterials. 2013;34:3891-901.

[168] Zhang J, Duan Y, Wei D, Wang L, Wang H, Gu Z, et al. Co-electrospun fibrous scaffold–adsorbed DNA for substrate-mediated gene delivery. Journal of Biomedical Materials Research Part A. 2011;96A:212-20.

[169] Mao Z, Shi H, Guo R, Ma L, Gao C, Han C, et al. Enhanced angiogenesis of porous collagen scaffolds by incorporation of TMC/DNA complexes encoding vascular endothelial growth factor. Acta Biomaterialia. 2009;5:2983-94.

[170] Elangovan S, D'Mello SR, Hong L, Ross RD, Allamargot C, Dawson DV, et al. The enhancement of bone regeneration by gene activated matrix encoding for platelet derived growth factor. Biomaterials. 2014;35:737-47.

[171] Huang YC, Simmons C, Kaigler D, Rice KG, Mooney DJ. Bone regeneration in a rat cranial defect with delivery of PEI-condensed plasmid DNA encoding for bone morphogenetic protein-4 (BMP-4). Gene Ther. 2005;12:418-26.

[172] Szymczak-Workman AL, Vignali KM, Vignali DA. Design and construction of 2A peptide-linked multicistronic vectors. Cold Spring Harb Protoc. 2012;2012:199-204.

[173] Lei Y, Huang S, Sharif-Kashani P, Chen Y, Kavehpour P, Segura T. Incorporation of active DNA/cationic polymer polyplexes into hydrogel scaffolds. Biomaterials. 2010;31:9106-16.

[174] Galiano RD, Michaels VJ, Dobryansky M, Levine JP, Gurtner GC. Quantitative and reproducible murine model of excisional wound healing. Wound Repair and Regeneration. 2004;12:485-92.

[175] Li J, Chen J, Kirsner R. Pathophysiology of acute wound healing. Clinics in Dermatology. 2007;25:9-18.

[176] Li J, Zhang YP, Kirsner RS. Angiogenesis in wound repair: angiogenic growth factors and the extracellular matrix. Microsc Res Tech. 2003;60:107-14.

[177] Nissen NN, Polverini PJ, Koch AE, Volin MV, Gamelli RL, DiPietro LA. Vascular endothelial growth factor mediates angiogenic activity during the proliferative phase of wound healing. Am J Pathol. 1998;152:1445-52.

[178] Werner S, Grose R. Regulation of wound healing by growth factors and cytokines. Physiol Rev. 2003;83:835-70.

[179] Bao P, Kodra A, Tomic-Canic M, Golinko MS, Ehrlich HP, Brem H. The role of vascular endothelial growth factor in wound healing. J Surg Res. 2009;153:347-58.

[180] Hellberg C, Ostman A, Heldin CH. PDGF and vessel maturation. Recent Results Cancer Res. 2010;180:103-14.

[181] Hao X, Silva EA, Månsson-Broberg A, Grinnemo K-H, Siddiqui AJ, Dellgren G, et al. Angiogenic effects of sequential release of VEGF-A165 and PDGF-BB with alginate hydrogels after myocardial infarction. Cardiovascular Research. 2007;75:178-85.

[182] Richardson TP, Peters MC, Ennett AB, Mooney DJ. Polymeric system for dual growth factor delivery. Nat Biotechnol. 2001;19:1029-34.

[183] Chen R, Silva E, Yuen W, Mooney D. Spatio–temporal VEGF and PDGF Delivery Patterns Blood Vessel Formation and Maturation. Pharmaceutical Research. 2007;24:258-64.

[184] Zhang H, Jia X, Han F, Zhao J, Zhao Y, Fan Y, et al. Dual-delivery of VEGF and PDGF by double-layered electrospun membranes for blood vessel regeneration. Biomaterials. 2013;34:2202-12.

[185] Salimath AS, Phelps EA, Boopathy AV, Che P-l, Brown M, García AJ, et al. Dual Delivery of Hepatocyte and Vascular Endothelial Growth Factors via a Protease-Degradable Hydrogel Improves Cardiac Function in Rats. PLoS One. 2012;7:e50980.

[186] Davies NH, Schmidt C, Bezuidenhout D, Zilla P. Sustaining Neovascularization of a Scaffold Through Staged Release of Vascular Endothelial Growth Factor-A and Platelet-Derived Growth Factor-BB. Tissue Eng Pt A. 2012;18:26-34.

[187] Heldin C-H, Westermark B. Mechanism of Action and In Vivo Role of Platelet-Derived Growth Factor. Physiological Reviews. 1999;79:1283-316.

[188] Curtin CM, Tierney EG, McSorley K, Cryan S-A, Duffy GP, O'Brien FJ. Combinatorial Gene Therapy Accelerates Bone Regeneration: Non-Viral Dual Delivery of VEGF and BMP2 in a Collagen-Nanohydroxyapatite Scaffold. Advanced Healthcare Materials. 2015;4:223-7.

[189] He S, Xia T, Wang H, Wei L, Luo X, Li X. Multiple release of polyplexes of plasmids VEGF and bFGF from electrospun fibrous scaffolds towards regeneration of mature blood vessels. Acta Biomaterialia. 2012;8:2659-69.

[190] Huh S-H, Do H-J, Lim H-Y, Kim D-K, Choi S-J, Song H, et al. Optimization of 25kDa linear polyethylenimine for efficient gene delivery. Biologicals. 2007;35:165-71.